A MODEL FOR ORE-GENESIS IN THE HANSONBURG MINING DISTRICT, NEW MEXICO

by

Roger J. Allmendinger

Submitted in Partial Fulfillment
of the Requirements for the Degree of
Doctor of Philosophy

NEW MEXICO INSTITUTE OF MINING AND TECHNOLOGY

Socorro, New Mexico

December, 1975

LIST OF CONTENTS

LIST OF FIGURES

LIST OF TABLES

ABSTRACT

The Hansonburg mining district contains open-space fillings and replacements of fluorite, barite, quartz, and galena in fractured Pennsylvanian limestones. Normal faulting associated with mid-Tertiary rifting of the Rio Grande trough has exposed over 800 feet of limestones and arkoses in the north-trending, westward-facing scarps of the Sierra Oscura. This Pennsylvanian sequence rests unconformably on Precambrian granites and metasedimentary rocks. Mineralization appears to be Oligocene or Miocene in age. Fluid inclusions indicate that most of the mineralization took place from a 2 to 3 molal NaCl solution at temperatures between 140° and 200° C. Present-day temperature gradients in this area are inadequate to provide for these temperatures at the estimated 1100-1500 meter depth at which mineralization took place. Mid-Tertiary dikes and sills in the area probably contributed to high heat flow.

Early sulfides precipitated during a period of increasing temperatures, while later fluorite mineralization occurred as temperatures decreased. Barite deposition overlapped between the sulfide and fluorite stages. Organic material identified in some inclusions was probably derived from nearby petroliferous limestones; these organics may have played a role in the precipitation of early sulfides. Sulfur isotopes indicate that nearly all of the sulfide and sulfate sulfur was probably derived from Permian evaporites found in the local stratigraphic column. Chemical analyses of various

country rocks suggest that they may have been the source of the hydrothermal mineral-forming constituents. Estimates of Oligocene-Miocene hydrologic flow patterns and a reinterpretation of lead isotopes are compatible with such a sedimentary-hydrothermal origin of the deposits.

Comparison with similar deposits elsewhere in North America suggests that the proposed model for mineralization of the Hansonburg mining district could account for numerous other deposits. The Hansonburg mining district has many similarities with Mississippi Valley-type mineralization.

INTRODUCTION

The Hansonburg mining district lies two and one-half miles south of U.S. highway 380 at Bingham, New Mexico (Figure 1). The northern boundary of the White Sands Missile Range forms the southern boundary of the mining district and has curtailled exploration and development in that direction. The primary ore and gangue minerals: fluorite, barite, galena and quartz occur as open-space fillings and replacements in silicified Pennsylvanian limestones. Normal faulting thought to be associated with rifting of the Rio Grande trough has exposed rocks of Precambrian to Permian age immediately south of the mining district. This mid-Tertiary (?) fault zone has bisected a Laramide (?) anticline nearly along its axial plane, thus resulting in the north-trending Sierra Oscura overlooking the Jornada del Muerto to the west. Normal faulting, erosion, and extensive mining activity have formed excellent exposures of the host rocks. Elevations in the district vary from less than 5500 feet to more than 6526 feet.

The Hansonburg mining district was New Mexico's largest producer of barite, 34,868 tons or 96.5% of New Mexico's production from 1951 to 1960 (Williams et al., 1964), and significant amounts of fluorite and galena also have been mined. The 1973-74 energy crisis and its effect on the economics of barite (used in drilling muds) should provide a catalyst to renewed exploration activity for this mineral. An understanding of the source and environment of deposition of ore-forming elements is an essential exploration tool.

Figure 1

Index map showing the locations of Bingham, New Mexico, and the area covered in the generalized geologic map of central New Mexico (Figure 2).

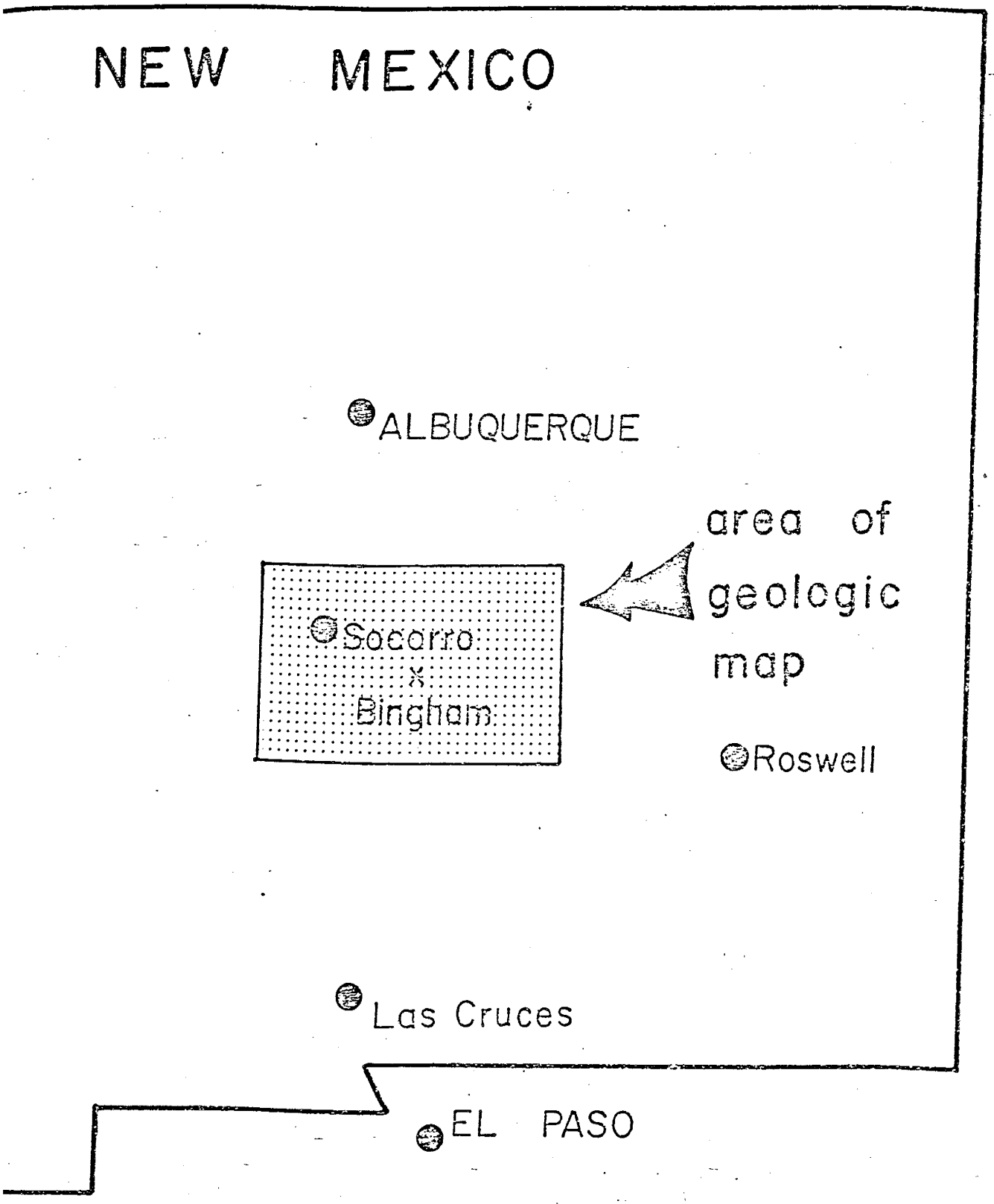
NEW MEXICO
ALBUQUERQUE
area of geologic map
Socorro
Bingham
Roswell
Las Cruces
EL PASO

Statement of purpose

The purpose of this investigation is to determine as closely as possible the environment of deposition of hypogene minerals in the Hansonburg mining district and to establish a model for the genesis of the hydrothermal fluids and their dissolved constituents. A secondary effort will be to compare the Hansonburg deposits and similar deposits in central New Mexico with the lead-zinc-barite-fluorite deposits of the central, cratonic United States. Several more specific questions may be posed in the light of this problem. These include:

1. Is the "source-bed" model of ore genesis a feasible explanation for mineralization in the Hansonburg district?
2. What were the relative roles of regional tectonics, magmatism and hydrology in the genetic model?
3. What similarities and differences does the Hansonburg mining district have with the so-called Mississippi Valley-type deposits in North America?

Investigatory processes and previous studies

Fluid inclusions have long been used as a primary source of information on the chemical characteristics of mineralizing solutions. Roedder (1967) has presented a bibliography and introduction to the theory, applications, and limits of fluid inclusion studies. This work has been expanded and updated (Roedder, 1972) in the form of a geochemical handbook. Although the majority of studies have used nondestructive techniques (homogenization and freezing temperatures), some have sampled the trapped fluids in

an attempt to directly measure their chemistry (c.f. Roedder, 1958; Hall and Friedman, 1963; Roedder et al., 1963; Rye and Haffty, 1969; Sawkins, 1968; and Ohmoto, 1968, 1971). The minerals in the Hansonburg district are, for the most part, transparent, large, euhedral crystals, particularly amenable to fluid inclusion analyses. Homogenization temperatures with a pressure correction will place limits on fluid temperatures. Freezing temperatures can be used to estimate approximately the total salt content (or ionic strength).

Fluid inclusion studies have been particularly useful for investigating the nature of fluids responsible for Mississippi Valley-type ore deposits. From the variations in salinity, cation ratios, and stable isotopes Hall and Friedman (1963) were able to suggest that connate waters mixed with possible magmatic waters followed by meteoric waters during the mineralization of the Cave-in-rock district. In a similar study Sawkins (1966) indicates that mixing of a juvenile hydrothermal solution with high-barium connate waters was responsible for fluorite-barite zoning in the North Pennine ore field. Roedder (1971) working in the Southern Appalachian Valley district concluded that deeply circulating connate brines were the most probable ore fluids. Some indication of mixing of these brines with small amounts of surface waters was also observed.

The isotopic chemistry of hydrogen and oxygen has been shown to be a useful indicator of the source (e.g. magmatic or meteoric) and the circulation history of a hydrothermal

solution. Craig (1963) first described the "oxygen shift", or departure from the meteoric water line, of waters associated with geothermal systems. This oxygen shift is commonly interpreted as the result of interaction of meteoric water with the host rock at elevated temperatures. Craig (op. cit.) then went on to define a region in δD- and $\delta^{18}O$-space which characterizes juvenile water. The size of this "magmatic box" has been increasing with continued research and a recent study (Ohmoto and Shettel, 1974) indicates that the isotopic composition of magmatic water is dependent on other phases which may be in equilibrium with the water, such as H_2, CH_4, CO_2 and CO.

The stable isotopes of carbon and sulfur may provide some clues regarding the source of these elements, as well as narrowing the chemical conditions of ore deposition. Sakai (1968) and Ohmoto (1972) have shown how pH and f_{O_2} of a hydrothermal system affect the stable isotope distribution by controlling the dominant aqueous species at equilibrium.

Recently, data from fluid inclusions and stable isotopes have been combined to study the hydrothermal processes involved with ore genesis (c.f. Rye, 1966, 1974; Ohmoto, 1968; Landis, 1972; Robinson and Ohmoto, 1973; and Rye and Sawkins, 1974). These studies have utilized temperature and composition estimates obtained from fluid inclusions in conjunction with stable isotope data from mineral phases and trapped fluids to determine the relative importance of magmatic and meteoric components during mineralization and to place restrictions

on the physiochemical parameters of the mineralizing fluid(s). Data from isotope and fluid inclusion analyses can aid in the application of mineral stability diagrams to an understanding of hydrothermal processes. Thermodynamic data for chemical species of geologic interest are becoming increasingly available and more refined (Stull, 1965; Helgeson, 1968; Robie and Waldbaum, 1968; Rosini et al., 1969), and may be used in conjunction with diagrams which graphically represent stability ranges of minerals in terms of compositional variables and temperature.

Thermodynamic, stable isotope, and fluid inclusion data are the primary input of this study. Inherent in the possibility that the element concentrations observed in the mineral deposits were derived from the country rock are problems involving mass transfer and hydrodynamics. Few investigators have appreciated the limit which can be placed on hydrothermal processes by the theories of regional groundwater dynamics in a conceptual model of ore genesis. This study will propose a model which is compatible with regional hydrologic dynamics as described by Toth (1962 and 1963) and Freeze and Witherspoon, (1966, 1967, and 1968).

The Hansonburg mining district has been mapped and the geology discussed in detail. The host rocks, ore and gangue mineralogy, structure and production were described by Lasky (1932); Talmage and Wootton (1937); and Rothrock et al. (1946). Later geologic studies include Kottlowski (1953); Kopicki (1962); Williams et al. (1964); Williams (1966); and Lewchalermvong (1973). Roedder et al. (1968) studied the

filling and freezing temperatures of fluid inclusions in sphalerite, barite, fluorite, and quartz at one mine in the district and Ames (1958) investigated the chemical composition of fluid inclusions. Austin and Slawson (1961) and Slawson and Austin (1962) studied the isotopic composition of lead in galena from the Hansonburg district. Consequently much preliminary and supplementary work has been completed, giving this author a large data base upon which to build.

Acknowledgments

Theses and dissertations in general require a large amount of time, patience and effort from persons other than the student; this study is certainly no exception. Advisor, Dr. Richard Beane deserves more than a simple "thank you" for the many long and late hours he has spent reviewing and criticizing the substance and structure of this dissertation. This assistance was essential to the study and is appreciated very much. However, it is this student's opinion that the personal involvement and guidance of his advisor, throughout the graduate program, is the most important contribution to this research. Although adequate appreciation cannot be described here, it is appropriate that this generosity be gratefully acknowledged.

Dr. Jacques Renault spent much time helping with the rock analyses and interpretation of the data. Both he and Dr. Charles Chapin devoted much time reviewing the manuscript and evaluating the geologic implications; this time often detracted from their own research efforts and is very much appreciated. Dr. Hiroshi Ohmoto of the Pennsylvania State

University and Dr. Austin Long of the University of Arizona very generously permitted the use of their complete stable isotope laboratories. This required a great amount of time for orientation and personal instruction in the use of laboratory equipment and analytical instrumentation. Dr. Ohmoto, especially, gave invaluable expertise in both the theories of stable isotope behavior and analytical precedures. In addition, his skills as laboratory technician and glass blower were called upon frequently throughout the study. Dr. Ohmoto and Dr. Gary Landis of the University of New Mexico made many suggestions and criticisms related to the original manuscript. Portions of the text were reviewed by Dr. Robert Weber and Roy Foster at the New Mexico Bureau of Mines; the considerable comments from these reviews are all gratefully acknowledged.

This research was made possible by a graduate assistantship from the New Mexico Bureau of Mines and Mineral Resources. In addition "the Bureau" allowed Drs. Jacques Renault and Charles Chapin to act as committee members, thus diverting their attention from other Bureau projects. Lynn Brandvold, chemist for the Bureau, kindly did the fluoride analyses of the rock samples.

The many drafts of this manuscript have been typed by my wife, Diane. She has done this with the same love and understanding I have enjoyed from her throughout the researching and writing of this dissertation.

Mr. Leslie Taylor of Taylor Mining Enterprises Co. is to be thanked for allowing access to all the property studied

in the Hansonburg mining district. Many important portions of this study could not have been made without substantial financial aid. The Society of Sigma Xi and the Geoscience Department of the New Mexico Institute of Mining and Technology both gave generous amounts for the analytical work. The New Mexico Geological Society donated funds for travel and drafting expenses. Some of the stable isotope analyses were paid by a National Science Foundation grant received by Dr. Ohmoto (Grant Number GA-31901A #1).

GEOLOGIC SETTING

The geology in the vicinity of the Hansonburg mining district is not well known beyond those areas which show economic potential. Wilpolt and Wanek (1951) included the Hansonburg district in their 1:62,500 map of east-central Socorro County. Weir's (1965) water-supply paper includes a 1:125,000 geologic map of the northern parts of the Jornada del Muerto and Tularosa Basin including the Sierra Oscura and northern San Andres Mountains. Figure 2 is a generalized geologic map of the terrane surrounding the mining district. Kottlowski (1953), Kopicki (1962), and Lewchalermvong (1973) discussed the geology of the district in some detail. The description of geology in this text will be largely a condensation and integration of the above references.

Stratigraphy

Rocks which crop out in the immediate vicinity of the Hansonburg mining district consist of Pennsylvanian limestones, siltstones, and arkosic sands and conglomerates. Other rocks which may have been important to the mineralization history include Precambrian granites and metasedimentary rocks and Permian siltstones, sandstones, mudstones, arkoses, evaporites, and limestones. Mesozoic rocks probably only affected mineralization in that they added to the overburden. Numerous mid-Tertiary (?) dikes and sills occur in the area but have no obvious spacial relationship to the open-space barite-fluorite-galena mineralization.

Figure 2

Generalized geologic map of central New Mexico showing the locations of Hansonburg mining district and related geologic features mentioned in the text (modified from Dane and Bachman, 1965). Figure 22 is an enlarged map of the shaded region labelled "Hansonburg and vicinity." Places abbreviated on the base and overlay are:

S	Socorro
SM	San Marcial
B	Bingham
GQ	Gran Quivera
C	Carrizozo
JCD	Jones Camp dike

The generalized geologic rock units are:

Qv	Quaternary volcanic rocks
Qs	Quaternary sedimentary rocks
Tv	Tertiary volcanic rocks
Ts	Tertiary sedimentary rocks
TKi	Tertiary-Cretaceous intrusive rocks
Mz	Mesozoic sedimentary rocks
Pz	Paleozoic sedimentary rocks
pE	Precambrian metamorphic rocks

PRECAMBRIAN ROCKS

Wilpolt and Wanek (1951) mapped undifferentiated Precambrian rocks south of the mining district along the base of the eroded fault scarp of the Sierra Oscura. These rocks include granites, schists, quartzites, rhyolites, and granitized metasediments. Granite containing large, poikilitic crystals of orthoclase and quartz, a dark-green mica schist and a mica-rich gneiss crop out in a canyon about one mile south of the Blanchard mine. Weir (1965) mapped over 2000 vertical feet of Precambrian rocks in T. 12S., R. 5E., on the east side of the San Andres Mountains about 45 miles to the south of Bingham. He notes (p. 14) that granite and quartzite predominate but some gneiss and schist also occur. A generalized stratigraphic column is shown in Figure 3.

PALEOZOIC ROCKS

Only a few hundred feet of Pennsylvanian limestones and sandstones intervene between the hydrothermal mineral deposits in the Council Spring limestone and the underlying Precambrian rocks. Overlying the Pennsylvanian rocks is a thick (3100 feet) sequence of Permian redbeds, evaporites and limestones.

Pennsylvanian rocks.

Mapping of Pennsylvanian rocks in the study area has been done on two scales. Wilpolt and Wanek (1951), mapping on a regional scale, divided the Pennsylvanian into the Sandia and Madera Formations. Only the upper clastic member of the Sandia Formation as described by Thompson (1942), is present in the northern Sierra Oscura. According

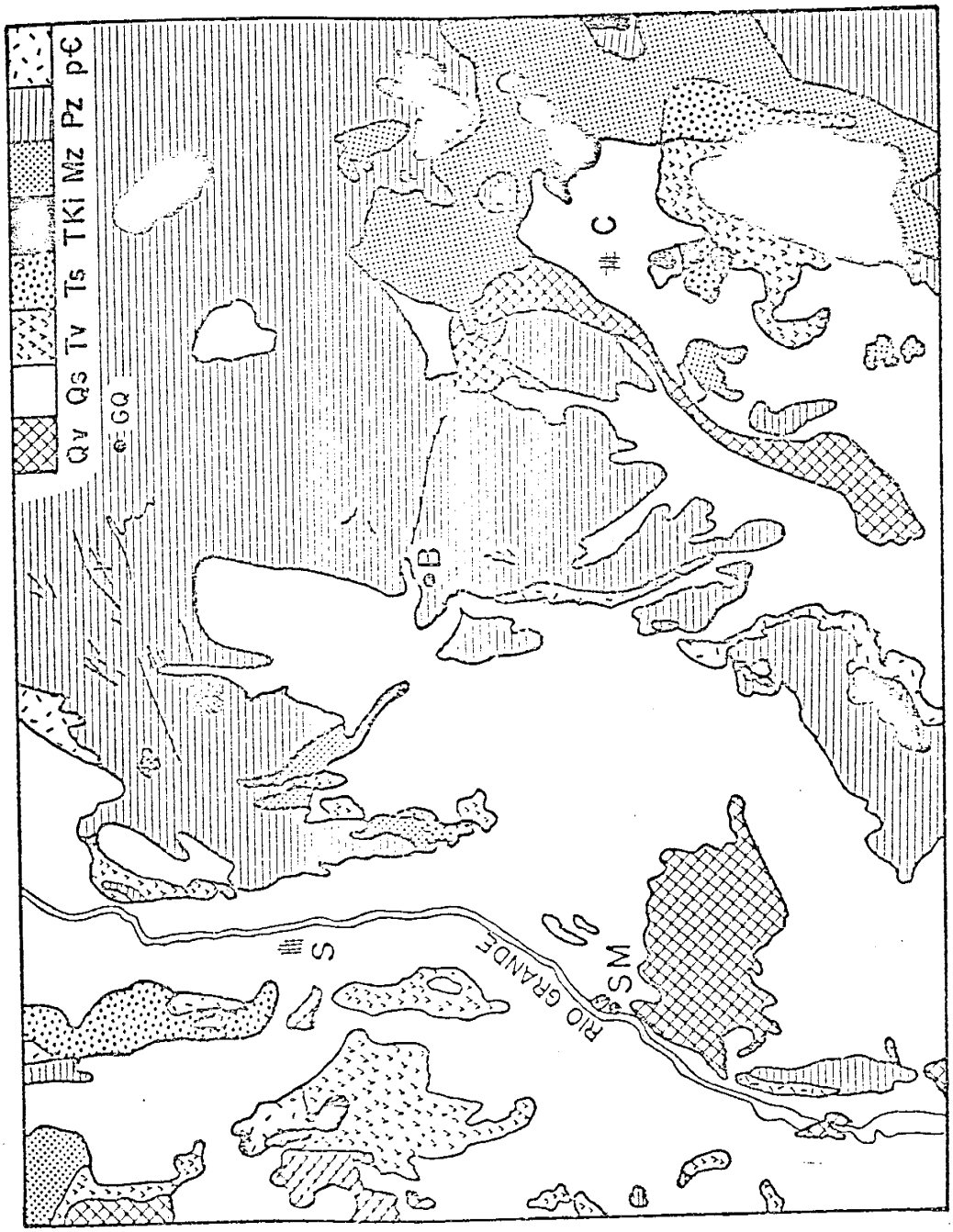
Qv Qs Tv Ts TKi Mz Pz p€
GQ
B
C
S
SM
RIO GRANDE
SCALE
15
30
MILES

Figure 3

Columnar section of Pennsylvanian and Permian rocks exposed in the vicinity of the Hansonburg mining district showing the correlation of Thompson's (1942) units with Wilpolt and Wanek's (1951) units (modified from Kottlowski, 1953).

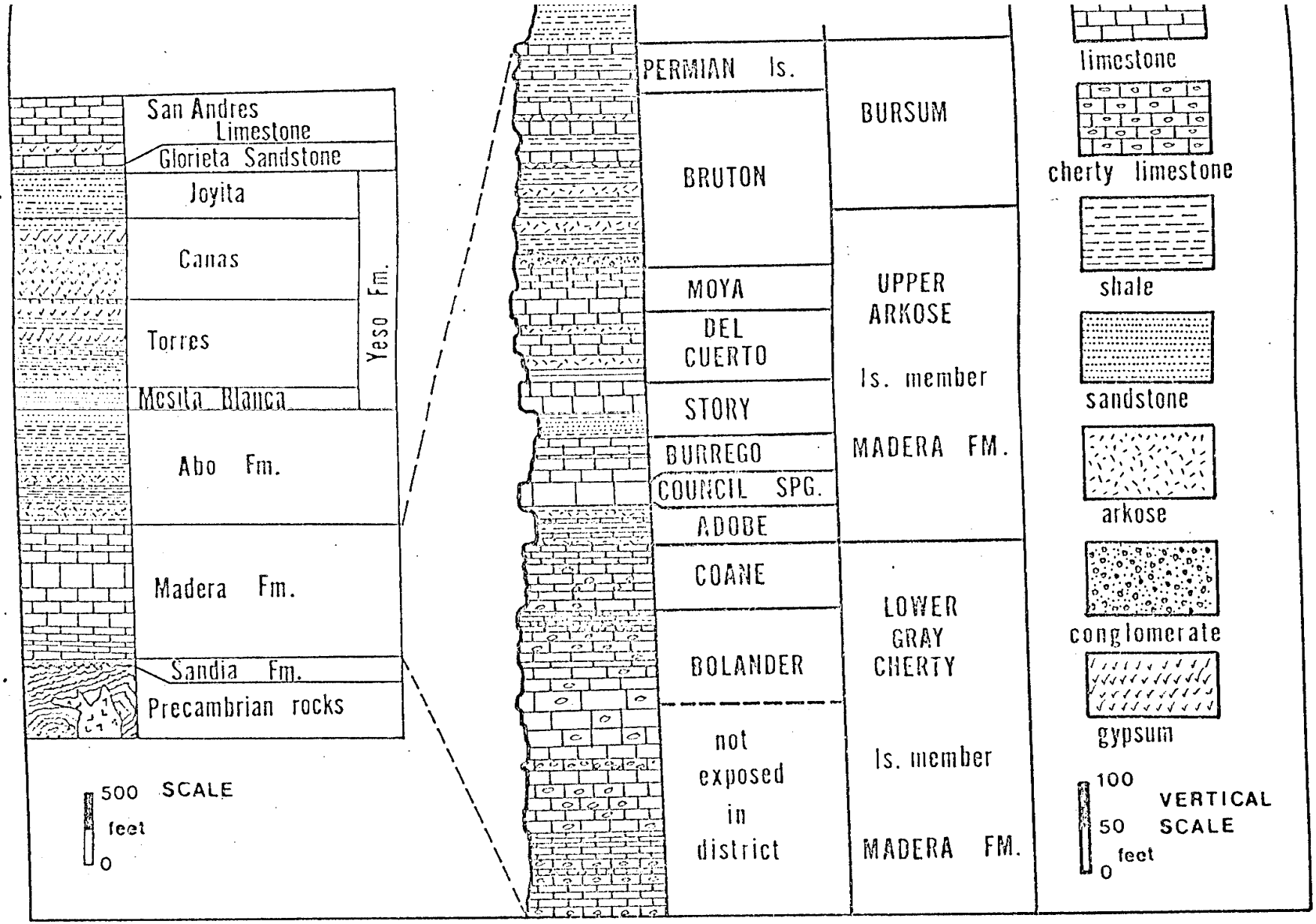
San Andres Limestone
Glorieta Sandstone
Joyita
Canas
Torres
Yeso Fm.
Mesita Blanca
Abo Fm.
Madera Fm.
Sandia Fm.
Precambrian rocks
500 SCALE
feet
0
PERMIAN ls.
BRUTON
MOYA
DEL CUERTO
STORY
BURREGO
COUNCIL SPG.
ADOBE
COANE
BOLANDER
not exposed in district
BURSUM
UPPER ARKOSE
ls. member
MADERA FM.
LOWER GRAY CHERTY
ls. member
MADERA FM.
limestone
cherty limestone
shale
sandstone
arkose
conglomerate
gypsum
100
50
0
feet
VERTICAL SCALE

to Kottlowski (1953, p. 4), this member consists of dark-gray, gray, black, and green sandy limestones, carbonaceous shale, sandstone and a quartz conglomerate, ranging in total thickness from 15 to 41 feet.

Conformably overlying the Sandia Formation is the Madera Formation which Wilpolt and Wanek (1951) divided into a lower gray limestone member and an arkosic limestone member. According to Wilpolt and Wanek (op. cit.), the lower gray limestone member thickens from 370 feet in the northern Sierra Oscura to 700 feet in the central Sierra Oscura. They describe this member as consisting of ". . . massive to thin-bedded, cherty, medium- to dark-gray limestone with small amounts of gray and green shale, sandstone and conglomerate." The arkosic limestone member (as much as 700 feet in total thickness) ". . . consists of thin-to thick-bedded, medium- and light-gray limestone that generally contains much less chert than the underlying member; gray, black, and red shale; and green, brown, and gray arkosic sandstone. Fresh pink feldspar grains are numerous in the basal sandstone and conglomerate beds of this member."

Thompson (1942) has subdivided the Pennsylvanian into much smaller units based on detailed stratigraphic and fusulinid studies. These units are useful for paleontologic studies but are not mappable rock units and are difficult to work with on a regional basis. Because this author is emphasizing the importance of regional controls on the ore-forming system, the classification of Wilpolt and Wanek (1951) will be emphasized. However,

previous workers (Kottlowski, 1953; Kopicki, 1962; and Lewchalermvong, 1973) limited the bulk of their work to the immediate vicinity of the mining district and found Thompson's classification more useful. Figure 3 is modified from Kottlowski (1953, Figure 1) and shows the relationship between the two nomenclatures. Difficulty in correlating units arises when trying to compare the Burton and Bursum Formations; Thompson considers the Burton to be Pennsylvanian in age while Wilpolt and Wanek consider their supposedly-equivalent Bursum to be Permian in age. Upper limestones in the Bursum Formation appear to be definitly Permian in age (Kottlowski, op. cit.). The problem, then, is in placing the Pennsylvanian-Permian time line between the Moya Limestone and the limestones capping the Bursum Formation.

The total Pennsylvanian rock section near the mining district may be about 915 feet thick.

Permian rocks.

Permian rocks include (in ascending order) the Abo, Yeso, and San Andres Formations. Sedimentation in Permian times in central New Mexico progressed from terrestrial red mudstones and siltstones, to marine sandstones and evaporites, to marine limestones. The total Permian rock section near the Hansenburg mining district may be more than 3100 feet thick.

The Abo Formation conformably overlies the Permian limestones of the Bursum Formation. The Abo comprises red, terrestrial mudstones, siltstones, sandstone, shales

and conglomerates containing abundant mudcracks, ripple marks and plant imprints. Wilpolt and Wanek (1951) suggest that this unit may be about 790 feet thick in the vicinity of the mining district. Differential weathering and erosion expose the sandy units while tending to cover the shaley units.

The Yeso Formation consists of four members: Meseta Blanca, Torres, Canas, and Joyita Members. All contacts within the Yeso Formation are conformable and gradational making them difficult to perceive in most instances. The basal Meseta Blanca Member, a uniform, reddish-brown sandstone unit, grades upward into the Torres Member which is an alternating sequence of sandstone, siltstone, limestone and gypsum. The Canas gypsum member, consisting of thick, white gypsum interbedded with minor gypsiferous siltstone and limestone, overlies the Torres Member and underlies the Joyita Member. The Joyita Member ranges from siltstone to sandstone and may be orange-red, pale tan, and yellow in color. The Yeso Formation does not crop out in the Hansonburg mining district but may be as thick as 1700 feet less than 8 miles to the south. Of this 1700 feet, nearly 1200 feet comprise the gypsum-rich Torres and Canas Members.

Above the Yeso Formation Wilpolt and Wanek (1951) map the Glorieta Sandstone and the San Andres Formation. Kottlowski (1963) has mapped the Glorieta sandstone member as a separate formation. The upper member of the San Andres Formation described by Wilpolt and Wanek as ". . . orange-red silty sandstone containing local thin beds of dark-gray limestone." may have been partially eroded during Triassic

times (Bates et al., 1947). The San Andres Limestone then, is an altermating sequence of dark-gray, thin- and medium-bedded, petroliferous limestone, white gypsum, and gray and orange-red sandstones. The Glorieta Sandstone is between twenty-five and fifty feet thick in the southern part of Chupadera Mesa (Kottlowski, 1963, p. 67) and the San Andres Limestone may be between 500 and 600 feet thick (Weir, 1965, p. 20).

MESOZOIC ROCKS

Mesozoic rocks are difficult to map in the vicinity of the mining district because they have been generally eroded from the elevated lands and covered in the basins; many of these rocks were probably eroded during Eocene times. Wilpolt and Wanek (1951) map small, isolated outcrops of Cretaceous and Triassic rocks in the area of the Torres syncline, suggesting that they may underlie a large region of Quaternary alluvium west and northwest of the Hansonburg mining district. Thus Mesozoic rocks probably add to the sedimentary column in lands adjacent to the mineralized region. No Jurassic rocks are known to exist in the southern half of New Mexico.

Triassic rocks.

The Dockum Group of Late Triassic age is only locally exposed in widely-spaced outcrops in the area of interest. Wilpolt and Wanek (op. cit.) estimate the maximum thickness of these rocks to be 500 feet, east of Socorro. Triassic rocks thin southward mainly because of ". . . truncation beneath

basal Cretaceous conglomerates and sandstones." (Kottlowski, 1963, p. 71). Smith (1964, p. 94) has mapped 250 feet of Santa Rosa Sandstone and from 200 to 400 feet of Chinle Formation in the Little Black Peak Quadrangle eight miles north of Carrizozo, New Mexico. This indicates a possible composite thickness of Late Triassic Dockum Group of between 450 and 650 feet. Foster (1974, pers. commun.) suggests that there may have been as much as 750 feet of Triassic Rocks in the Hansonburg mining district prior to Laramide erosion. These rocks have been eroded from Chupadera Mesa and the Sierra Oscura but crop out sporadically in the low hills north of U.S. Highway 380 and west of Bingham.

Cretaceous rocks.

Cretaceous rocks, like those of Triassic age, are sparse in the area of interest and generally follow the outcrop patterns of Triassic rocks. Three rock units of Cretaceous age are known in the structurally complex highlands east of the Rio Grande near the latitude of Socorro: The Dakota Sandstone, Mancos Shale, and Mesaverde Formation. Occurrences of these rocks in central New Mexico are mapped and described by Wilpolt and Wanek (1951).

The Dakota Sandstone consists of 71 to 110 feet of thick-bedded, medium-grained sandstone with some basal gray shales. The Mancos Shale contains about 800 feet of calcareous shale and limestone and medium- to fine-grained, medium-bedded sandstone. The Mesaverde Formation represents the last Cretaceous sedimentation in central New Mexico and consists

of sandstone, shale, and thin coal beds. This coal was mined in the Carthage area, 20 miles west of Hansonburg where the entire formation is only 200 feet thick. According to Wilpolt and Wanek (op. cit.), this is because the upper surface is erosional and the bulk of the formation has been removed. They point out that 987 feet of Mesaverde was penetrated by the Stackhouse No. 3 drill hole in Sec. 1, T. 5S., R. 2E. (op. cit., p. 2).

Smith measured 144-182 feet of Dakota Formation and 600 to 700 feet of Mancos Shale in the Little Black Peak Quadrangle (located on Figure 2). No Mesaverde rocks were noted there. Budding (1964) estimated 120-200 feet of Dakota, 410 feet of Mancos, and at least 415 feet of Mesaverde rocks are present in the Jicarilla Mountains.

It appears therefore, that between the Carthage coal field and the area north of Carrizozo, the Dakota thickens to the east slightly, the Mancos shales thin from 800 to 410 feet and the Mesaverde thins from 987 to 415 feet below an irregular erosion surface. In the Little Black Peak Quadrangle the Mancos is overlain by a volcanic breccia of Tertiary age. Near the Jicarilla Mountains, Ogallala-type conglomerates (Pliocene?) overlie the Dakota Sandstone in part. Cretaceous rocks as a whole probably thin eastward from about 1900 feet in the Carthage area to about 985 feet in the Carrizozo area. The top erosional surface is irregular and the erosion likely occurred over a long period of time from place to place. A rough estimate of the amount of Cretaceous cover, since eroded from the Hansonburg area,

would be about 1500 feet.

LATE CRETACEOUS - EARLY TERTIARY SEDIMENTARY ROCKS (LARAMIDE)

Sedimentation may have continued from the Cretaceous into early Tertiary times. Because this sedimentation was occurring during Laramide deformation (ca. 75-50 million years ago), distribution of the sediments would be controlled largely by the local upwarps and downwarps associated with the orogeny. Uplifted areas may have been sites of degradation while downwarps were receiving locally eroded detritus a short distance away. The Cub Mountain Formation as defined by Weber (1964, p. 105) may be such a unit. The Cub Mountain Formation is about 500 feet thick beneath the Sierra Blanca volcanics and may be late Cretaceous or early Tertiary in age (Kottlowki, 1963, p. 74). Deposition in this locale may have been related to downwarping of the Sierra Blanca basin; most of the debris in the basin was derived from Triassic and Cretaceous rocks (Kelley and Thompson, 1964, p. 117).

A similar unit exists in the vicinity of Elephant Butte Reservoir where the McRae Formation is well exposed. Bushnell (1955, p. 86) describes two members in the type locality, the Jose Creek Member and the Hall Lake Member. The lower, 394-foot-thick, Jose Creek Member is very local in nature. The upper Hall Lake Member may be Cretaceous in age near the type section but the upper beds are probably equivalent to the Tertiary Baca and Galesteo Formations to the north (Bushnell, p. 87).

The Baca Formation is a name given to 684 feet of Eocene conglomerate, light-gray sandstone, and red shale at the type locality in the Bear Mountains northwest of Socorro. One thousand to as much as 2000 feet of Baca Formation has been reported (Anonymous, 1963, p. 100) in the Carthage area, where it is deposited unconformably upon upper Triassic and Cretaceous rocks. Debris of Paleozoic and Precambrian rocks in the Baca indicate that considerable local degradation occurred. It is quite probable that the Baca, McRae, and Cub Mountain Formations are partially equivalent in age and depositional environment but not demonstrably deposited in a contiguous basin (Weber, 1974, pers. comm.). These erosional units are the result of Laramide orogenic activity in central New Mexico.

There is no evidence which would suggest that lands adjacent to the Hansonburg mining district were ever buried by significant amounts of Late Cretaceous or early Tertiary material. Weber (1963, p. 135), writing about isolated outcrops below Datil volcanic rocks on the western side of the Jornada del Muerto, states that the Baca ". . . is evidently very thin and contains channel conglomerates with boulders of granite and gneiss up to 8 feet in diameter." The Cub Mountain Formation probably does not extend much farther west than Cub and Chaves Mountains in southern Carrizozo Quadrangle (Weber, 1964, p. 105).

POST EOCENE ROCKS

Middle Tertiary volcanic rocks were the last rocks which might have been deposited near the Hansonburg mining district.

No Datil volcanic rocks are now exposed east of the axis of the Torres syncline and no Sierra Blanca volcanic rocks are known to exist within about 35 miles of the Hansonburg district. Although these rocks are equivalent in age (Oligocene?), evidence as to whether or not they were contiguous is lacking. Outflow facies of ash-flow tuffs from major cauldrons in the Magdalena and San Mateo Ranges and from vents in the Sierra Blanca area probably coalesced across the Hansonburg district but their presence and thickness can only be conjectured (Chapin, oral commun., 1975).

TERTIARY INTRUSIVE ROCKS

Dikes and sills are very common in the Hansonburg area but none seem to be spacially related to mineralization. Bates et al. (1947, p. 36-39) describe numerous dike and sill occurrences in the Gran Quivira Quadrangle north of the Hansonburg mining district, where hornblende diorites and diabases were intruded into the Yeso, Glorieta, and San Andres Formations. The host rocks have been upwarped by these injections but evidence of baking or thermal alteration is lacking. These authors (Bates et al., p. 36) also note that a water well in Section 25., T. 2S., R. 8E. penetrated six sills in less than 250 feet; these sills were five to 45 feet thick.

Dikes are common throughout this central part of the state and Kelley and Thompson (1964, p. 115) indicate that as much as one mile of east-west extension may have been

involved with dike intrusion in the southern part of the Capitan Quadrangle. The east-trending Jones dike of southern Chupadera Mesa is about 10 miles long and reaches a maximum width of 575 feet (op. cit., p. 115). This suggests there also may have been some extension in the north-south direction.

A dioritic dike, about six feet wide, occurs 2 and one-half miles north of the Hansonburg mining district and a sill of considerable extent is mapped by Wilpolt and Wanek (1951) about 3 miles east-southeast of the district. A small outcrop of diorite occurs in the northwest corner of Section 25., T. 5S., R. 5E. It is not known whether this small outcrop represents a dike or sill, however, it is not likely to be a stock of any large size because the adjacent Permian limestones and redbeds are not noticeably altered. There is no hydrothermal mineralization areally associated with this intrusion although a small replacement deposit of barite occurs 1/4 mile to the northeast in fractured Abo siltstones.

A previously unmapped sill, about 3 feet thick, was located in Abo redbeds about 1 1/2 miles east of the Hansonburg district; this sill has minor barite associated with it. About one mile farther east, a dike trends N. 70E. for about 1/2 mile before rolling over upwards into a sill. The dike is about 4 feet wide whereas the sill may exceed 15 feet in thickness, however, much of the sill has been eroded. These rocks all intrude about the same horizon and could have been continuous prior to erosion.

These abundant dikes and sills are indicative of a mid-Tertiary magmatic episode which would increase the heat flow in the region around Hansonburg. The Jones Camp dike and a large dike near Chupadera, New Mexico have been dated by Chapin at 27.2 ± 1.1 and 29.4 ± 2.0 million years, respectively (Beane and Titus, 1973). Several other unpublished dates on dikes and stocks in Socorro County are in the range of 27-30 million years (Chapin, oral commun., 1975). This widespread epoch of epizonal plutonism in central New Mexico may represent the initial stage of regional extension related to the Rio Grande rift (op. cit., oral commun., 1975). Beane and Titus (op. cit.) conclude that massive magnetite replacements and skarns associated with the larger dikes resulted from thermal interaction of ground water and the heated host rocks. The consistant assymetric geometry between dike and mineralization was attributed to regional groundwater movement. It is not known whether these intrusives vented to form a volcanic rock cover in this region.

QUATERNARY ROCKS

Quaternary deposits cover much of the valley fill immediately west of the Sierra Oscura. These comprise alluvial detritus derived from the Paleozoic and Precambrian rocks of the Sierra Oscura and transported westward by arroyos which deeply dissect the uplifted rocks. Well-developed alluvial fans occur along the base of the westward-facing scarp and merge with the valley floor of the Jornada

del Muerto. The surface deposits in the basin consist of fine-grained alluvium, blowsand, and playa deposits. A Quaternary basalt flow covers a large area east of the Rio Grande near San Marcial (Figure 2). These are recent features and probably are not related to mineralization in the Hansonburg mining district.

Structural history

Kopicki (p. 29) groups the faults in the Hansonburg district into three periods: "(1) possible pre-Burrego faults, . . . (2) faults formed prior to and coincident with mineralization . . . (3) a few faults which may have been formed during a post-mineralization period." The first period of faulting is represented by only one good example, which Kopicki believed may have been a conduit for later hydrothermal fluids.

The major landmasses contributing detritus to Pennsylvanian and Permian basins in New Mexico were the Uncompahgre, Penasco, Pedernal, Zuni and Joyita uplifts (Kottlowski and Stewart, 1970, p. 3). Figure 4 shows the generalized locations of the Pedernal landmass and associated clastic sediments for the Pennsylvanian of central New Mexico. Kottlowski and Stewart (op. cit.) have proposed the existence of a Wolfcampian uplift in the Joyita Hills area, where hydrothermal mineralization very similar to that at Hansonburg is found.

Laramide compressional deformation in central New Mexico is evident from broad anticlinal and synclinal folds, high-angle thrusting along reverse faults subparallel to

fault blocks. Southward from Loma de las Canas the general structure is a faulted anticlinorium plunging toward the Carthage area (Wilpolt & Wanek, op. cit.). The trend of the structural fabric is north-south but strikes of individual faults vary widely. East of the Montosa fault (approximately R. 2E.) the mid- to late-Tertiary structure becomes less apparent. Gentle Laramide flexures dominate the structure for approximately 15 miles eastward to the Sierra Oscura.

The Oscura fault is buried beneath alluvium about one mile west of the present location of the Oscura escarpment. Displacement on this N. 15E. trending normal fault decreases to the north where it dies out in the Oscura anticline (Kottlowski, 1953, p. 6). A second, nearly parallel fault trends along the base of the escarpment where the western limb of the Oscura anticline has been down-faulted about 550 feet into the Jornada del Muerto. This fault also dies out northward. A third fault bordering the zone on the east, is the Hansonburg fault which bifurcates to the south and probably dies out rapidly. The Hansonburg fault extends north-to-northeastward for about four miles. Many minor faults and fissures occur in the limestone exposed between the two major faults on the east. Presumably, these minor fractures occur westward at least as far as the Oscura fault but they are buried below Quaternary alluvium. Total displacement across this fault zone may be 800 to 900 feet as indicated by the position of the Bursum Formation in the Hansonburg Hills and eastward of the Blanchard prospects.

folds and erosion of pre-Laramide rocks on the uplifts. Laramide folds in the area (Figure 2) are, from west to east: the Prairie Springs anticline, Torres syncline, and Oscura anticline. Similar structures may have existed farther to the east and west but were broken and disguised by later complex normal faulting (Wilpolt & Wanek, 1951). The axes of these folds trend from N. 35E. to N-S; the Oscura anticline plunges northward but both the Prairie Springs anticline and Torres syncline plunge southward. Thrusting occurred along the Montosa fault (Figure 2) during Laramide times but the movement reversed after compression subsided (Wilpolt et al., 1946).

Most of the normal faulting in the Rio Grande Valley, Jornada del Muerto, and Tularosa Basin is associated with rifting of the Rio Grande trough and believed to be of mid-Tertiary and younger in age. McLean (1970, p. 16) and Strain (1969, p. 122) indicate that mountain building and basin filling may have begun by early- to mid-Miocene times. Regional extension began in the Socorro-Magdalena area at about 29 million years with the earliest fanglomerate deposits dated at 25 million years (Chapin, oral commun., (1975).

The "eastern structural border of the Rio Grande basin" is an area defined by Wilpolt and Wanek (1951) as lying between the West Joyita and Montosa faults (see Figure 2) extending southward from the Joyita Hills to the Carthage coal field. The structural complexity of this area is a result of normal faulting which produced numerous tilted

Figure 4

Generalized map showing areal distribution of Pedernal landmass, arkosic detritus, and evaporite deposits associated with Pennsylvanian geology (modified from Kottlowski, 1963).

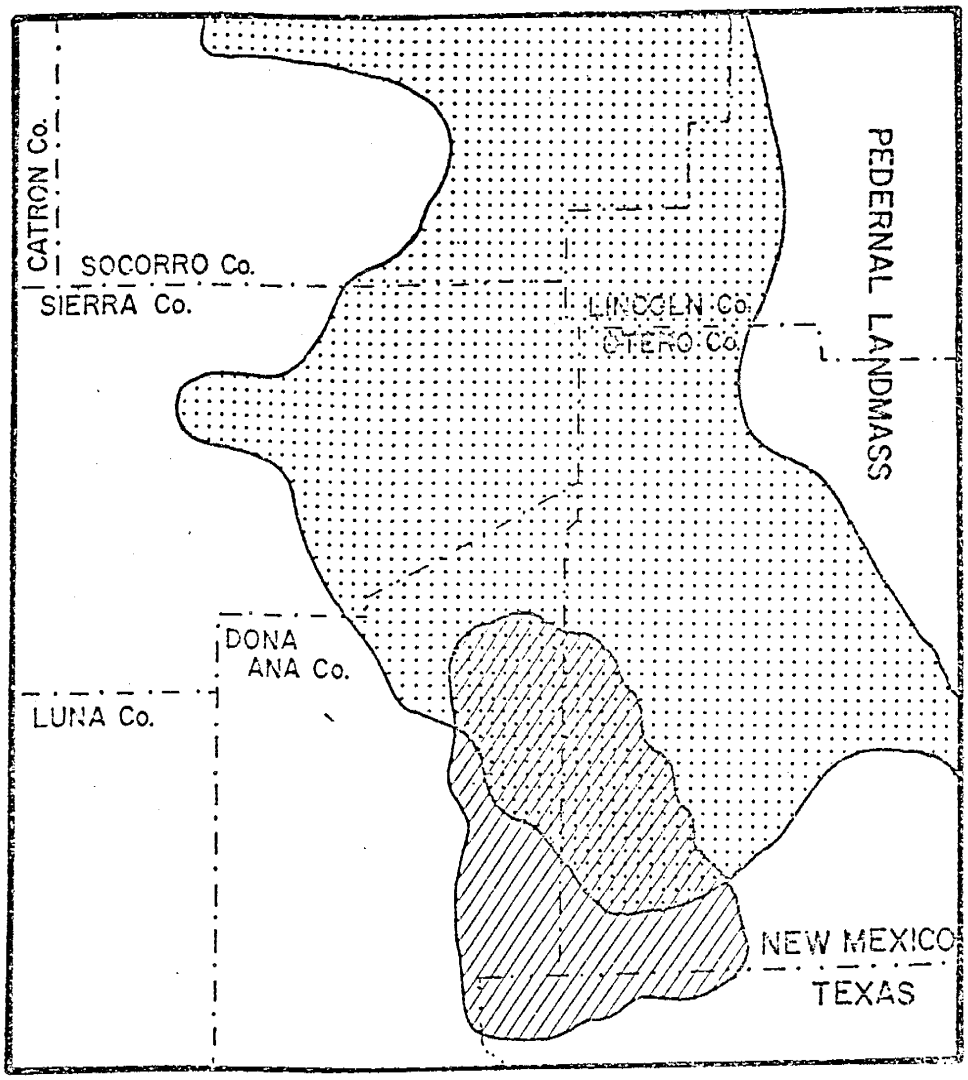

SCALE

0 25 50

MILES

LEGEND

GYPSUM

ARKOSE OR FELDSPATHIC SANDSTONE

Another fault of major proportions was mapped along the western margin of the Hansonburg Hills by Wilpolt and Wanek (1951). Here the San Andres Formation has been downfaulted into contact with the Bursum Formation near its (Bursum) type section, thus indicating displacement of more than 2500 feet. At this latitude, the Jornada del Muerto is likely a step-faulted graben-like basin. Sanford (1968, p. 4 and Figure 5) describes "a sharp fault" bounding the western margin of the Jornada del Muerto in the Carthage Quadrangle and believes that the Jornada is as deep as the Rio Grande depression in the adjacent quadrangle.

In summary, the structural relations in the area of the Sierra Oscura and Jornada del Muerto at approximately the latitude of the Hansonburg mining district are as follows. The north end is dominated by alternating, Laramide anticlines and synclines, while south of U.S. highway 380 mid- to late-Tertiary normal faulting predominates. At the north end, the switch from Laramide compression to later Tertiary extension was accomodated by reversal of fault movement and a wide, complex system or normal faulting east of the Rio Grande. Southward, the same purpose was served by a narrower band of complex faulting close to the Rio Grande and the large normal faults bounding the Jornada del Muerto on the east and west.

ANALYTICAL METHODS AND TECHNIQUES

Several analytical techniques were utilized to quantify the basic data necessary for this study. These included thermal analyses of fluid inclusions, x-ray fluorescence analyses of country rocks, and stable isotope analyses of ore minerals and some country rocks. In addition, past studies which have examined the lead isotope compositions of the Hansonburg and other hydrothermal deposits will be considered in this investigation. The results of these analytical methods will be used in conjunction with data derived from predictive methods for aqueous species and plotted on activity diagrams to aid definition of the chemical environment of hydrothermal mineral deposition. These methods and techniques are described below.

Activity diagrams

Diagrams which graphically represent stability ranges of minerals in terms of compositional variables and temperature may be used in conjunction with data from isotope and fluid inclusion analyses to aid in understanding hydrothermal processes. Eh, pH, and fugacity diagrams are specialized forms of activity diagrams which have been found to be particularly useful. Usually only two variables can be graphically expressed in two dimensions, however; several techniques can be utilized for expressing three or more variables on one illustration. Several examples follow which demonstrate the types and applications of activity

Figure 5

Distribution of aqueous sulfur species in P_{O_2} and pH space (modified from Barnes and Kullerud, 1961). Heavy lines separate fields dominated by the various aqueous sulfur species; light lines are contours on the fugacity of sulfur gas.

diagrams which will be utilized in this investigation. Figure 5 is a diagram showing the fields of predominence for the aqueous sulfur species in pH-P_{O_2} space. Construction of this diagram requires that pressure, temperature, ionic strength, and total dissolved sulfur be fixed. The solid lines enclose fields where the indicated species predominate. Figures 6 and 7 show how the mole fractions of two of these species are distributed at 200° C. Figures 8 and 9 show how the logarithm of the equilibrium constants for reactions between silicate phases vary as a function of temperature in terms of activities of K^+, Na^+, and H^+. Figure 10 is a composite a_{K^+}, a_{Na^+}, a_{H^+} (activity) diagram constructed from these equilibrium constants at 200° C. Helgeson et al. (1969) present over two hundred computer-drawn theoretical activity diagrams which describe a large number of mineral stability relations between 0° and 300° C.

Activity diagrams can be used to trace reaction paths for a particular paragenetic sequence. Evidence for equilibrium between two or more minerals can often be shown to demonstrate the presence of a chemical buffer. Referring to Figure 10, it can be demonstrated that if a_{K^+} is fixed then the coexistence of microcline and muscovite or albite and paragonite indicates a pH-buffered system at a given temperature. Activity diagrams are used in this study to help place limits on the composition of fluids which were responsible for alteration and mineralization at Hansonburg.

Figure 6

Distribution of the sulfide (S^{2-}) ion in f_{O_2} - pH space at 200°C and an ionic strength of 2.0. Contours are of mole fraction S^{2-} relative to total dissolved sulfur as calculated from the relations in Table B.

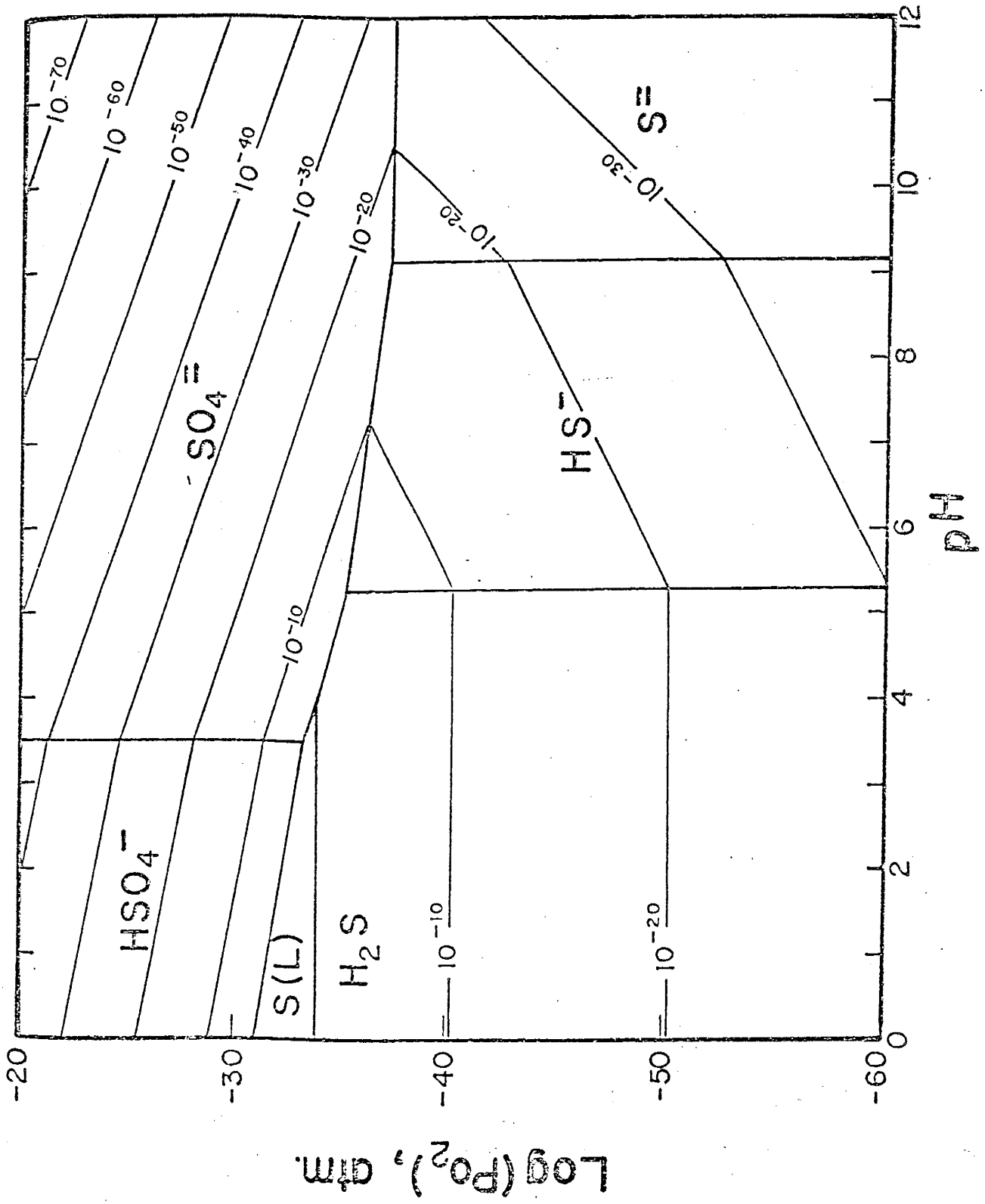
Log (P_{O_2}), atm.
pH
HSO_4^-
$SO_4^=$
S(L)
H_2S
HS^-
$S^=$
10^{-70}
10^{-60}
10^{-50}
10^{-40}
10^{-30}
10^{-20}
10^{-10}
10^{-30}
10^{-20}
10^{-10}
10^{-20}
-20
-30
-40
-50
-60
0
2
4
6
8
10
12

Figure 7

Distribution of aqueous H_2S in f_{O_2} - pH space at 200°C and an ionic strength of 2.0. Contours are of mole fraction H_2S relative to total dissolved sulfur.

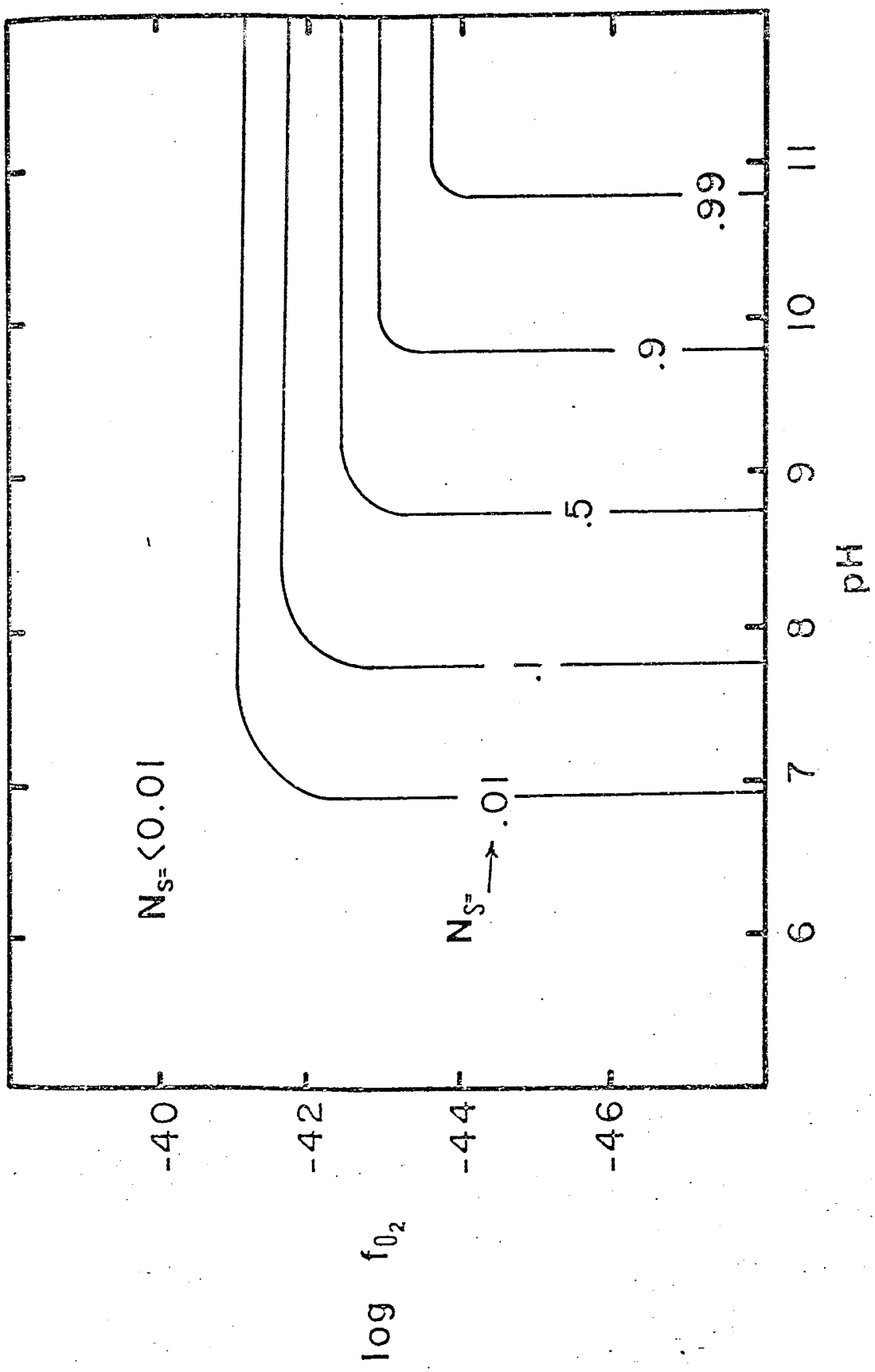
-40
-42
-44
-46
log f_{O_2}
6
7
8
9
10
11
pH
.01
.1
.5
.9
.99
$N_{S^=}$
$N_{S^=}$ <0.01

Figure 8

Plot of equilibrium constants for reactions between potassium-silicate pairs in terms of the logarithm of the potassium-hydrogen activity ratio and temperature. Equilibrium constants were obtained by adding the appropriate hydrolysis reactions and the corresponding equilibrium constants as listed by Helgeson (1969, Table 12).

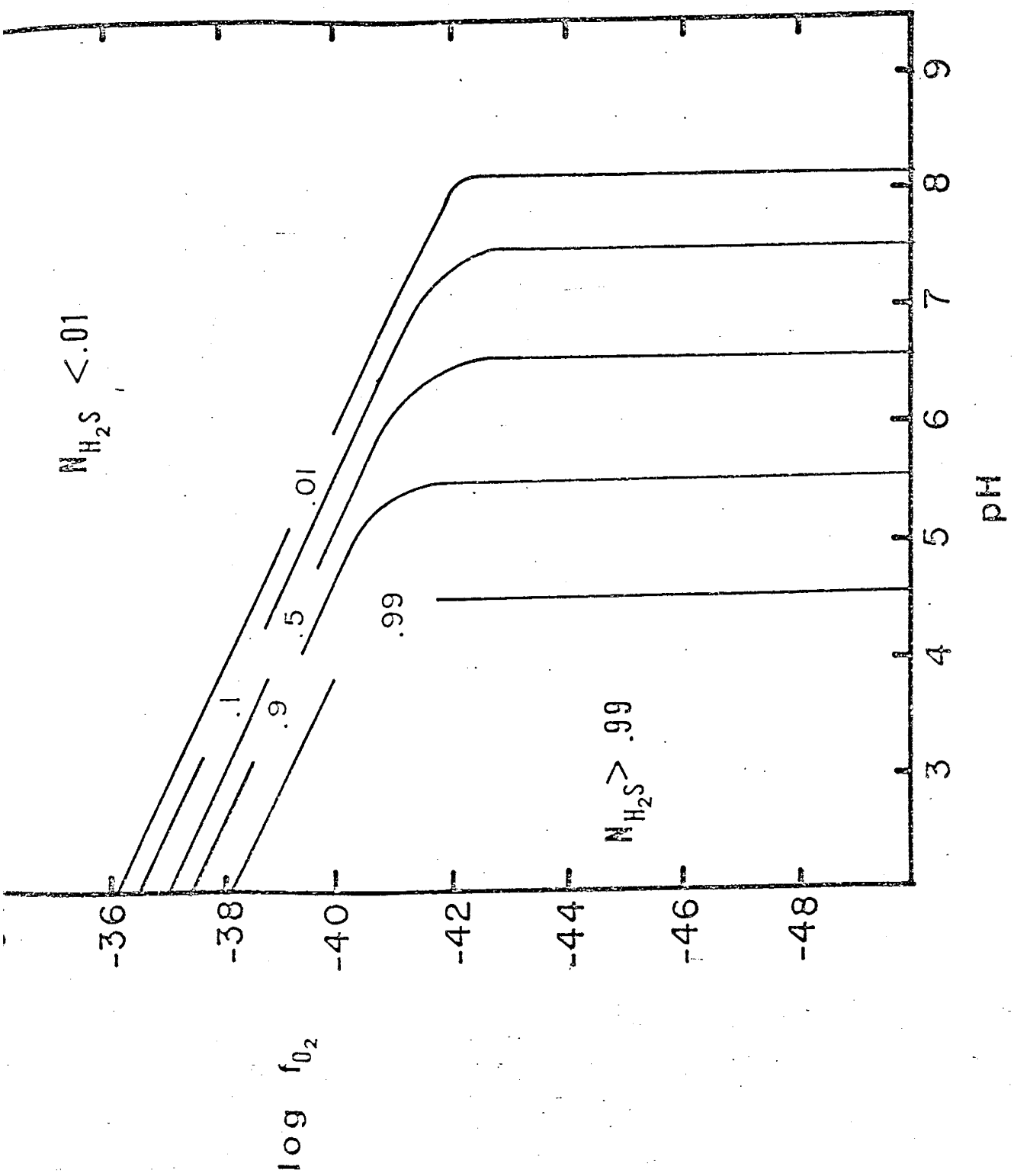
N_{H_2S} < .01
.01
.1
.5
.9
.99
N_{H_2S} > .99
-36
-38
-40
-42
-44
-46
-48
log f_{O_2}
3
4
5
6
7
8
9
pH

Figure 9

Plot of equilibrium constants for reactions between sodium-silicate pairs in terms of the logarithm of the sodium-hydrogen activity ratio and temperature. Equilibrium constants were obtained by adding the appropriate hydrolysis reactions and the corresponding equilibrium constants as listed by Helgeson (1969, Table 12).

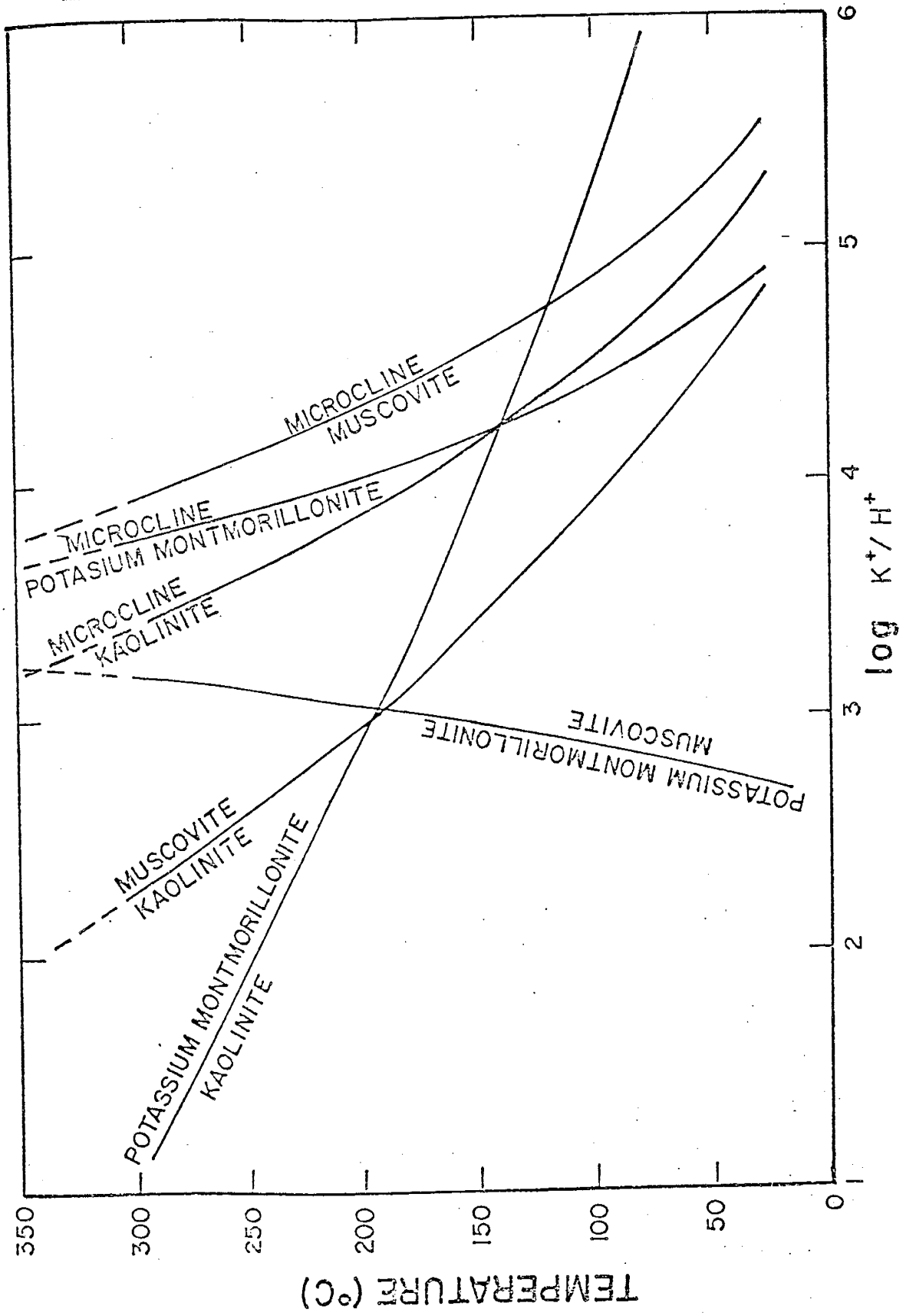
MICROCLINE
MUSCOVITE
MICROCLINE
POTASIUM MONTMORILLONITE
MICROCLINE
KAOLINITE
POTASSIUM MONTMORILLONITE
MUSCOVITE
MUSCOVITE
KAOLINITE
POTASSIUM MONTMORILLONITE
KAOLINITE
log K+/H+
TEMPERATURE (°C)
350
300
250
200
150
100
50
0
1
2
3
4
5
6

Figure 10

Activity diagram of sodium and potassium silicate minerals in terms of log a_{Na^+}/a_{H^+} and log a_{K^+}/a_{H^+} at 200°C using the data of Figures 8 and 9.

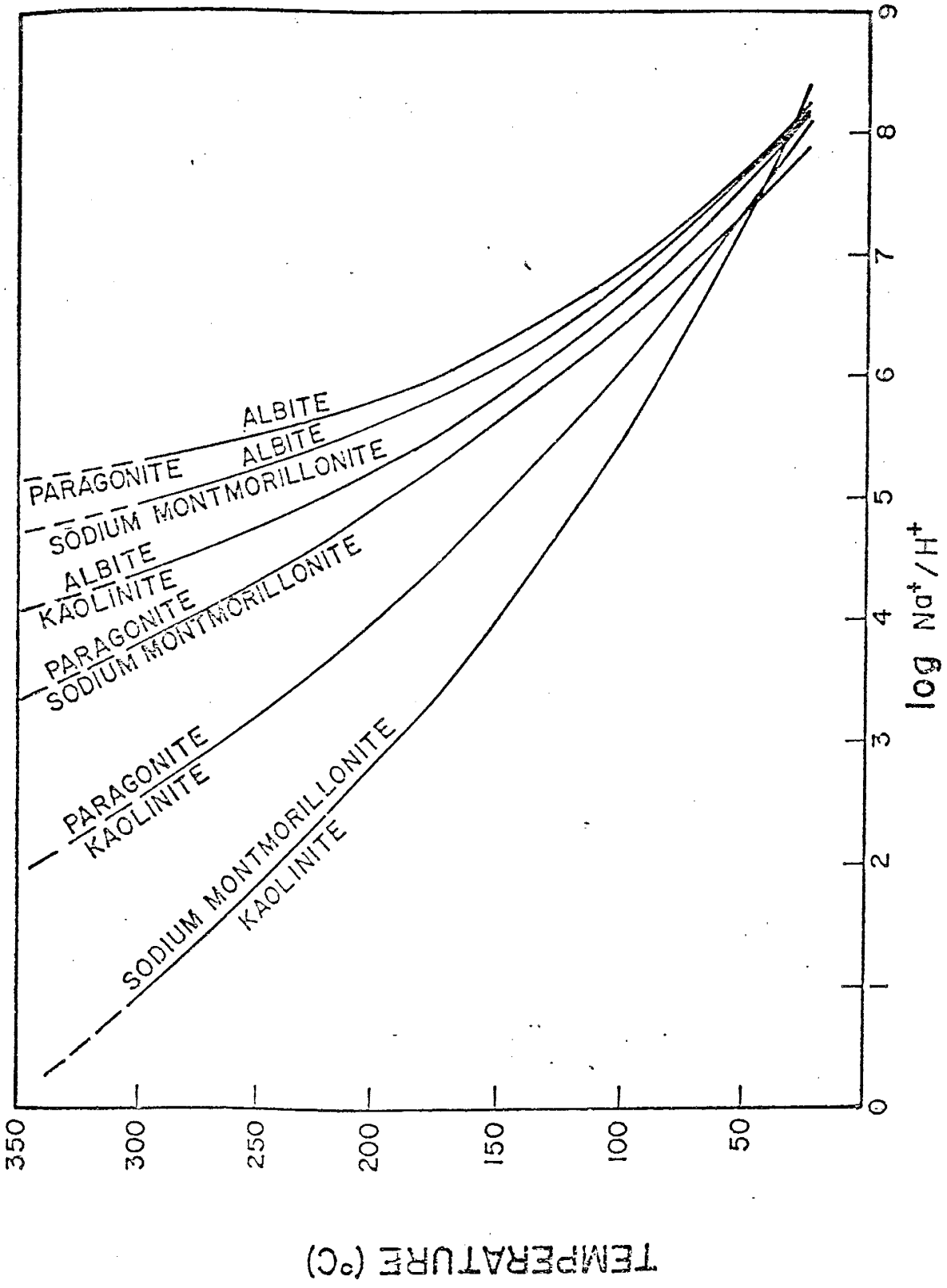
ALBITE
PARAGONITE
ALBITE
SODIUM MONTMORILLONITE
ALBITE
KAOLINITE
PARAGONITE
SODIUM MONTMORILLONITE
PARAGONITE
KAOLINITE
SODIUM MONTMORILLONITE
KAOLINITE
log Na+/H+
0
1
2
3
4
5
6
7
8
9
350
300
250
200
150
100
50
TEMPERATURE (°C)

Fluid inclusions

Fluid inclusions are small (usually less than one millimeter) samples of fluids trapped by growth imperfections on the crystal surface or by "healed fractures" during some period of the crystal's history. Fluid inclusions are classified as primary, secondary, or pseudosecondary depending on the model and timing of entrapment. Primary inclusions are those which are trapped by irregularities on the growth surface of the crystal and which are overgrown as crystal growth continues. Secondary inclusions form after the crystal has ceased precipitating from the fluid phase and has reached its final dimensions. This happens when the crystal is fractured and fluid leaks into the fracture. The fluid once "trapped" by the fracture, dissolves and reprecipitates the crystal material in such a manner as to produce a more stable cavity (system of lower surface energy). Thus, a plane of inclusions results outlining the former fracture. Often these inclusions take on a crystallographic orientation and shape; these are called negative crystals. Pseudosecondary inclusions form in the same manner as secondary inclusions but during crystal growth, hence the outer extent of planes of pseudosecondary inclusions will lie entirely within the crystal, unlike planes of secondaries which extend to the crystal edge. Often times, healing of the original fracture has been so complete that secondary and pseudosecondary inclusions become sufficiently isolated so as to render identification of their planar genesis difficult or impossible.

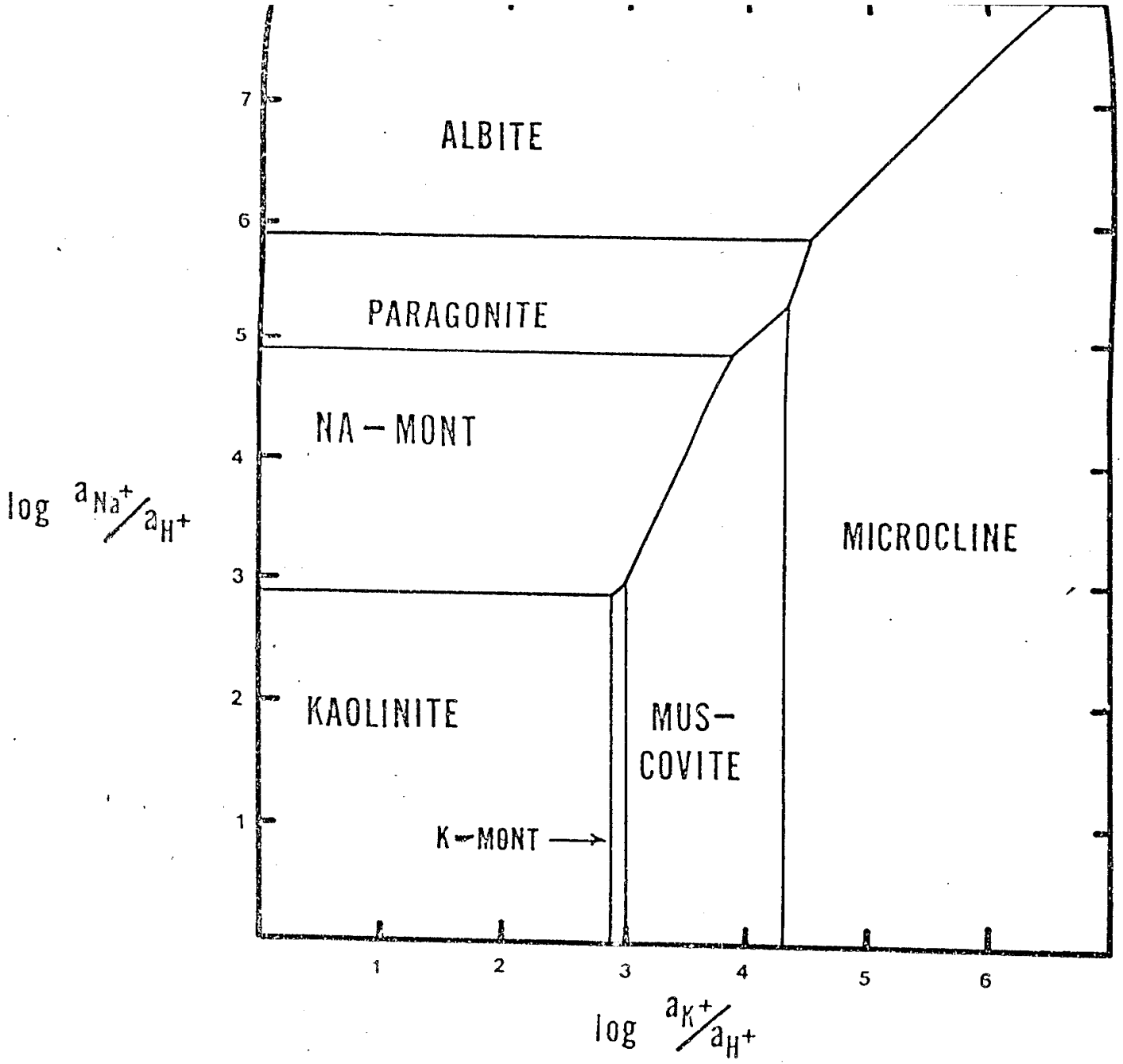
ALBITE
PARAGONITE
NA – MONT
MICROCLINE
KAOLINITE
MUS–
COVITE
K–MONT
7
6
5
4
3
2
1
1
2
3
4
5
6
log a_{Na^+}/a_{H^+}
log a_{K^+}/a_{H^+}

polished plate (about 1 mm thick) of the mineral is placed in the heating stage and the temperature is slowly increased until the vapor-phase bubble completely disappears. The temperature at which the vapor phase disappears is recorded as the filling temperature for that inclusion.

Filling temperatures are lower limits on the actual temperature at which that inclusion was trapped. When these temperatures are corrected for pressure they can be very accurate estimates of the temperature at which precipitation (or crystallization) took place. The difference between the filling temperature and the actual trapping temperature is a function of the filling pressure. Thus, if the pressure on the system during trapping is greater than the vapor pressure of the fuild, then the fluid will be compressed slightly. After this fluid has been trapped, it must be cooled the amount of the "pressure correction" before a vapor bubble can form (Kvenvolden and Roedder, 1971, p. 1225). The present study involves only the measurement of filling temperatures of fluid inclusions. A heating stage was built from plans of Ohmoto and Rye (1970) with few minor modifications. Temperatures were initially determined with a chromel-alumel thermocouple in conjunction with a balancing millivolt meter; later a Doric (DS350) digital thermocouple indicator was substituted for the millivolt meter. Filling temperatures were reproduceable to within 0.1° C for many inclusions. Figure 11 was used in conjunction with overburden and salinity estimates to determine the appropriate pressure correction. Freezing temperatures

The importance of being able to distinguish between the three types of inclusions lies in fact that the trapped fluids are representative of different periods relative to their position in the crystal. Primary inclusions are most important because they are contemporaneous with that portion of the crystal immediately adjacent to them. Fluids trapped in pseudosecondary inclusions are representative of fluids from which some part of the crystal precipitated but not necessarily that part directly surrounding the inclusion. Finally, fluids trapped in secondary inclusions may have no genetic relation to the fluids from which the crystal precipitated.

Simple fluid inclusions contain a liquid and vapor phase at room temperature. This closed two-phase system may have evolved by two means. First, the sample is trapped as a gas phase and later cooling results in condensation of a second (liquid) phase. Alternatively, a liquid phase may have been trapped, which upon cooling contracted more rapidly than the host mineral leaving a vapor-phase vacuole. The latter type of fluid inclusion is much more common than the former. Other phases are commonly found in fluid inclusions such as "bubbles" of liquid carbon dioxide and hydrocarbons and daughter minerals such as halite, sylvite, hematite, gypsum, barite and calcite.

Filling temperatures of fluid inclusions are the temperatures at which the liquid phase (in this instance) upon heating, completely fills the inclusion void at the expense of the gas phase. In practice, a cleavage plate or doubly

Figure 11

Contours of equal density in pressure-temperature space used to estimate pressure correction of fluid inclusion homogenization temperatures (from Ohmoto, 1968).

determined by Roedder et al. (1968) indicated that the fluid contained ten weight percent (or more) equivalent NaCl; thus the dashed curves in Figure 11 were used.

The procedure for determining filling temperatures follows. Cleavage fragments or doubly-polished plates are placed in the heating stage adjacent to the thermocouple probe and an inclusion is located while the stage is heating. The first heating run is made at a high rate (∿ 10° C/min.) to determine the approximate filling temperature. The stage and mineral plates are then allowed to cool until the vapor phase re-segregates from the liquid phase. A heating curve is then chosen which will allow temperatures to approach the approximated filling temperature at a slow rate (1° C/(5-10) min.). Several runs are made at the slow heating rate and the temperature noted when the vapor phase completely homogenizes with the liquid phase. If temperatures from successive runs are within 1° C of each other the temperature is recorded as the filling temperature. A large variation (more than 2-3° C) between successive runs on the same inclusion indicates leakage and the filling temperature data are unuseable.

Stable isotopes

It is believed that sulfur isotope analyses contribute significantly to this study for several reasons. First, sulfur-bearing hypogene minerals are common throughout the district, whereas hydrogen- and carbon-bearing minerals are sparse. Hypogene calcite, although common, occurs late in the paragenetic sequence and probably does not relate

directly to hypogene processes responsible for most of the mineralization. Several carbon-13 analyses were made and these will be discussed later. Oxygen isotopes would be useful for geothermometry but fluid inclusions serve the same purpose at a much lower cost. Oxygen and hydrogen isotopes are often used to distinguish magmatic waters from meteoric waters. Unfortunately the Hansonburg mining district lies in a geographic location not suited to this analyses. Sulfur will serve as the isotopic indicator of geochemical environment for this study.

The sulfur isotopes used in geologic investigations are ^{32}S and ^{34}S. Abundances of the natural sulfur isotopes are as follows: ^{32}S - 95.0%, ^{33}S - 0.76%, ^{34}S - 4.22%, and ^{36}S = 0.014% (Heath, 1973, p. B-256). ^{34}S of a sample is related to ^{32}S by the ratio $^{32}S/^{34}S$ which is compared with a standard. Variations from the standard are noted either simply as that ratio or by delta notation (δ). Most recent literature used the delta notation:

$$\delta^{34}S \text{ ‰} = \frac{(^{34}S/^{32}S)x - (^{34}S/^{32}S)s}{(^{34}S/^{32}S)s} \times 1000 \qquad (1)$$

where the subscripts x and s refer to the unknown and standard respectively and ‰ refers to parts per thousand (per mil). The standard to which all sulfur isotope values are referred is troilite (FeS) of the Canyon Diablo meteorite. Canyon Diablo Troilite (CDT) is defined to have a $^{34}S/^{32}S$ ratio of 0.0451145 and a permil value of 0.0 (Macnamara and Thode, 1950; Ault and Jensen, 1963).

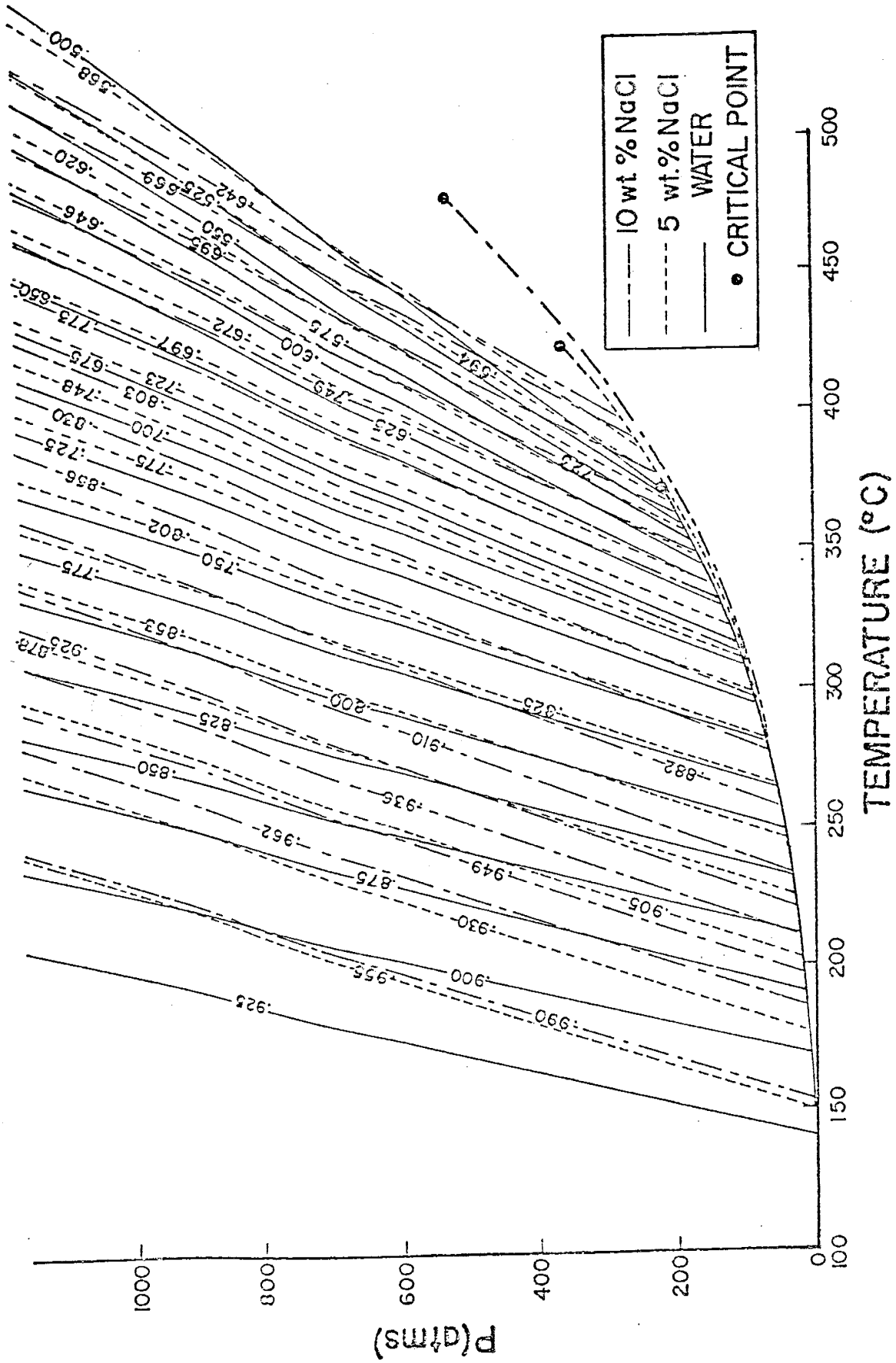
10 wt % NaCl
5 wt.% NaCl
WATER
CRITICAL POINT
TEMPERATURE (°C)
P(atms)
100
150
200
250
300
350
400
450
500
200
400
600
800
1000

Figure 12

Isotopic fractionation factors between H_2S and other aqueous sulfur species as a function of temperature (from Ohmoto, 1972).

Stable isotopes are useful because their ratios vary in a predictable thermodynamic manner under equilibrium conditions. Simply put, isotopes of higher mass favor positions of higher bond strength, or lighter isotopes favor higher energy environments. Sakai (1968) was first to explain some of these fractionation patterns in terms of thermodynamic theory.

Figure 12 shows the isotopic enrichment factors (Δ_i) of the important hydrothermal sulfur species. Δ_i is the difference of $\delta^{34}S$ values of the i-th species and H_2S. Two points should be obvious from this figure: 1) at some theoretical infinite temperature there is no isotopic fractionation between species but with decreasing temperatures these fractionations become considerable and 2) in the temperature range of most hydrothermal systems, the fractionation between the sulfate and sulfide species is much larger than that among the sulfide species alone. Although experimental data are not conclusive, it appears that fractionation between the various ionic sulfate species are negligible (Ohmoto, 1972, p. 554). According to Sakai (1968, p. 35), the largest isotopic fraction among sulfate species would be between anhydrite and aqueous sulfate ion, and this enrichment would be less than 3 ‰ at 25° C.

Ohmoto (1973) used the enrichment factors among $H_2S°$, HS^-, S^{2-}, SO_4^{2-}, and HSO_4^- to illustrate how pH and f_{O_2} control the isotopic composition of a hydrothermal fluid. The basic procedures outlined by Ohmoto will be implemented here to

show how they may be applied to the Hansonburg district. The first step is to consider the basic equations which control the distribution of aqueous sulfur species in pH and f_{O_2} space and their equilibrium constants (K). These equations and their log K's at 150° and 200° C are presented in Table A. Ohmoto (1972, pp. 552-556) shows how these equations can be rewritten in terms of log K, pH, f_{O_2}, molalities and activity coefficients and an expression for mass balance to yield the following expression for mole fraction of H_2S (N_{H_2S}):

$$N_{H_2S} = {}^{1}/C \qquad (2)$$

where

$$C = 1 + \left[\frac{K_{H_2S} \cdot \gamma_{H_2S}}{a_{H^+} \cdot \gamma_{HS^-}}\right] \cdot \left[1 + \frac{K_{HS^-} \cdot \gamma_{HS^-}}{a_{H^+} \cdot \gamma_{H^{2-}}}\right] + \left[\frac{f_{O_2}^2 \cdot \gamma_{H_2S}}{K_{SO_4^{2-}} \cdot a_{H^+}^2}\right] \cdot$$

$$\left[\frac{1}{\gamma_{SO_4^{2-}}} + \frac{a_{H^+}}{K_{HSO_4^-} \cdot \gamma_{HSO_4}} + \frac{a_{K^+}}{K_{KSO_4^-} \cdot \gamma_{KSO_4^-}} + \frac{a_{Na^+}}{K_{NaSO_4^-} \cdot \gamma_{NaSO_4^-}}\right] \qquad (3)$$

Mole fractions of the remaining species can be obtained by multiplying N_{H_2S} by m_i/m_{H_2S} where m_i is the appropriate expression for the molality of species i. Thus, the series of expressions in Table B follow. Mole fractions of the various sulfur species are then a function of the equilibrium constants, activity coefficients of species, activities of K^+, Na^+, and H^+ and f_{O_2}. The equilibrium constants and activity coefficients are a function of temperature and pressure. An expression showing the dependence of mole

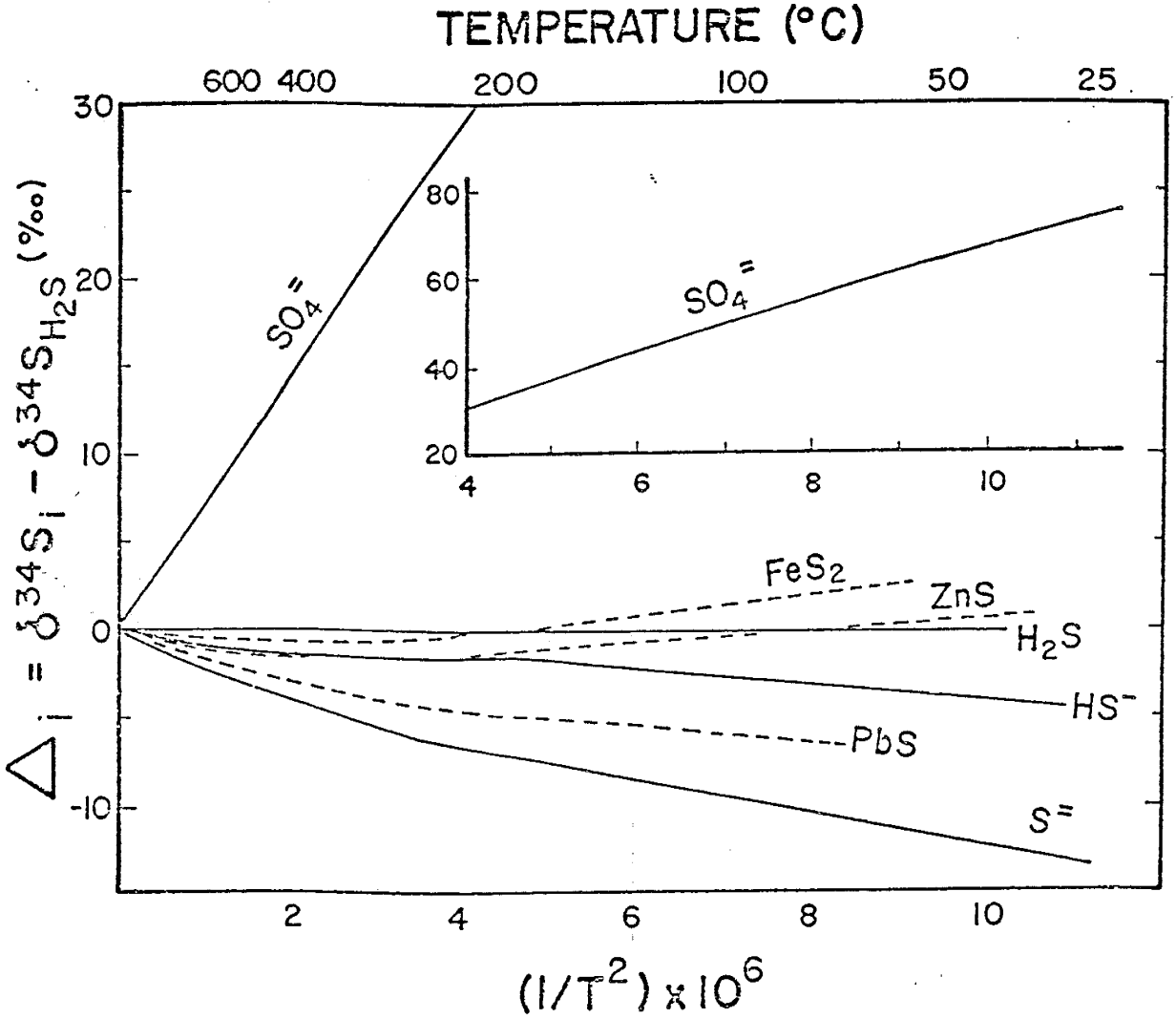
TEMPERATURE (°C)
600 400
200
100
50
25
30
20
10
0
-10
$\Delta_i = \delta^{34}S_i - \delta^{34}S_{H_2S}$ (‰)
$SO_4^=$
80
60
40
20
4
6
8
10
$SO_4^=$
FeS_2
ZnS
H_2S
HS^-
PbS
$S^=$
2
4
6
8
10
$(1/T^2) \times 10^6$

Table A Equations used to describe the distribution of aqueous sulfur species and the logarithm of their equilibrium constants (log K) at 150° and 200° C. Data for first 6 equations is from Ohmoto (1972, p. 556); data for equilibrium constant for equations 7 and 8 are from Figure 20.

	Equation	log $K_{150°}$	log $K_{200°}$
1.	$H_2S = H^+ + HS^-$	-6.72	-6.96
2.	$HS^- = H^+ + S^{2-}$	-10.76	-9.57
3.	$2H^+ + SO_4^{2-} = H_2S^\circ + 2O_2$	-79.31	-67.13
4.	$HSO_4^- = H^+ + SO_4^{2-}$	-3.74	-4.49
5.	$KSO_4^- = K^+ + SO_4^{2-}$	-1.60	-1.94
6.	$NaSO_4^- = Na^+ + SO_4^{2-}$	-1.60	-1.94
7.	$CaSO_4^\circ = Ca^{2+} + SO_4^{2-}$		-3.60
8.	$BaSO_4^\circ = Ba^{2+} + SO_4^{2-}$		-3.76

fractions on chemical environment may then be written as:

$$N_i = f\ (T,\ f_{O_2},\ pH,\ I). \qquad (4)$$

Assuming that the total sulfur isotopic composition is constant ($\delta^{34}S_{\Sigma S} = k$) and that the fractionation factors are constant (i.e. temperature is fixed), then the $\delta^{34}S$ of the individual species is directly related to its mole fraction. Figure 13 represents this relationship for a binary system at 200° C. If mole fractions of aqueous sulfur species can be contoured in pH and f_{O_2} space such as Figures 6 and 7, and if the isotopic composition of a species is directly related to its mole fraction, then it should be possible to contour lines of equal δ values (isodels) in pH and f_{O_2} space. Several such diagrams are presented by Ohmoto (op. cit.) and Figure 14 shows the theoretical distribution at 200° C, an ionic strength of 2.0, and a $\delta^{34}S_{\Sigma S}$ of 0.0 ‰. Similar treatment of carbon species and fractionation factors results in analogous expressions which describe the distribution of ^{13}C among the various aqueous species in terms of Equation 4 above.

Measurement of sulfur isotope ratios were made on a 6"-60° dual gas inlet, rationing mass spectrometer at the Pennsylvania State University. Sphalerite, galena, and barite samples were crushed to about 0.5 mm and then hand separated under a binocular magnifier. The sulfides were ground in an agate mortar with excess copper oxide and then oxidized at 1000° C for five minutes. The evolving gases were separated under vacuum by a series of cold traps and

Table B Expressions for mole fractions (N_i) of aqueous sulfur species. C is defined by Equation 3. K_1 is the equilibrium constant of Equation 1 in Table A.

$$N_{H_2S^\circ} = 1/C$$

$$N_{HS^-} = \frac{K_1 \cdot \delta_{H_2S^\circ}}{C \cdot a_{H^+} \cdot \delta_{HS^-}}$$

$$N_{S^{2-}} = \frac{K_1 \cdot K_2 \cdot \delta_{H_2S^\circ}}{C \cdot a_{H^+}^2 \cdot \delta_{S^{2-}}}$$

$$N_{SO_4^{2-}} = \frac{f_{O_2}^2 \cdot \delta_{H_2S^\circ}}{C \cdot K_{SO_4^{2-}} \cdot a_{H^+}^2 \cdot \delta_{SO_4^{2-}}}$$

$$N_{HSO_4^-} = \frac{f_{O_2}^2 \cdot \delta_{H_2S^\circ}}{C \cdot K_3 \cdot K_4 \cdot a_{H^+}^2 \cdot \delta_{HSO_4^-}}$$

$$N_{KSO_4^-} = \frac{f_{O_2}^2 \cdot m_{K^+} \cdot \delta_{K^+} \cdot \delta_{H_2S^\circ}}{C \cdot K_3 \cdot K_5 \cdot a_{H^+}^2 \cdot \delta_{KSO_4^-}}$$

$$N_{NaSO_4^-} = \frac{f_{O_2}^2 \cdot m_{Na^+} \cdot \delta_{Na^+} \cdot \delta_{H_2S^\circ}}{C \cdot K_3 \cdot K_6 \cdot a_{H^+}^2 \cdot \delta_{NaSO_4^-}}$$

Figure 13

Schematic illustration showing how differing mole fractions of ionic sulfur species in equilibrium effect the distribution of ^{34}S. (Modified from Ohmoto, pers. commun.)

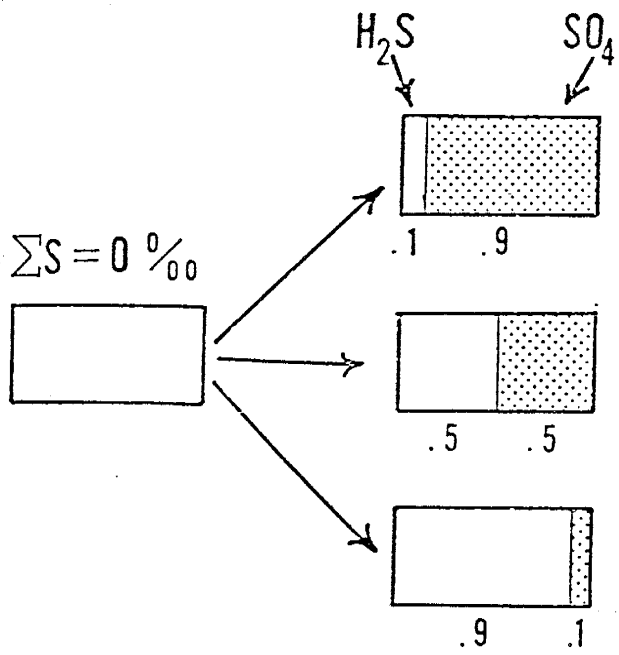

H_2S	SO_4
−28.8	+3.2
−16	+16
−3.2	+28.8

Figure 14

Distribution of isodels (relative to H_2S) in pH - f_{O_2} space at 200°C, an ionic strength of 2.0, and total dissolved sulfur equal to 0.0 per mil.

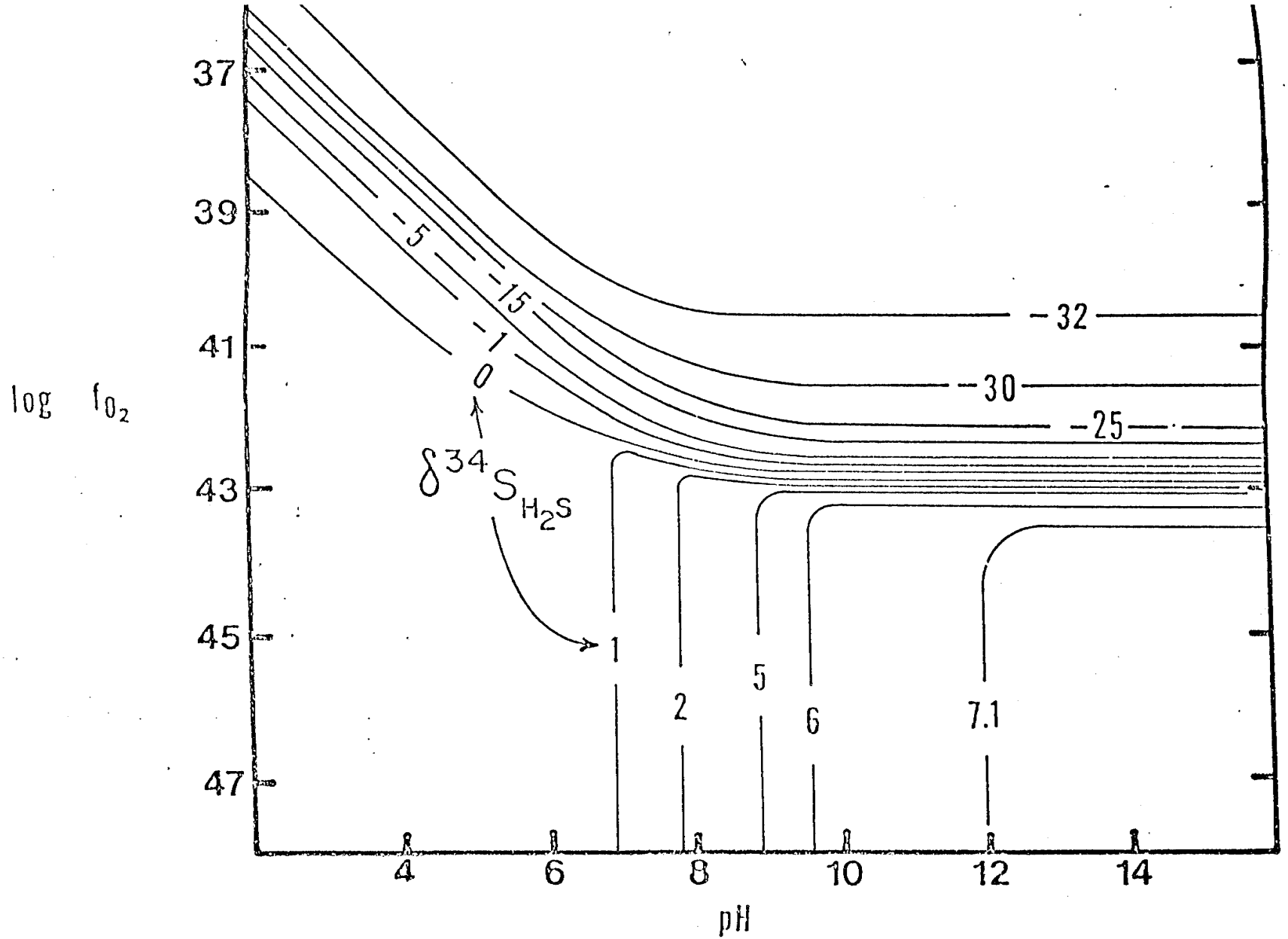
log f_{O_2}
37
39
41
43
45
47
-5
-15
-1
0
-32
-30
-25
$\delta^{34}S_{H_2S}$
1
2
5
6
7.1
4
6
8
10
12
14
pH

the SO_2 stored in a breakseal until a number of samples were thus prepared for analysing in the mass spectrometer. Barite samples were first reduced to BaS in the presence of excess graphite powder at 1100° C. The resulting barium sulfide was dissolved in hot H_2O and converted to silver sulfide by addition of 0.1 normal $AgNO_3$. This silver sulfide was then treated in the same manner as sphalerite and galena. The SO_2 samples were introduced into the mass spectrometer where the $^{34}S - ^{32}S$ ratio was measured against the working standard. These numbers were recalculated as a δ (permil) variation from the Canyon Diablo Troilite (CDT) standard. Accuracy of the measured values is believed to be $\pm$ 0.5 ‰.

Calcite samples were prepared according to the technique of McCrea (1950). Ground samples are place in a two-chamber reaction vessel with excess phosphoric acid. The vessel was evacuated and the chamber containing the calcite was heated to remove most of the hydrocarbons. After cooling, the phosphoric acid was allowed to enter the calcite chamber and thus release CO_2. The CO_2 was separated from water and oxygen before being collected in a breakseal. These gas samples were analyzed on a Micromass 602C mass spectrometer at the University of Arizona. The ^{13}C analyses were calculated as δ (permil) variations relative to the PDB standard and are believed to be accurate to $\pm$ 0.5 ‰.

Lead isotopes

No new analytical studies have been made with respect to lead in this study but previous published data have been reinterpreted. Four isotopes of lead are common in the

geologic environment: ^{204}Pb, ^{206}Pb, ^{207}Pb, and ^{208}Pb. The ^{204}Pb isotope is stable, and its abundance has not been affected by radioactive decay of other elements. Therefore, all ^{204}Pb is primeval lead, that is, lead which was p·esent at the time of formation of the earth. Leads -206, -207, and -208 are, in part, radiogenic leads resulting from the decay of ^{238}U, and ^{235}Th, respectively, and therefore, the abundance of radiogenic leads are continuously changing in a system containing uranium and thorium. "Common leads" are those which are found in minerals containing no uranium or thorium (Stacey et al., 1968, p. 798); such leads have not changed in their relative isotopic abundances since mineralization. Leads contained in feldspars or galenas then, would be representative of the isotopic composition of the fluid from which they precipitated or crystalized.

Lead isotopes in conjunction with uranium and thorium often provide an effective tool for dating geologic events. Single stage leads are considered to have evolved in a closed lead-uranium-thorium environment until the time of their final mineralization. Multistage or anomalous leads are those which have evolved from more than one Pb-U-Th system prior to final mineralization (Stacey et al., op. cit.). Multistage leads have additional concentrations of radiogenic lead representing contributions from uranium and thorium decay for each stage (Figure 15). As a dating tool, these leads are useless because they indicate anomalously young and even future "dates". These are the J-type leads so common to Mississippi Valley-type deposits.

Figure 15

Diagram showing (a) the t-isochron and growth curves for varying initial values of $^{238}U/^{204}Pb$ and (b) the development of leads in a two-stage model (both from Stacey et al., 1962).

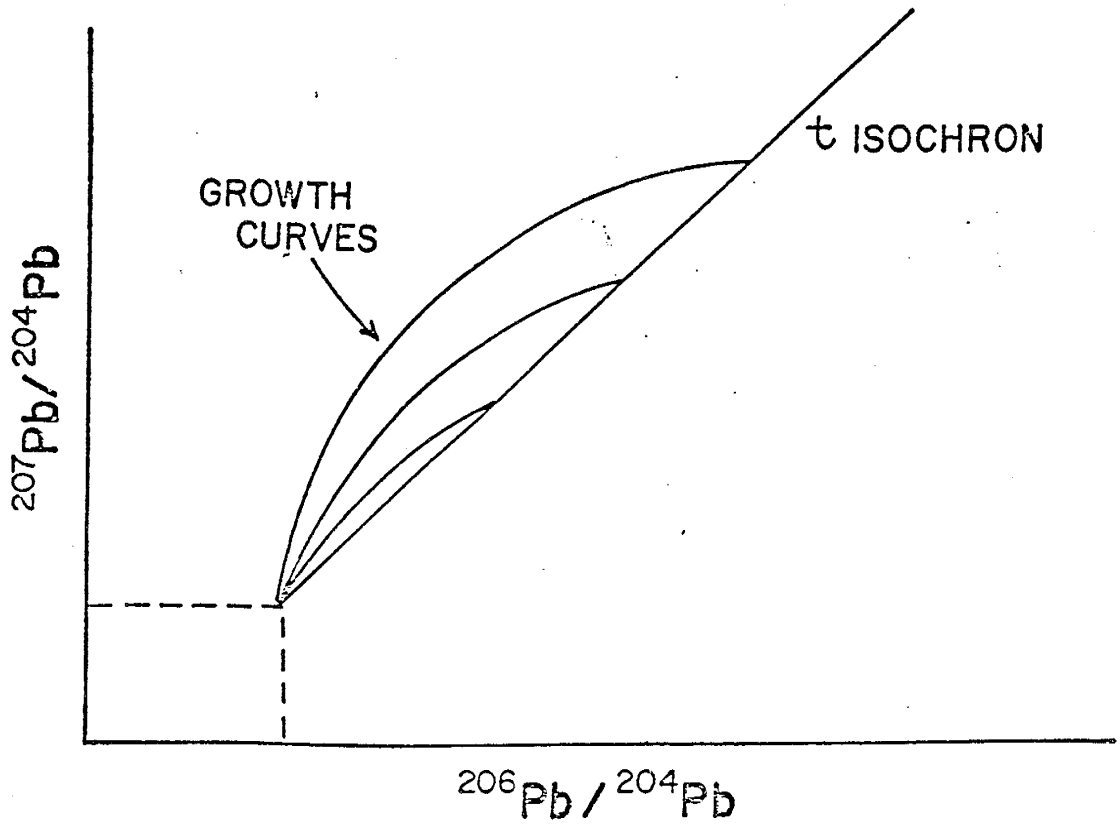
t ISOCHRON
GROWTH CURVES
$^{207}Pb/^{204}Pb$
$^{206}Pb/^{204}Pb$

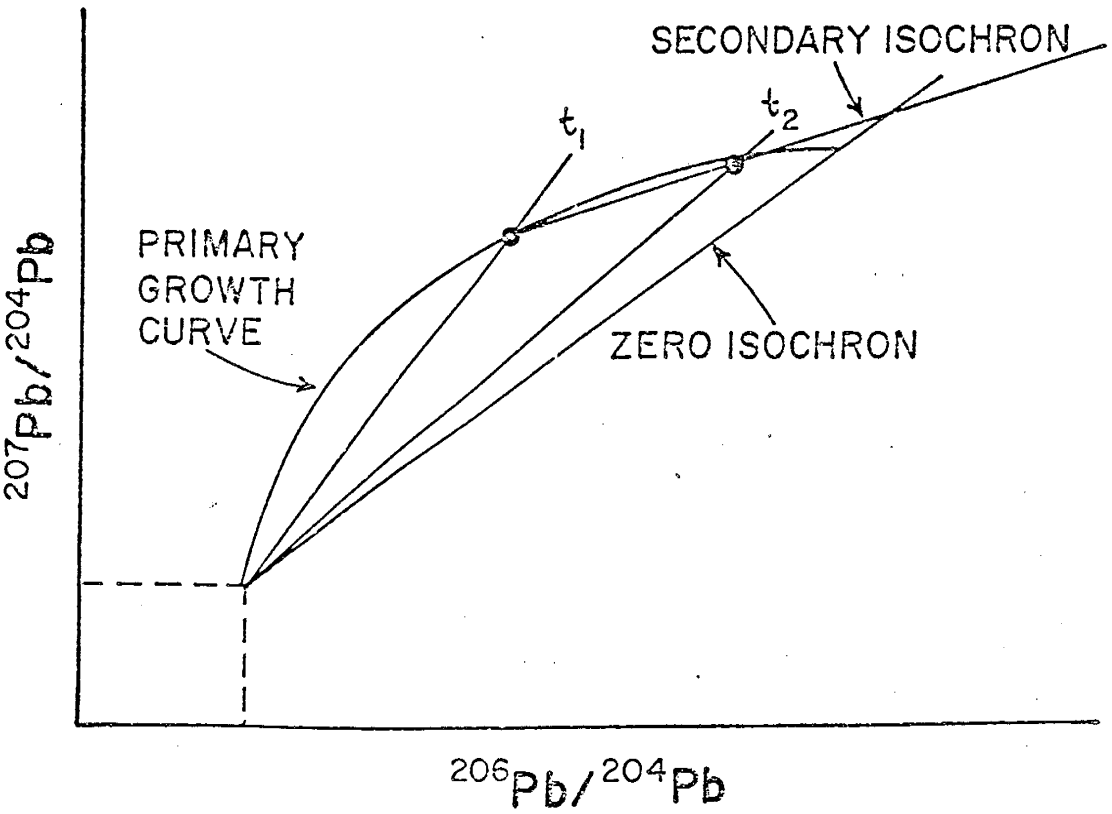
SECONDARY ISOCHRON
t_1
t_2
PRIMARY GROWTH CURVE
ZERO ISOCHRON
$^{207}Pb/^{204}Pb$
$^{206}Pb/^{204}Pb$

Chemical analyses

Pennsylvanian limestone, Permian arkoses and evaporites, Precambrian granites and metasediments and Tertiary intrusive rocks were analyzed to determine any anomalous concentrations or depletions of ore-forming elements which could suggest a mechanism for mineralization which otherwise might not be recognized. The above listed rocks were analyzed for sodium, potassium, calcium, magnesium, total iron, strontium, alumnium, silicon, and sulfur by X-ray fluorescence. These elements were determined on a Norelco X-ray spectrometer with the instrumental settings listed in Table C. Barium, lead, and some potassium and strontium concentrations were determined by atomic absorption on a Perkins-Elmer 403 spectrophotometer. Fluorine was determined with a Fisher specific ion electrode.

Standards and rock samples were prepared in a similar manner for X-ray fluorescence analyses. Rock samples were first broken down with steel-faced mechanical jaw crushers and then ground to powder in a tungsten-lined puck mill. This powder was finally ground in a ceramic ball mill and mixed mechanically prior to construction of briquettes. Briquettes were formed by applying pressure only (not heat) to approximately six grams of sample powder in a bakelite shield. A "drift pellet" was kept in the number eight position of the sample holder during all analyses to act as a reference sample. The ratio of the number of counts measured on this sample to the number of counts on the "unknown" is defined as R and is a linear function of concentration of the element analyzed. The ratio, R, was plotted versus concentration of each element

Table C Instrumental settings for X-ray fluorescence analyses.

Element	Kv/ma	HV	E	ΔE	Gain	Columnator	Detector	Crystal	$2\theta_{peak}$	$2\theta_{bkg}$
Na	50/35	2900	0.08	0.27	20	C	CH_4	Gyp	73.10	72.00
K	40/20	1760	0.06	0.52	20	F	P-10	Qtz	68.15	67.15
Ca	20/10	1720	0.04	0.28	20	F	P-10	Qtz	60.35	59.35
Mg	50/35	2800	0.02	0.20	20	C	CH_4	Gyp	51.35	50.00
Sr	40/30	940	.05	.16	6	C	Scint	LiF(200)	25.28	26.00
Fe	30/15	950	0.11	0.32	18	F	Scint	Qtz	33.60	34.60
Al	50/35	1780	0.08	0.38	12	C	P-10	Gyp	36.30	37.30
Si	50/35	1780	0.04	0.44	8	C	P-10	Gyp	25.65	26.65
S	50/25	1780	0.10	0.48	16	C	P-10	Qtz	107.20	106.00

analyzed in the standards, and the deviation from linearity was considered the overall error in the analytical procedure. This error, e, is formally defined in Figure 16, and tabulated in Table D.

The relative error in the analyses made by atomic absorption and specific ion electrode is considered to be less than 10 percent, except that samples containing very large amounts of barium may have an analytical error of 50 percent for that element.

Predictive methods for aqueous species

A chemical system is defined in terms of the Gibbsian parameters: pressure (P), temperature (T), and composition (N). The composition of a system is described by the sum of its components. Because the dissolved constituents of an aqueous system can interact strongly, it is necessary to describe not only the individual components but also the degree of their interaction. The interaction of aqueous species can be defined by chemical reactions which in order to be thermodynamically valid, must be written in terms of activities. Activities are related to concentrations by

$$a_i = \gamma_i m_i \tag{5}$$

where a_i is the activity of the i-th species, m is molality and γ is the activity coefficient. The activity coefficient of species i is dependent on the total solution chemistry as demonstrated by the Debye-Huckel equation:

$$-\log \gamma_i = \frac{A z_i^2 \sqrt{I}}{1 + \overset{o}{a}_i B\sqrt{I}} \tag{6}$$

Figure 16

Schematic illustration of error estimation for X-ray fluorescence analyses. Measured values of R were plotted versus the "known" concentration of prepared samples. The error, e, was than calculated as the deviation from a best fit straight line by the relationship shown in the figure. N is the number of points used in the calculation. Errors thus calculated are listed in Table D.

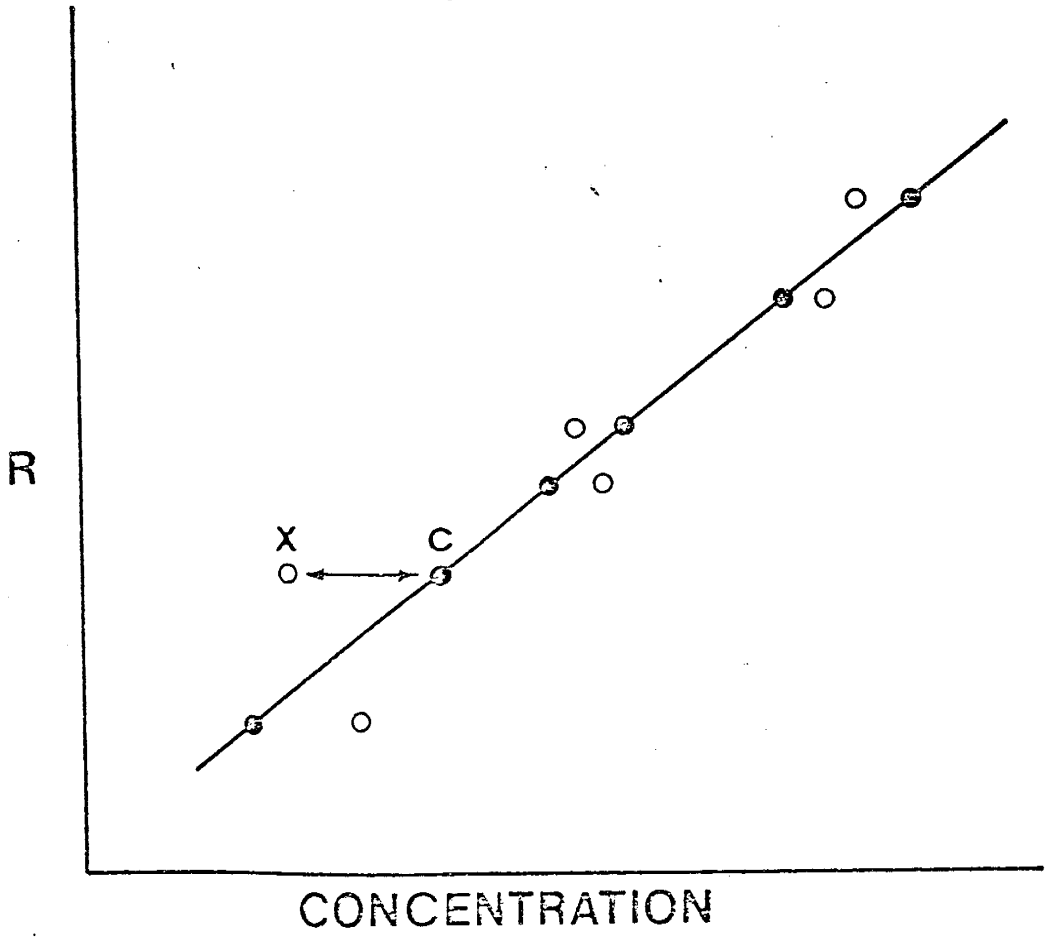

$$e = \sqrt{\frac{\sum \left(\frac{X - C}{C}\right)^2}{N}}$$

Table D Errors (e defined in Figure 16) calculated for X-ray fluorescence analyses of oxide components.

Element	e	Element	e
Silicon	.085	Sodium	.40
Aluminum	.39	Potassium	.084
Calcium	.057	Magnesium	.12
Sulfur	.086	Manganese	.050
Phosphorous	.028	Iron	.32

where A and B are temperature dependent constants characteristic of the solvent, z_i is the charge on the i-th species and I is the ionic strength of the solution, defined as:

$$I = 1/2 \Sigma m_i z_i^2 \quad (7)$$

where the summation is taken over all the dissolved species. If ions did not associate, it would be a simple matter to define the chemical composition of an aqueous system, but this is generally not the case and cations such as Pb^{2+}, Ca^{2+}, etc., are found to form various associated species with CO_3^{2-}, SO_4^{2-}, Cl^-, F^-, and other anions.

Complexing or association of dissolved species can be represented by the reaction:

$$\text{€}^{+x} + nL^{-y} = \text{€}L_n^{x-ny} \quad (8)$$

where € is a cation with a +x charge, nL is n number of L anions with -y charge, and $\text{€}L_n^{x-ny}$ is the resulting complex. The stability of the complex is described by the equilibrium constant for reaction (8) which, if considered as proceeding to the right, is an association constant. If the reaction were written as proceeding to the left, the equilibrium constant is a dissociation constant (K_d).

Helgeson (1967) developed an expression for dissociation constants at elevated temperatures using a fundamental electrostatic-nonelectrostatic approach. The entropy of dissociation ($\Delta S_d°$) is divided into electrostatic ($\Delta S_e°$)

and nonelectrostatic ($\Delta S_n°$) terms so that:

$$\Delta S_d° = \Delta S_e° + \Delta S_n° \tag{9}$$

A general expression was then proposed for the entropy of dissociation at elevated temperatures:

$$\Delta S°_{d,T} = \Delta S°_{e,T_r} \cdot f(T) + \Delta S°_{n,T_r} \cdot g(T) \tag{10}$$

where the subscript T_r refers to the contribution of the reference-state entropies. An expression for the electrostatic contribution to the free energy of dissociation was written as:

$$\Delta G°_{e,T} = B + A/\varepsilon_T \tag{11}$$

where ε_T is the dialectric constant of the solvent, A is a slope parameter and B is the integration constant of $- \int \Delta S°_{e,T} dT$. The dialectric constant of water can be written as a function of temperature:

$$\varepsilon_T = \varepsilon_o \exp(-\exp(b+aT) - T/\Theta) \tag{12}$$

where a and b are 0.01875 and -12.741 respectively, ε_o is 305.7, and Θ is 219. From this basis, an expression for the dissociation constant of an associated species at elevated temperatures can be written:

$$\log K_{d,T} = \frac{\Delta S°_r}{2.303RT}(T_r - \frac{\Theta}{w}(1-\exp(\exp(b + aT) - C + (T-T_r)/\Theta)) - \frac{\Delta H°_r}{2.303RT} \tag{13}$$

where the subscript r designates reference state conditions

(25° C, 1 bar). This equation, which requires only a reference state entropy and enthalpy for the given reaction, enables computation of dissociation constants at elevated temperatures which are generally in good agreement with measured values (Helgeson, op. cit., p. 3131).

Unfortunately, equation (13) holds only for temperatures up to about 150° C. In order to extend the calculation of dissociation constants to temperatures greater than 150° C, an equation of the form

$$\log K_T = \log K_{Tr} - \frac{\Delta H^\circ_r}{2.303R}\left(\frac{1}{T} - \frac{1}{T_r}\right) - \frac{1}{2.303RT}\int \Delta C_p dT$$

$$+ \frac{1}{2.303R}\int \Delta C_p d \ln T \qquad (14)$$

is used where ΔC_p is the heat capacity of dissociation.

Values of $\log K_{d,T}$ derived to 150°C from equation (13) can be treated so as to determine values of ΔC_p at elevated temperatures. These ΔC_p values can then be regressed using a power function of the form $\Delta C_p = a + bT$ in order to estimate values of the dissociation constant to approximately 300° C.

The entropy and enthalpy of dissociation are related to the free energy of dissociation by:

$$\Delta G^\circ_d = \Delta H^\circ_d - T\Delta S^\circ_d, \qquad (15)$$

and

$$\Delta G^\circ_d = -2.303RT\log K_d \qquad (16)$$

Thus, if a single $\log K_d$ at given temperature can be obtained from published compilations, only ΔH°_d or ΔS°_d of dissociation

need be established to carry out the calculations described above. In a dissociation reaction of the form

$$(\text{€L}_y)^{x-yz} = \text{€}^x + y\text{L}^z \qquad (17)$$

the entropy of dissociation may be written:

$$\Delta S^\circ_r = S^\circ_{\text{€}}x + yS^\circ_L z - S^\circ(\text{€L}_y)x-yz \qquad (18)$$

where S°_i is the standard conventional third law entropy of the i-th species and ΔS°_r is the desired entropy of reaction. A means to determine the entropies of unknown species by entropy correlation has been developed for the simple ions by Powell and Latimer (1951) and for the oxy-anions and complex ions by Cobble (1953 and 1953a) and Helgeson (1969) respectively. The necessary parameters for this correlation using the correspondence principle are the effective radius, charge, and mass of the ion. The effective radius is usually a modified form of Pauling's crystal radii. For the simple ions, this effective radius (r_e) is:

$$r_e = (r_p + a) \qquad (19)$$

where r_p is the Pauling crystal radius and a is 1 for anions and 2 for cations (Powell and Latimer, 1951, p. 1139).

The equation for ionic entropy as developed by Powell and Latimer (op. cit.) is:

$$S^\circ_i = 3/2\ R\ln M + 37 = 270\ z/r_e^2 \qquad (20)$$

where R is the gas constant, M is the atomic mass, z is the ionic charge and r_e is the effective ionic radius.

Cobble (1953a) determined that the appropriate equation for oxy-anions (SO_4^{2-}, CO_3^{2-}, PO_4^{3-}, etc.) is:

$$S_i^\circ = 3/2\ R\ln M + 66 = 81\ (z/\rho) \qquad (21)$$

where ρ is r_{12}/f. r_{12} is the interatomic distance of the elements in the oxy-anion and f is a structural factor. For example, the structural factor for sulphate is 0.74 (op. cit., Table 1).

The equations which will be applied to the complex ions are taken from Helgeson (1969, p. 738) and have the form

$$\Delta S_d^* = a + b/(r_1 + r_2) \qquad (22)$$

where r_1 and r_2 are the radii of the cation and anion, and ΔS_d^* is related to ΔS_d° by:

$$\Delta S_d^\circ = y(S_L^\circ - S_{H_2O}^\circ) - \Delta S_d^* \qquad (23)$$

where y is the number of ligands in the complex and S_L° and $S_{H_2O}^\circ$ are the third law entropies of the ligand and water respectively. Thus, estimated values of ΔS_d° for the complexes can then be used in conjunction with the free energy (ΔG_d° from a given log K_d) to define an enthalpy of reaction (ΔH_d°) using equations (15) and (16).

Figures 17 and 18 show the plots of known values of ΔS_d^* for chloride and sulfate complexes. The plot for the chloride complexes was taken directly from Helgeson (1969, Figure 1), and was constructed by plotting ΔS_d^* values of complexes whose entropies of dissociation (ΔS_d°) are known from experimental data, versus $1/(r_1 + 1.81)$ where 1.81 is the radius ($\mathring{A}$) of the

Figure 17

Correlation plot of ΔS_d^* for metal chloride complexes versus the reciprocal sum of the ionic radii $(1/r_1 + r_2)$ in the complex (from Helgeson, 1968).

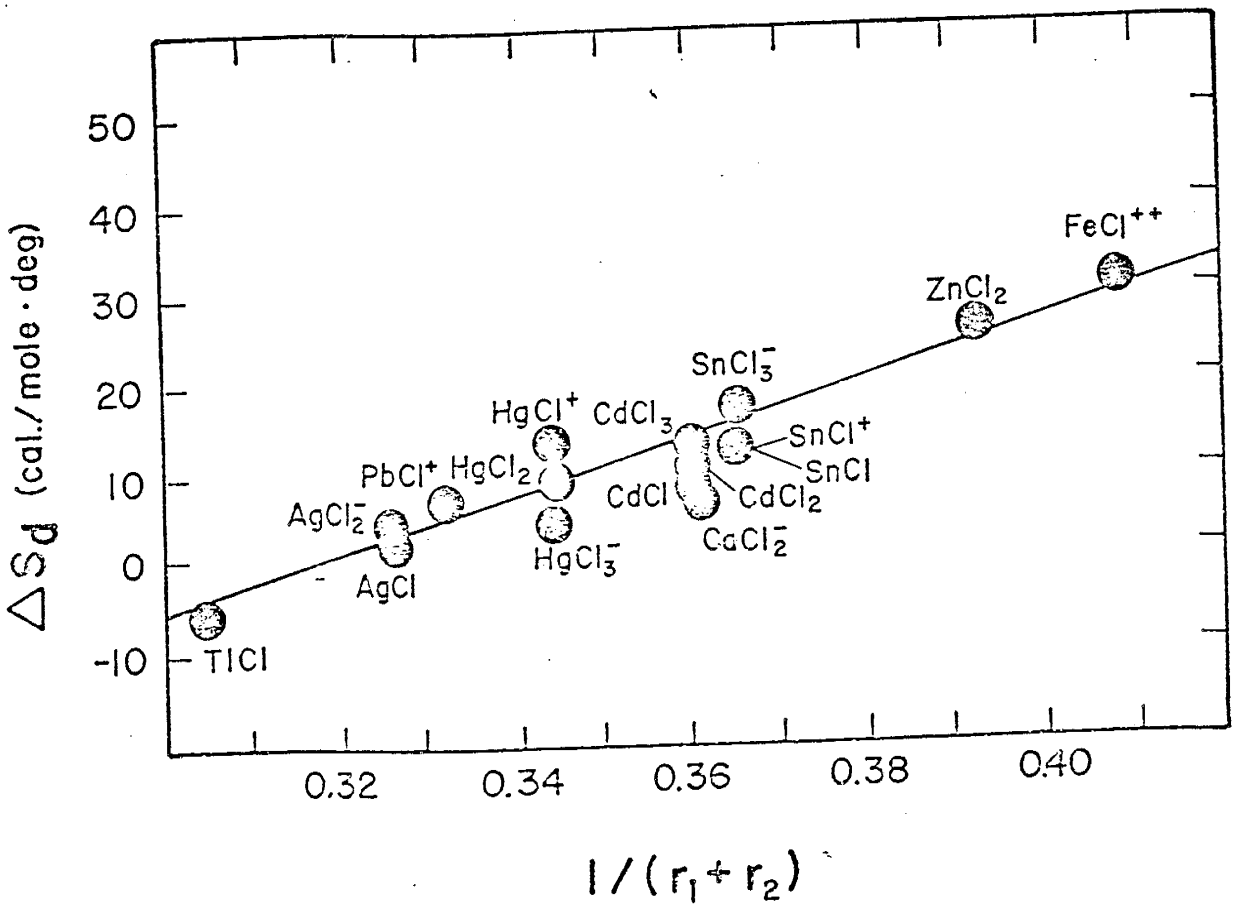
50
40
30
20
10
0
-10
ΔS_d (cal./mole · deg)
TlCl
AgCl
$AgCl_2^-$
$PbCl^+$
$HgCl_2$
$HgCl^+$
$HgCl_3^-$
$CdCl_3$
CdCl
$CdCl_2$
$CdCl_2^-$
$SnCl_3^-$
$SnCl^+$
SnCl
$ZnCl_2$
$FeCl^{++}$
0.32
0.34
0.36
0.38
0.40
$1/(r_1 + r_2)$

Figure 18

Correlation plot of ΔS_d^* for metal sulfate complexes versus the reciprocal sum of the ionic radii $(1/r_1 + r_2)$ in the complex. The first six complexes in Table E were used to regress the straight line which in the turn was used to estimate the ΔS_d^* for $BaSO_4^\circ$.

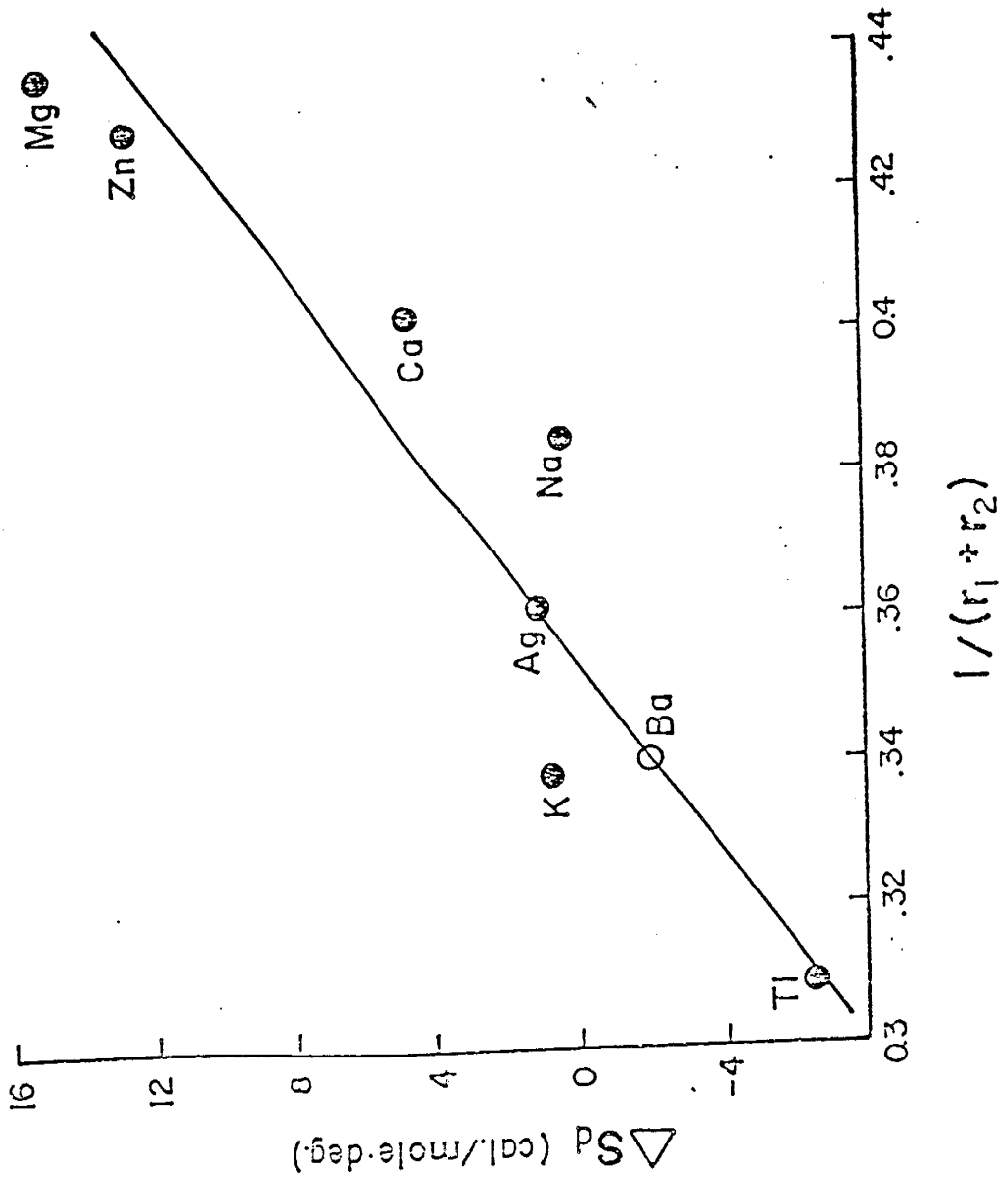
Mg
Zn
Ca
Na
Ag
Ba
K
Tl
16
12
8
4
0
-4
ΔS_d (cal./mole·deg.)
0.3
.32
.34
.36
.38
0.4
.42
.44
$1/(r_1+r_2)$

chloride ion. The curve in Figure 17 was regressed from the plotted points in the form of equation (22) and is, for the chroride complexes:

$$\Delta S_d^* = -102.5 + 325/(r_1 + 1.81) \qquad (24)$$

Figure 18 was constructed from the data in Table E for the sulfate complexes in the same manner as described above for the chloride complexes. These entropy data were then used in conjunction with experimentally defined equilibrium constants at some reference temperature to calculate the enthalpy of dissociation. These log $K_{d,T}$, ΔH_d°, and ΔS_d° were then used in equations (13) and (14) to determine the values for log K_T of dissociation which are plotted in Figures 19 and 20 for the chloride and sulfate ligands as a function of temperature. A plot of entropies versus ionic radius such as those constructed for the chloride and sulfate species (Figures 17 and 18) cannot be constructed for the fluoride and carbonate complexes because sufficient data are lacking.

An alternate method which makes use of the Fuoss electrostatic ion-pair theory can be used to predict ion-pair dissociation constants (Siebert, 1974). This theory describes the dissociation constant in terms of the energy of electrostatic interaction between the interacting cation and anion making use of the size and charge of the ions and the dielectric constant of the solvent (Robinson and Stokes, 1970, p. 552):

$$\ln K_F = A - B/\epsilon_T \qquad (25)$$

Table E Cation radii and ΔS_d^* values used to construct the correlation for plot for metal sulfate complexes (Figure 18). Ionic radii were taken from Huheey (1962) and values for ΔS_d^* were determined from the relationship:

$$\Delta S_d^* = S^\circ_{\epsilon Ly^{x-yz}} - S^\circ_{\epsilon^x} - yS^\circ_{H_2O}$$

(Helgeson, 1969, p. 738). The equation for the regressed straight line,

$$\Delta S_d^* = -5.26 + 148.9/(r_1 + 1.50),$$

was then used to estimate the ΔS_d^* of $BaSO_4$.

Complex	Cation Radius (Å)	$1/(r_\epsilon + 1.50)$	ΔS_d^*
$CaSO_4^\circ$	1.08	0.388	4.6
$MgSO_4^\circ$	0.80	0.455	14.9
$ZnSO_4^\circ$	0.83	0.430	12.6
$AgSO_4^-$	1.26	0.362	0.9
KSO_4^-	1.46	0.338	0.8
$NaSO_4^-$	1.10	0.385	0.39
$BaSO_4^\circ$	1.44	0.340	-1.99

Figure 19

Plot of dissociation constants (log K_d) for chloride complexes using the data in Figure 17 and the procedure of Helgeson (1969) as described in text.

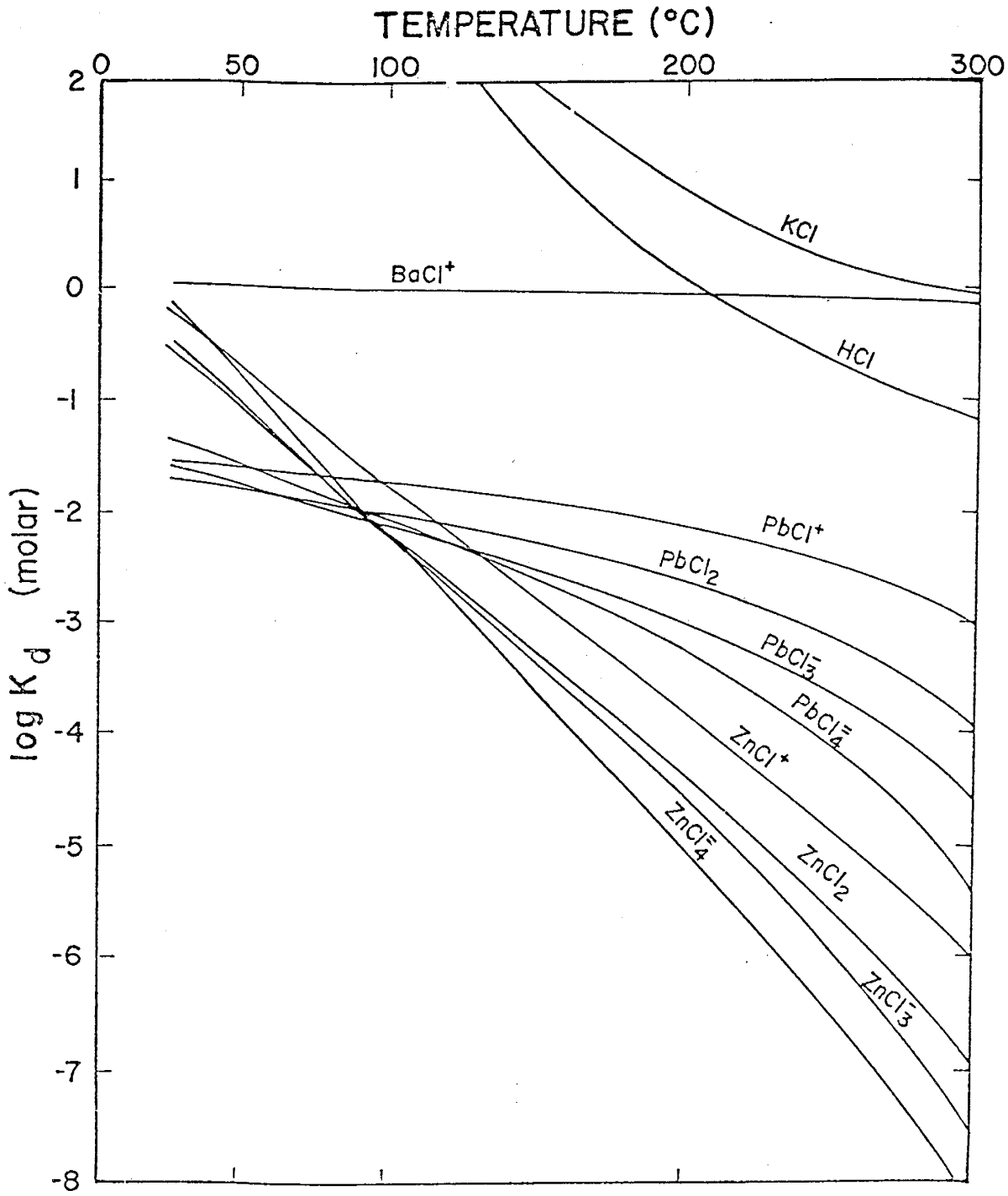
TEMPERATURE (°C)
0
50
100
200
300
2
1
0
-1
-2
-3
-4
-5
-6
-7
-8
log K_d (molar)
KCl
$BaCl^+$
HCl
$PbCl^+$
$PbCl_2$
$PbCl_3^-$
$PbCl_4^=$
$ZnCl^+$
$ZnCl_4^=$
$ZnCl_2$
$ZnCl_3^-$

Figure 20

Plot of dissociation constants (log K_d) for sulfate complexes using the data in Figure 18 and the procedure of Helgeson (1969) described in text.

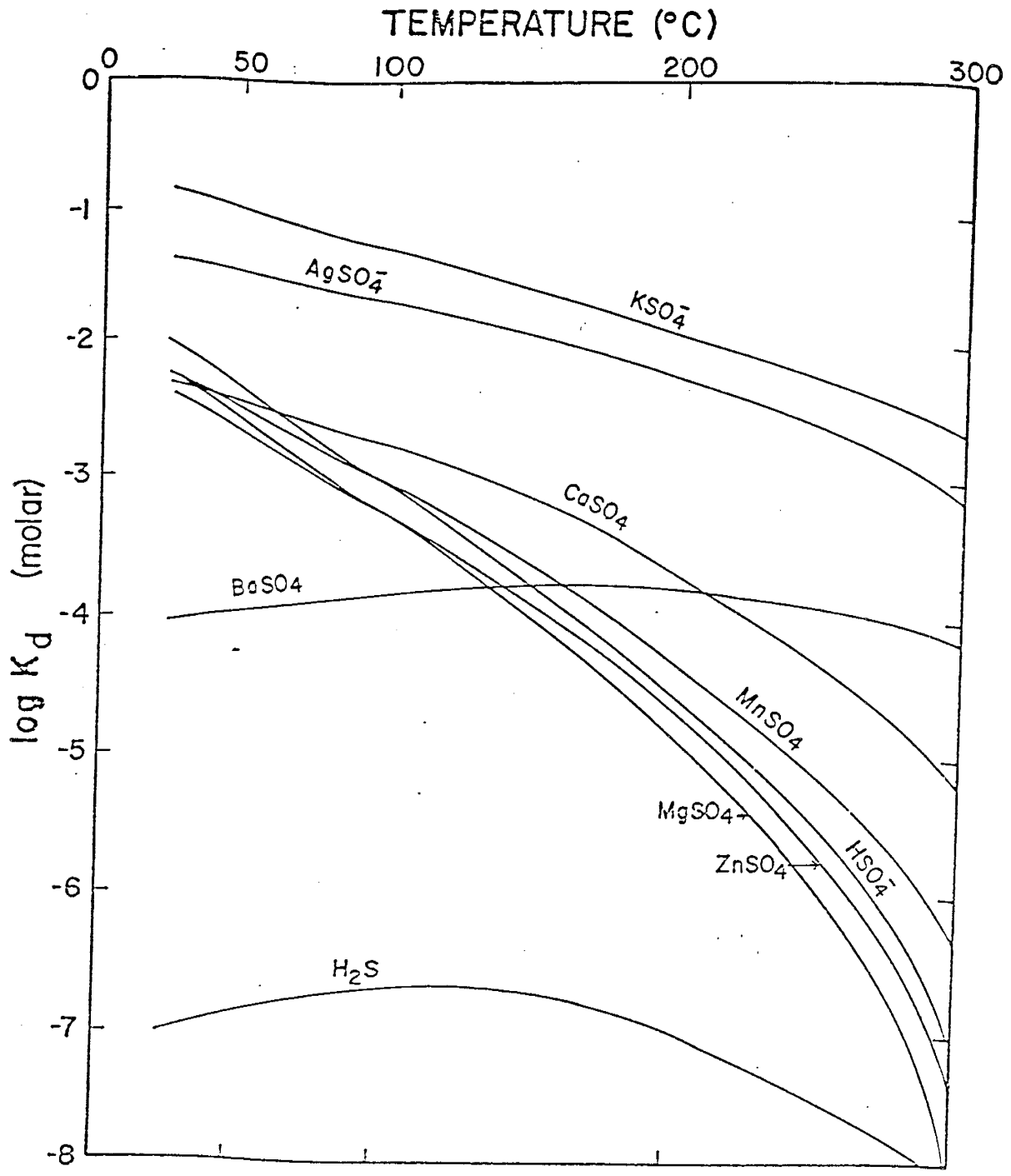
TEMPERATURE (°C)
0
50
100
200
300
-1
-2
-3
-4
-5
-6
-7
-8
log K_d (molar)
$AgSO_4^-$
KSO_4^-
$CaSO_4$
$BaSO_4$
$MnSO_4$
$MgSO_4$
$ZnSO_4$
HSO_4^-
H_2S

where: $A = \ln \frac{3000}{4\pi N a^3}$, $B = \frac{Z_1 Z_2 e^2}{ka}$

and:

ε = dielectric constant of solvent

T = temperature in degrees Kelvin

a = an ion size parameter

Z = appropriate ion charge

e = charge (esu) of the electron

N = Avogadro's number

K = Boltzman's constant

K_F = Fuoss dissociation constant.

Siebert (op. cit.) treats the ion-size parameter (a) as an adjustable parameter representative of the radius of the cation when in contact with the anion. The molal dissociation constant (K_m) can be related to the Fuoss dissociation constant by:

$$\ln K_m = \ln K_F - \ln \rho \qquad (26)$$

where ρ is the density of the solvent. The ion-size parameter (a) is determined by fitting the equation to a known $\ln K_F$ at some temperature. Thus, the ion-size parameter may be readily computed using an interval halving technique if the stability constant of a given complex is known from experimental work at a given temperature. It is then possible to extend the method to stability constants at elevated temperatures according to equation (25). Siebert (op. cit.) employed this procedure to predict the dissociation constants for

$CaHCO_3^+$, $MgOH^+$, $MgHCO_3^+$, and $MgCO_3^\circ$ at various temperatures and found that the predicted values were within the limits of error for the experimentally determined values.

The Fuoss method may be used to predict the dissociation constants of the remaining complex ions of concern which have insufficient data to justify the use of correlation plots (i.e. fluoride and carbonate complexes).

Although fluoride complexes may be of little significance to distribution of metal cation species, they could be important to the activity of the fluoride ion. This would be true if fluoride complexed with abundant (relative to total F) species such as H^+, Na^+, Ca^{2+}, Ba^{2+}, Pb^{2+}, or Zn^{2+}. Thermodynamic data for many of these species are lacking, but it is probable that HF° and NaF° are essentially non-existent at temperatures below 300° C. There appears to be no data in the literature which relates to base-metal-fluoride complexes, thus, the stabilities of such complexes as PbF^+ and ZnF_2° cannot be readily determined. Sillen and Martell (1964, p. 258) indicate that the log K_d of BaF^+ is greater than -0.45 and log K_d of CaF^+ is greater than -1.04 at 25° C. Table F is a listing of stability constants for some other alkaline earth fluoride complexes as determined by Cadek et al. (1971), which may be extended to higher temperatures with the Fuoss equation. Figure 21 shows how the stabilities of some complexes of interest to this study vary with temperature.

The abundances of the carbonate and bicarbonate ions may be evaluated in terms of pH and f_{CO_2} according to the following

Table F Metal fluoride dissociation constants (log K_d) at several temperatures as determined by Cadek et al. (1971).

	15°C	25°C	35°C	45°C	60°C
MgF^+	-18.9	-20.81	-22.5	-25.4	-30.6
CaF^+	-3.34	-3.7	-4.2	-4.5	-6.1
SrF^+	-0.82	-0.9	-1.1	-1.2	-1.5
BaF^+	-0.32	-0.4	-0.5	-0.7	-0.9

Figure 21

Molal equilibrium constants versus temperature as determined from Equations 25 and 26 using the procedure described on page 71 and the data in Table F and Equations 30-32.

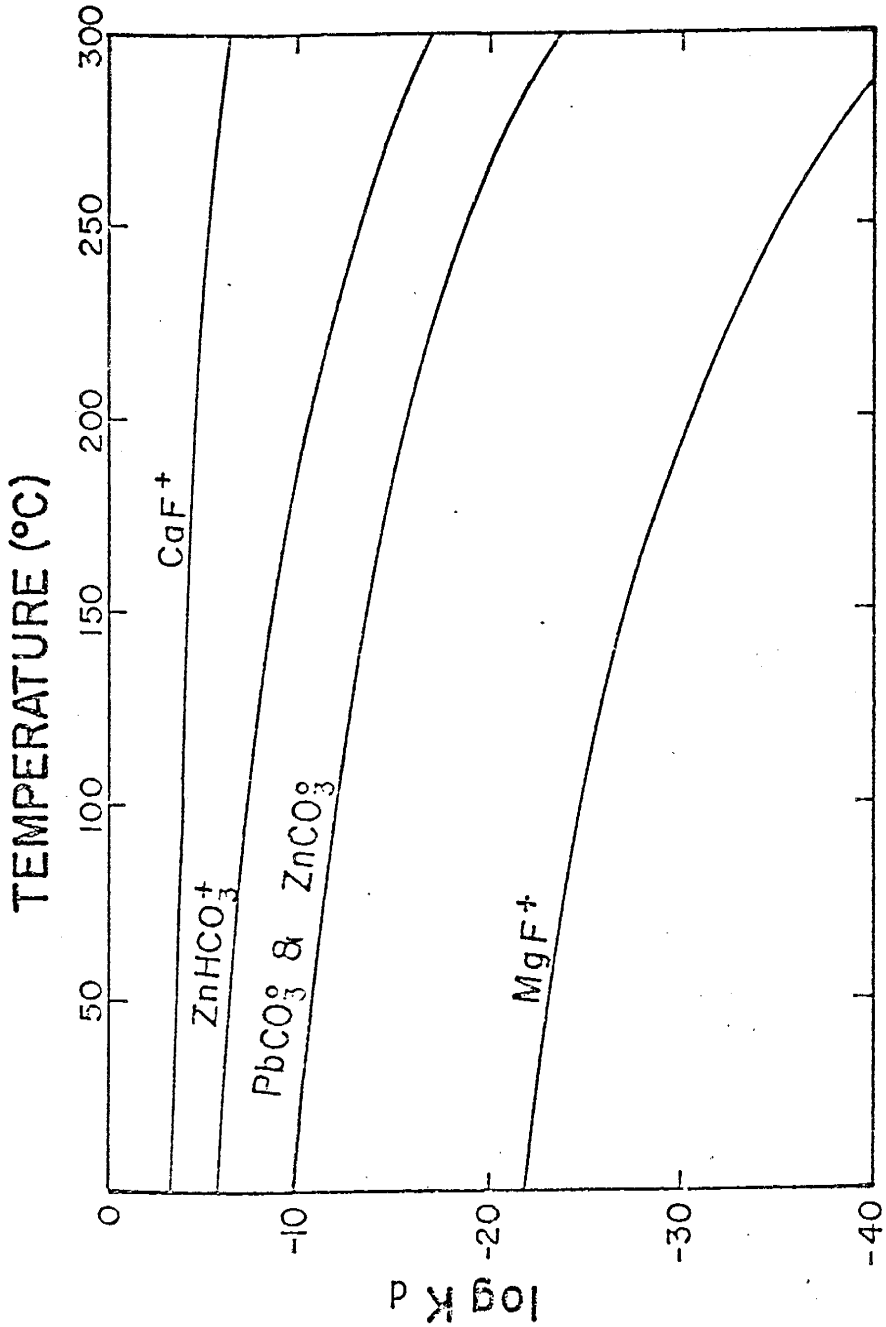
TEMPERATURE (°C)
0
50
100
150
200
250
300
log K d
0
-10
-20
-30
-40
CaF+
ZnHCO3+
PbCO3° & ZnCO3°
MgF+

equations:

$$CO_2 + H_2O = H_2CO_3 \quad (\log K_{200°} = -2.96), \tag{27}$$

$$H_2CO_3 = H_+ + HCO_3^- \quad (\log K_{200°} = -7.08), \tag{28}$$

and

$$HCO_3^- = H^+ + CO_3^= \quad (\log K_{200°} = -10.68). \tag{29}$$

The values for the equilibrium constants are from Helgeson (1969, Table 4).

Cations which may be affected by carbonate complexing are Pb^{2+}, Zn^{2+}, and Ba^{2+}. Sinclair (1972) indicates that lead probably complexes significantly with carbonate and bicarbonate especially at elevated temperatures. Sillen and Martell (1964, p. 134) give log K's for zinc and lead complex dissociation as:

$$ZnCO_3^\circ = Zn^{2+} + CO_3^{2-} \quad (\log K_{25°} = -10.31), \tag{30}$$

$$ZnHCO_3^+ = Zn^{2+} + HCO_3^- \quad (\log K_{25°} = -6.46), \tag{31}$$

$$PbCO_3^\circ = Pb^{2+} + CO_3^{2-} \quad (\log K_{25°} = -10.33). \tag{32}$$

These data can be used in conjunction with the Fuoss equation to calculate the complex stabilities at elevated temperatures (Figure 21). There appears to be no data in the literature which would indicate the stability of barium carbonate complexes.

GEOLOGY AND GEOCHEMISTRY OF THE ORE DEPOSITS

The ore deposits at Hansonburg are massive replacements and open-space fillings of barite, fluorite, galena, and quartz in highly silicified Pennsylvanian limestones, and occasionally in Permian redbeds. The major mines in the district are located in the massive, 19-foot-thick, Council Spring Limestone. These mines are, from north to south, the Royal Flush, Mountain Canyon, Mex-Tex, and Blanchard mines (Figure 22). Lewchalermvong (pp. 5-10) and Kopicki (pp. 2-9) discuss the history of the numerous mining attempts in the district. Scattered prospects are abundant and localized mineralization appears to be spread throughout the Pennsylvanian section occuring most commonly in the upper arkosic limestone member of the Madera Formation. Fluorite and barite mineralization with minor galena is also known to occur in the Abo Formation in the northern parts of Section 25, T. 5S., R. 5E., and in the Bursum Formation of Section 36, T. 5S., R. 5E.

Mineralogy and paragenesis

Kopicki (1962, Figure 3) lists 29 minerals (or solid solutions) from the northern part of the Hansonburg mining district in their paragenetic order. Many of these are exotic secondary lead, zinc, and copper carbonates and sulfates formed by supergene oxidation of metal sulfides. This study is concerned primarily with the hypogene minerals which presumeably precipitated directly from high-salinity, hydrothermal solutions. Sample locations for all paragenetic,

Figure 22

Generalized geologic map of the Hansonburg mining district and vicinity (modified from Wilpolt and Wanek, 1951). The major workings in the district are located with a symbol and the following abbreviations.

RB Red Bird
RF Royal Flush
MC Mountain Canyon
MT Mex-Tex
BL Blanchard

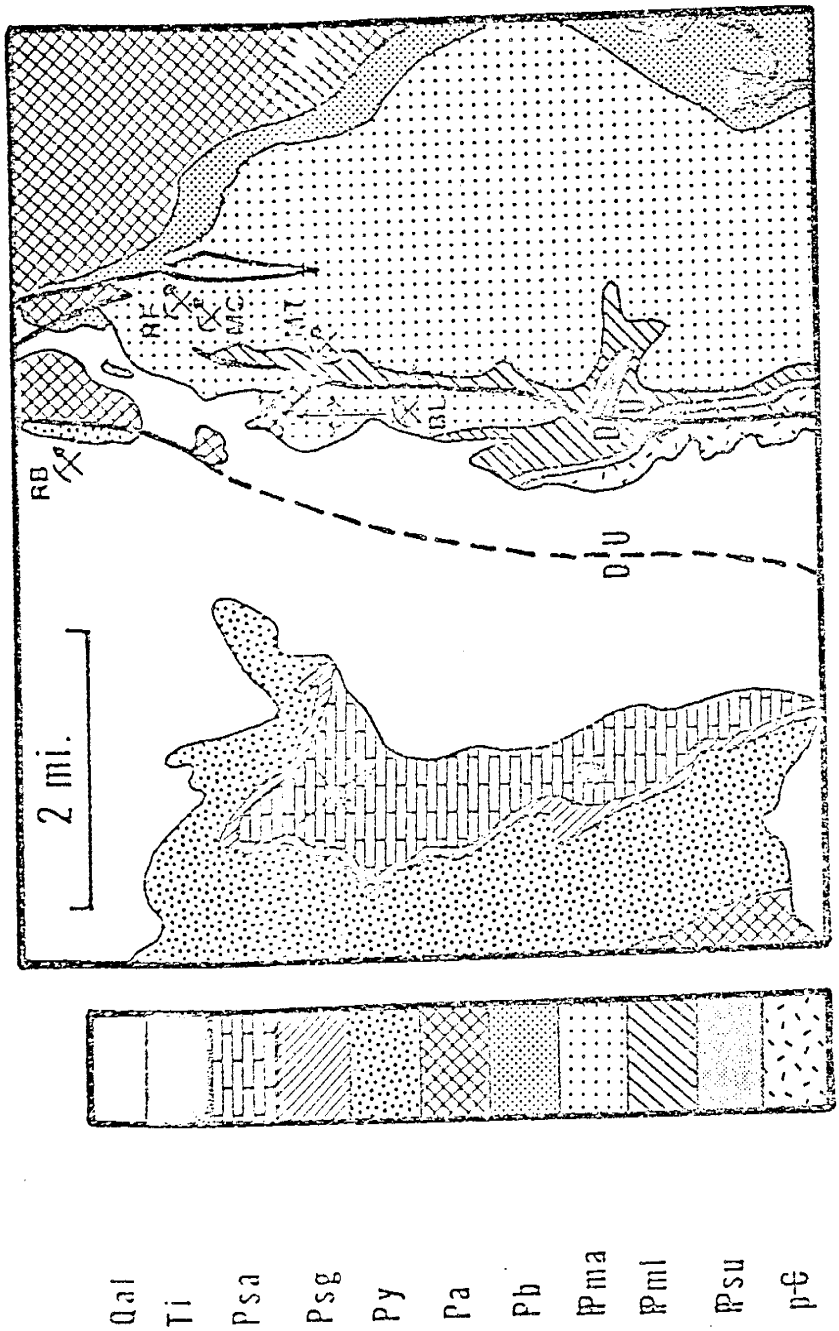
RB
RF
EX
MC
LT
BL
D
U
2 mi.
Qal
Ti
Psa
Psg
Py
Pa
Pb
Pma
Pml
Psu
p-€

fluid inclusion, and chemical analyses are shown in Figure 35.

In some instances, the primary (hypogene) or secondary (supergene) nature is difficult to determine. Such is the problem with some occurrences of anglesite ($PbSO_4$) and cerrusite ($PbCO_3$). For the present, the minerals which will be considered primary are sphalerite, pyrite, galena, chalcopyrite, barite, fluorite, quartz, and calcite. Sphalerite, pyrite, and chalcopyrite are very rare and difficult to find because of intense supergene oxidation. These minerals must have been more abundant prior to oxidation because of the abundance of the oxidation products (Fe-oxides and Cu-, Pb-, Zn-sulfates, and carbonates).

The Hansonburg mining district has long been a classic location for mineral collectors. Rare minerals of exceptional quality of rosasite $(Cu,Zn)CO_3 \cdot (Cu,Zn)(OH)$, linarite $(Pb,Cu)SO_4 \cdot (Pb,Cu)(OH_2)$, brochanthite $CuSO_4 \cdot 3Cu(OH)_2$, and museum specimens of fluorite, barite and galena have attracted many mineral collectors. The now nearly bare walls of many of the adits and drifts yield little information regarding crystal habit and paragenetic relationships. For this reason, the paragenesis as described by Roedder et al. (1968) and Kopicki (1962) will be employed for this study with little modification (Figure 23).

Sphalerite in the Hansonburg district is of the transparent, yellow-jack variety, indicating a small degree of iron substitution for zinc. The contemporaneity of sphalerite and pyrite as indicated by Kopicki (op. cit.) was not observed. Several samples containing both sphalerite and

Figure 23

Paragenetic sequence of hydrothermal mineral deposition. The relationships indicated by the filled bars were determined by Roedder et al. (1968) and found to be valid in all samples collected for this study. One additional fluorite stage was found which is located in the sequence as shown by the open bar.

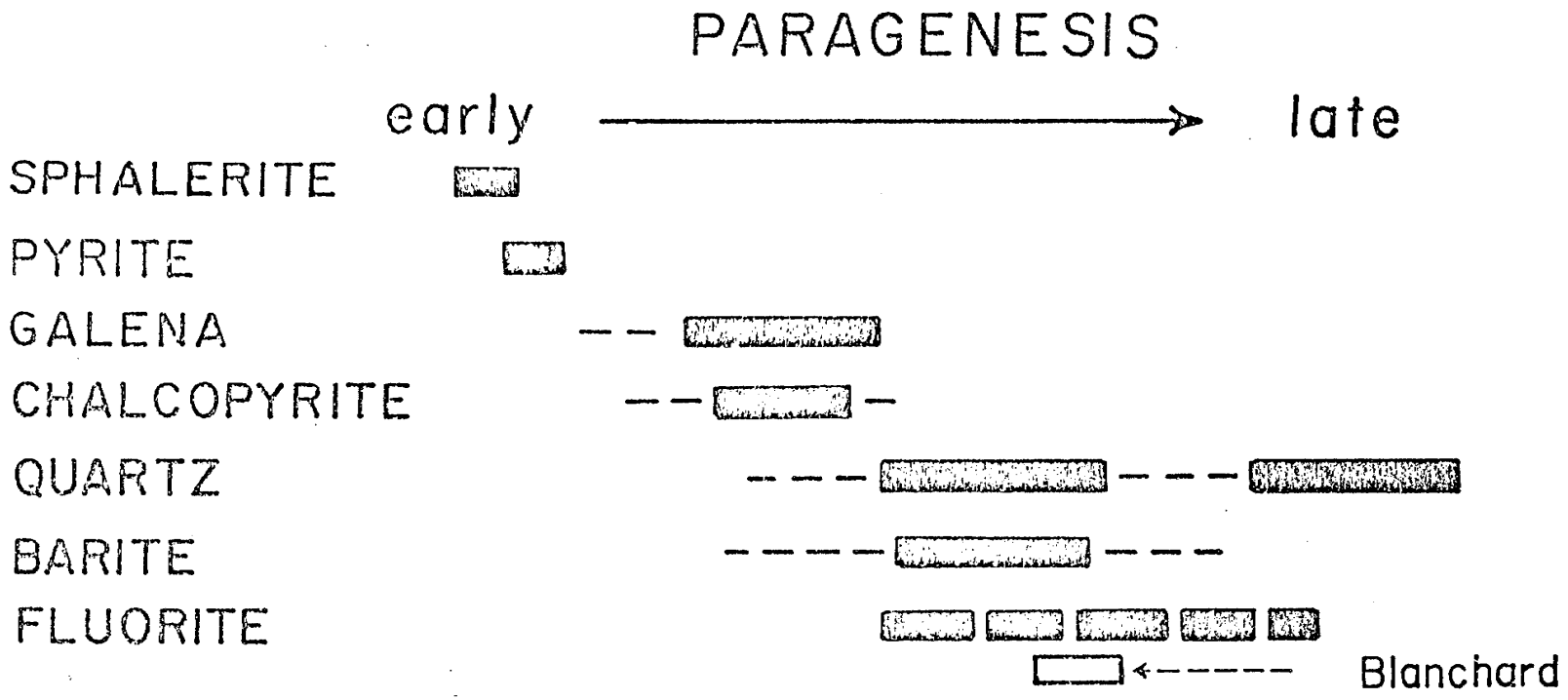
PARAGENESIS
early
late
SPHALERITE
PYRITE
GALENA
CHALCOPYRITE
QUARTZ
BARITE
FLUORITE
Blanchard

pyrite were collected from the Blanchard mine. All of these samples showed pyrite rimming sphalerite indicating that sphalerite was deposited first. The paragenetic position of chalcopyrite could not be determined because of oxidation. Chalcopyrite was observed at and near the Royal Flush and Mex-Tex mines where it occurred in arkosic units rather than limestone. Apparently, the porosity and permeability of these arkosic units remained high after primary mineralization, allowing later oxidizing fluids to react with the iron and copper sulfides. In contrast, some galena replacing silicified limestone was not oxidized, probably as a result of the protective silica shield. However, open-space galena in the same deposit is oxidized to alternating layers of cerrusite and anglesite. Thus, preservation of early sulfides appears to be, at least in part, related to the permeability of the host rocks and thus, accessibility for reaction with oxidizing fluids.

Galena is the last sulfide in the paragenic sequence and the only sulfide to approach economic concentrations. Galena occurs as euhedral cubes, commonly cut by octohedrons, in limestones as both open-space fillings and replacements. Nearly all of the galena has been oxidized to anglesite, cerrusite or both. One cube of galena collected from the Blanchard mine contained fractures which were filled by alternating bands of cerrusite and anglesite followed by barite. If this sequence represents a temporal progression ($PbS \rightarrow PbCO_3 + PbSO_4 \rightarrow BaSO_4$) it would place very definite limits on certain aspects of the solution chemistry. An

alternate possibility would be that the galena cube fractured prior to barite mineralization, filled with barite, and subsequent oxidizing fluids or ions migrated along the barite-galena boundary producing the banded carbonate-sulfate zone between the galena and barite.

Barite which follows galena and overlaps with several stages of fluorite in the mineralization sequence, often is the most common ore mineral. Mineralization at the Red Bird mine consists almost entirely of massive barite in red Abo shales and silstones. Elsewhere barite occurs as very large, massive, lenticular bodies parallel to bedding with a pronounced platy habit developed parallel to the short axis. Individual, tabular, euhedral crystals are not uncommon constituents of open-space fillings. Massive barite often occurs in layers alternating with fluorite and galena resembling the "coon tail" ore of Southern Illinois (Roedder et al., 1968, p. 338).

Five stages of fluorite mineralization were described by Roedder et al. (1968) at the Mex-Tex mine. These stages are defined by color zoning and crystal habit as follows (early to late):

STAGE I - rounded pale green crystals (parallel multiple-stepped cube facets)

STAGE II - pale green, well-formed cubes

STAGE III - slightly greenish-white cubes

STAGE IV - limpid blue to blue-green cubes

STAGE V - lavender, purple, and blue cubes and overgrowths.

A sixth stage of fluorite has been observed at the Blanchard

prospects; this fluorite is a pale blue to lavender, cubic variety. Its presence between stages II and III is well-defined by color zoning in large multiple-stage crystals; this fluorite is designated as stage IIa. Its presence in the paragenetic sequence is shown by the open box in Figure 23. At least some of this stage IIa fluorite precedes barite mineralization at the Blanchard prospects; no stage IIa fluorite has been observed outside the Blanchard prospects. All fluorite mineralization follows galena and most appears to follow barite. Occasionally, barite is found suspended in Fluorite I indicating that this stage is earlier or contemporaneous with barite. Roedder et al. (op. cit.) place Fluorite I prior to barite in their paragenetic scheme while stages II through V follow barite.

Fluorite appears to become more important southward in the district while barite shows an opposite trend. Earlier green fluorite predominates northward at the Royal Flush mine while later, banded, blue and purple fluorite predominates southward in the Blanchard mines. At the Royal Flush mine massive barite occurs in thick lenses and appears to be more abundant than fluorite. Southward in the Blanchard deposits fluorite predominates and barite occurs more as individual crystals or aggregates of intergrown fluorite and barite. Although massive lenticular bodies of barite can be seen in the Blanchard workings, they are much less common than in the Royal Flush mine. The mineral assemblages at the Mountain Canyon and Mex-Tex mines

probably are more similar to the Royal Flush assemblages rather than the Blanchard; the Mex-Tex may be more intermediate. These observations were made on pillars and remaining mine faces and have not been statistically verified.

Quartz occurs as both a fine-grained (cryptocrystalline) replacement of limestone, usually early in the paragenetic sequence, and as later, coarse, open-space crystals in vugs. Lewchalermvong (1973, pp. 26, 35, 36) has described the occurrence of silica in some detail. He discusses three types of occurrences: 1) cryptocrystalline, "jasperoid" quartz which is always associated with mineralization, 2) a coarsely-crystalline quartz, often comb-structured, filling vugs and cavities, and 3) a late stage, finely crystalline druse covering hypogene minerals. Roedder et al. (1968, p. 338) note the presence of smoky quartz at the Mex-Tex mine, where a pale rose and amethystine quartz are also found. Evidence that quartz mineralization continued throughout the late paragenetic sequence is the nearly ubiquitous presence of this mineral trapped as inclusions in barite and all stages of fluorite.

Dark brown calcite is a very common mineral filling the profuse veinlets observed on almost every limestone outcrop in the district. These veinlets are from a fraction of a millimeter to several centimeters in width. At one locale between the Mex-Tex and Mountain Canyon mines sufficient open space has allowed growth of calcite scalenohedrons up to two inches long.

Calcite fills cavities between earlier minerals and appears to be the last hypogene mineral to have been precipitated.

Wall rock alteration

Two types of wall rock alteration occur in the Hansonburg mining district corresponding to the two prominent rock types: limestones, and arkosic sandstones and mudstones. In general, the main alteration associated with limestones is silicification. An estimate of the amount of SiO_2 added to the limestones can be calculated from Lewchalermvong's (1973, Appendix II) descriptions of proven, probable, and potential ores in the district. This estimate (2×10^9 gms.) is low because none of the many, scattered, isolated silicified zones were included; nor did he consider Section 1, T. 6S., R. 5E. which includes the Blanchard mine and constitutes at least 25 percent of the mineralization in the district. The total amount of SiO_2 added to limestones in the district could easily have been on the order of 10^{10} gms.

The source of much of this silica may be accounted for by the second type of alteration in the district. This alteration is associated with coarse-grained arkoses of the Bursum Formation at the base of the scarp immediately below the Mex-Tex mine. The most obvious differences between the altered and unaltered Bursum Formation is color. The dark maroon to reddish-brown colors typical of the Bursum Formation in this area, have been extensively bleached to a dull white and pale grey. This is believed to be the result of

hydrothermal alteration by a hot NaCl-rich aqueous fluid as it moved upward through the fault zone. Thin sections show that most of the red color common to the Bursum Formation is from iron-oxide-stained, kaolinized feldspar clasts and interstitial hematite. In the altered arkoses the hematite appears to have been leached from the presently kaolinized feldspar and matrix. Other forms of alteration in the arkose are simple silicification and widespread dissolution of silicates. Figure 24 shows that the solubility of quartz is strongly temperature dependent between 50° and 300° C and thus quartz could be dissolved and reprecipitated within a short distance if temperature varied with time or over short distances.

A hot fluid in equilibrium with a silicate assemblage such as the Permian arkoses would be expected to dissolve considerable amounts of limestone and thus increase dissolved CO_2. Ohmoto (1974, pers. comm.) believes that experimental evidence indicates dissolved CO_2 may significantly reduce the solubility of SiO_2 in an aqueous solution. Such a mechanism could explain the silicification of Pennsylvanian limestones in the Hansonburg mining district.

Chemical parameters

The chemistry of the hydrothermal system responsible for hypogene mineralization will be described in terms of pressure, temperature, and composition using the methods and techniques described above. Pressure limits may be determined independent of the other parameters and, therefore, will be considered first.

Figure 24

Stabilities of quartz and amorphous silica in terms of log $a_{H_4SiO_4}$ as a function of temperature. Data from Helgeson (1969) and Okamoto et al. (1957).

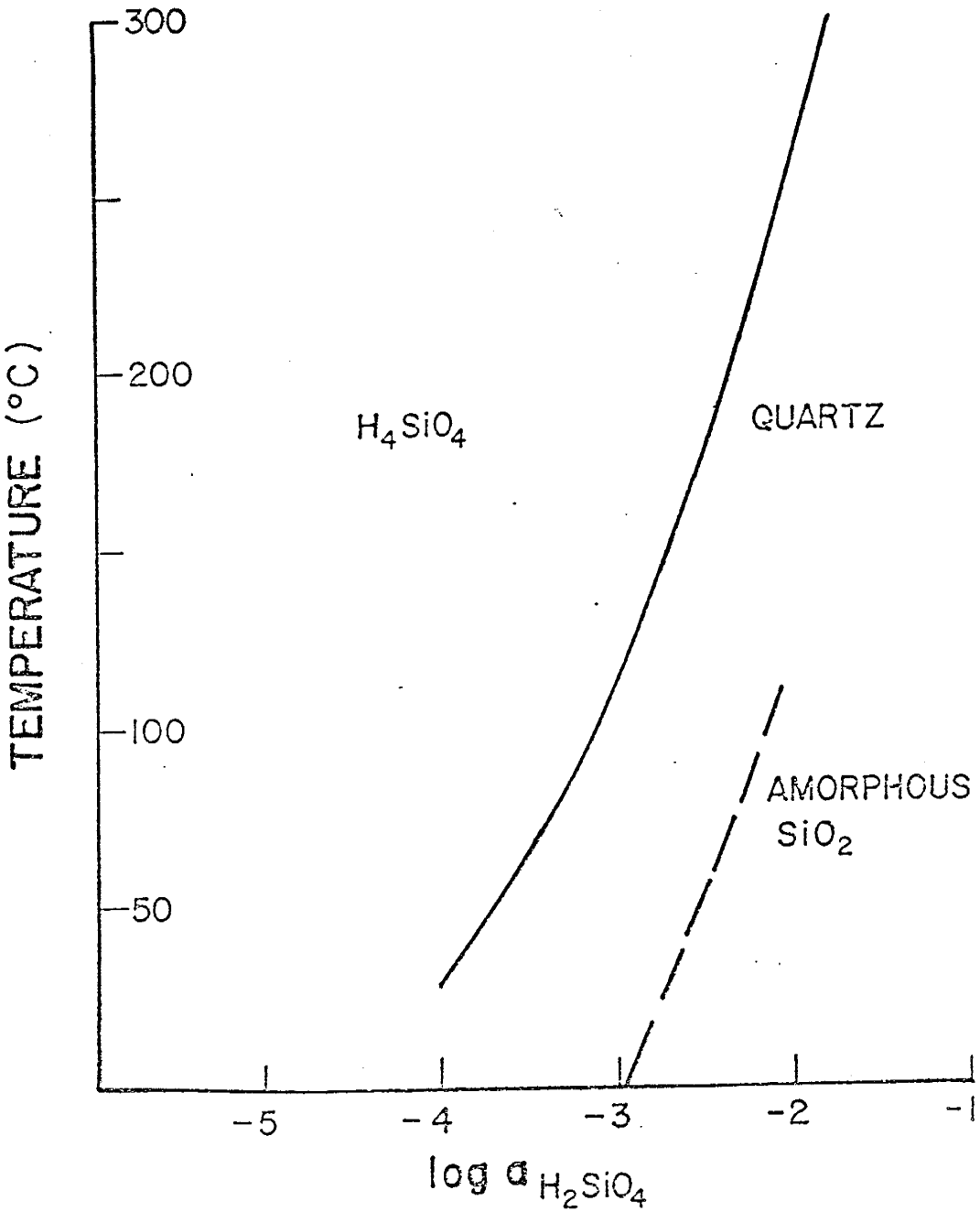
300
200
100
50
TEMPERATURE (°C)
H_4SiO_4
QUARTZ
AMORPHOUS
SiO_2
-5
-4
-3
-2
-1
log $a_{H_2SiO_4}$

PRESSURE

There are two ways to place limits on the depth (and hence, pressure) at which mineralization took place. One is to consider the physical behavior of fluid inclusions, and the other is to reconstruct the overburden at the time of mineralization. Minerals which precipitate from a boiling fluid occasionally trap the gas phase, resulting in a mineral containing primary inclusions some of which homogenize in the vapor phase, but most of which homogenize in the liquid phase. Because there is no fluid inclusion evidence at Hansonburg that the fluid was boiling, it is assumed that total pressure was above the liquid-vapor two-phase boundary. The fluid is known to be an aqueous solution containing 10 to 17 equivalent weight percent NaCl (Roedder et al., 1968). From the data of Haas (1971, p. 943) and Roedder et al. (op. cit.) it is shown that the minimum pressure necessary to keep the fluid in a liquid state at 200° C is 13.5 bars, or about 125 meters of hydrostatic pressure. This is a lower limit on the pressure. No upper limit can be obtained from simple two-phase inclusions.

Difficulty with attempting to reconstruct overburden for the Hansonburg district arises from the uncertainty in age of the deposits. A mid-Tertiary age will be given the deposits for two reasons: 1) the deposits are associated with mid-Tertiary (?), normal faulting and 2) the scattered dikes and sills dated at about 28 m.y., with syngenetic magnetite (Deane & Titus, 1973) represent a period of hydrothermal activity. As will be proposed in a following section, the many scattered dikes and sills occurring throughout this part of central New

Mexico probably contributed significantly to the heat budget required to account for the observed fluid inclusion filling temperature data.

Upon assuming a mid-Tertiary age for the deposits, the problem becomes one of estimating the thickness of strata removed by erosion between deposition of the Cretaceous Mesaverde Formation and mid-Tertiary times and the thickness of mid-Tertiary volcanic rocks. As indicated in a previous section (p. 22), it is doubtful that there were significant deposits of late-Cretaceous-Eocene Cub Mountain or Baca Formation equivalents overlying the Hansonburg mining district but there was probably some overlap of Datil-Sierra Blanca volcanic rocks across this area. An upper limit on overburden then would be 3100 feet of Permian rocks plus 750 feet of Triassic rocks plus 1500 feet of Cretaceous rocks plus a probable maximum of 1000 feet of mid-Tertiary volcanic rocks equals 6350 feet (1935 m.) of pre-Tertiary strata. This assumes that no erosion took place for the approximately 35 million years intervening between late Cretaceous and mid-Tertiary times. It is known however, (p. 22) that the Baca Formation truncates Cretaceous and some Triassic sediments a short distance westward in the Carthage area. Evidence that the Baca erosion surface truncates progressively deeper strata in a westward direction makes it unlikely that early Tertiary erosion cut much deeper than Triassic strata. Following early Tertiary degradation it is likely that some mid-Tertiary volcanic deposition occurred in the form of ash-fall and/or ash-flow sheets. Chapin (personal communication, 1975) notes

that a reconstruction of the probable extent of outflow aprons from recently discovered major ash-flow cauldrons indicates that the Datil and Sierra Blanca volcanics overlapped across the area of interest. The actual thickness is problematical but 1000 feet seems to be a reasonable maximum. It is probable that overburden during mineralization was between about 3600 and 5000 feet (1100-1800 m.). These estimates are similar to those of Roedder et al. (1968, p. 345). Thus, pressures were probably between 40 and 100 bars depending on whether hydrostatic or lithostatic loads are assumed. It would be reasonable to assume a mean total pressure of about 70 bars.

TEMPERATURE

Roedder et al. (op. cit.) made a detailed investigation of the fluid inclusion filling and freezing temperatures in minerals from the northern part of the Hansonburg mining district. The temperature correction used by Roedder et al. (op. cit., p. 345) was +10° C for hydrostatic pressure and +30° C for lithostatic pressure at the assumed depth of burial of 1500 meters. The results of their work is illustrated in Figure 25, and resulted from observations of more than 500 primary and 2500 pseudosecondary inclusions. Most of their work was with fluorite but several analyses were made in sphalerite, barite, and late quartz.

The measurements made in the present study were not intended to improve on Roedder et al.'s (op. cit.) comprehensive work, but instead were designed to determine the validity of extending their work to other mines and

Figure 25

Fluid inclusion data from studies of sphalerite, barite, and fluorite. Filled bars represent data from primary inclusions and open bars indicate planes or groups of pseudosecondary inclusions (data from Roedder et al. 1968). The shaded bars indicate the results of observations made on primary inclusions in the present study. A pressure correction of +15° C must be added to the homogenization temperatures (T_H). No freezing temperatures (T_F) were determined for this study.

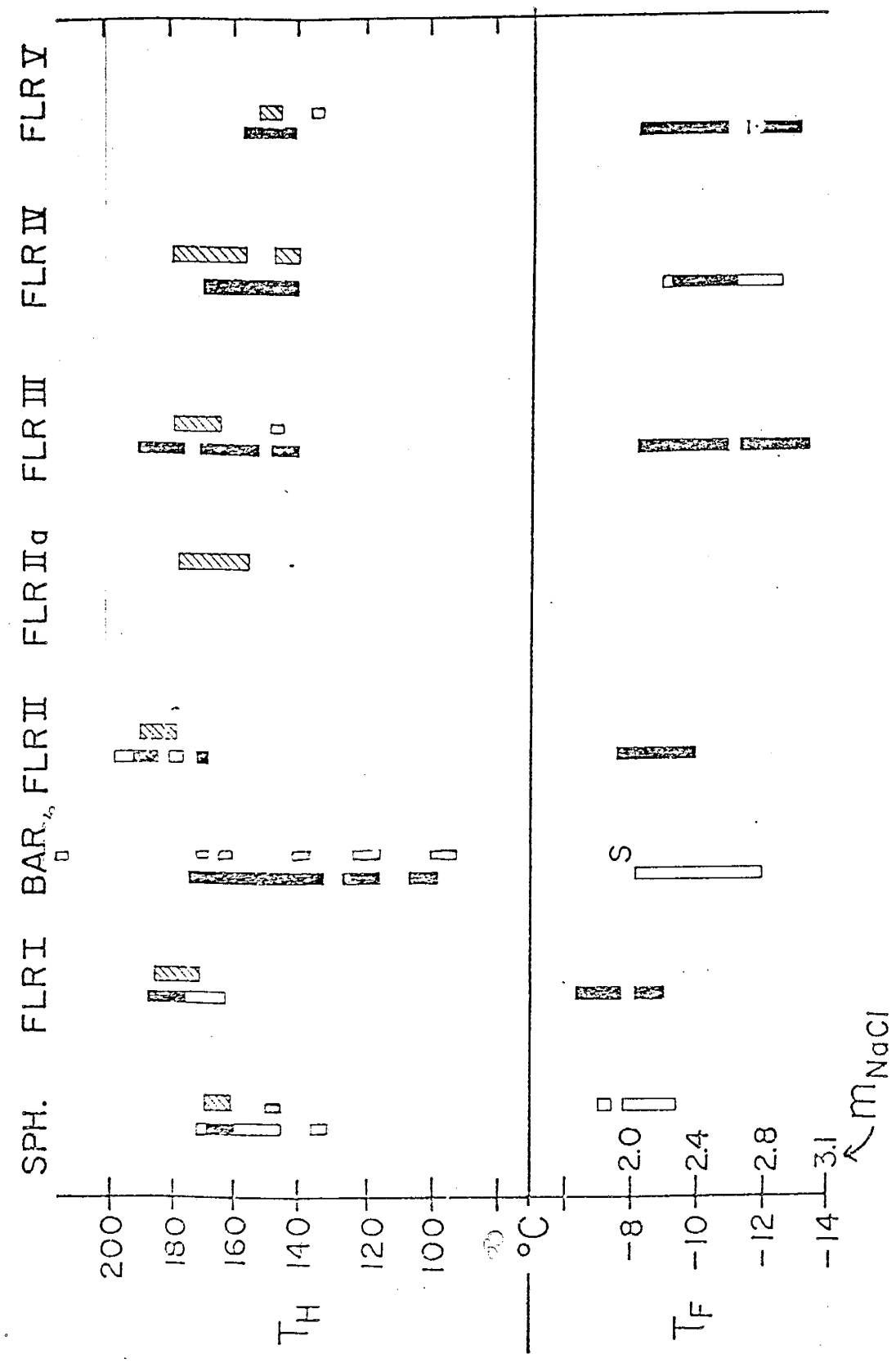
SPH.
FLR I
BAR.
FLR II
FLR IIa
FLR III
FLR IV
FLR V
S
200
180
160
140
120
100
°C
-8
-10
-12
-14
2.0
2.4
2.8
3.1
T_H
T_F
m_{NaCl}

prospects throughout the district. Further, the possibility of aerial and/or vertical temperature zoning in the district could be essential to arguments concerning the origin and source of the fluids. With this in mind, samples of barite, fluorite, and sphalerite were collected from many mines, prospects, and unworked veins (see Figure 22). The results, which are shown in Figure 25, indicate close agreement with those studied by Roedder et al. (op. cit.).

The fluid inclusion data indicate that temperatures of mineralization (including a pressure correction of +15° C) were about 180° C for sphalerite, increasing to about 200° C for early fluorite and then decreasing to less than 165° C for late fluorite. Roedder's (op. cit.) study indicated that temperature continued to decline through the late quartz stage to less than 140° C. Sixty-one primary inclusions from fluorite, six from sphalerite, and nine secondary (?) inclusions in barite were examined and found to have filling temperatures reproduceable within $\pm$ 3° C. Analyses of these inclusions did not show any vertical or areal variation within the district. The close agreement of temperatures among the diverse sample locations is indicative of an environment of uniform temperatures over a relatively large area at a particular paragenetic stage and thus suggests good hydrologic communication among cavities and fissures of the fault zones during mineralization.

SOLUTION COMPOSITION

The freezing temperatures determined by Roedder et al. (op. cit.) are considered representative of the Hansonburg

district; it seems unlikely that salinity would vary from place to place any more than temperature would for the same inclusions. The results of their freezing stage determinations are shown in Figure 25 and indicate a salinity of between 10 and 17% equivalent NaCl. This is equivalent to a 1.9 to 3.3 molal NaCl solution. For purposes of chemical calculation it is considered that this amount of salt is large relative to the amount of cations or anions which would be added or depleted from the fluid during the course of mineralization. Thus, NaCl will be considered a supporting electrolyte maintaining an ionic strength of between approximately two for the early stages and three for the later stages. Because the bulk of mineralization of interest to this study occurred during the early stages, most of the calculations will consider an ionic strength of two.

OXYGEN FUGACITY

Stability diagrams can be used to place limits on the fugacity of oxygen in the ore-forming fluid. The Hansonburg mining district contains a number of minerals which reflect the oxidation-reduction conditions during mineralization. Using galena as an example, the following equation shows how the presence of a sulfide mineral indicates an upper limit on the oxygen fugacity.

$$PbS + 2O_2 = PbSO_4 \qquad (33)$$

The equilibrium constant for this reaction is related to oxygen fugacity by : $\log K = -2 \log f_{O_2}$. The oxygen fugacity

is thus limited by -1/2 log K of the reaction. Figure 26 shows the range of stability of galena in terms of the above equation in log f_{O_2} - T space. The analogous stability boundaries are shown for sphalerite and barite. The sulfides place individual upper limits on f_{O_2} while barite defines a lower limit. The range of permitted oxygen fugacities is narrowed markedly if hematite is considered as a stable phase. Specular hematite has been observed in association with several dikes north and east of the Hansonburg mining district. These dikes have been extensively altered and the hematite may be a product of this alteration. Furthermore, Beane and Titus (1973, pp. 543-544) indicate that oxygen fugacity was buffered by the magnetite-hematite assemblage during mineralization of magnetite associated with similar monzonitic dikes. The hematite-magnetite buffer is also plotted in Figure 26 and indicates a narrow range of f_{O_2}.

AQUEOUS SPECIES

Modern subsurface waters collected from Lake Lucero, in the White Sands National Monument will be considered analogous to the hot saline waters which interacted with the arkoses. These waters are thought to be chemically similar to the Hansonburg brines for several reasons. 1) They accumulated in a large adjacent basin which is the same age as the Jornada del Muerto. 2) The waters resulted from interaction with the same Permian section as the Hansonburg hydrothermal fluids under very similar hydrologic conditions (Allmendinger, 1971). 3) Lake Lucero waters have the same NaCl molality ($\sim$ 3) as the Hansonburg fluids. 4) The Na^+/K^+ ratios of the modern brines

Figure 26

Equilibrium constants for reduction-oxidation equations as a function of temperature. The shaded region contains the range of possible positions of the reaction

$$- C_{(graphite)} + O_2 = CO_2$$

where P_{CO_2} can vary from 10 to 100 bars. (Data from Helgeson, 1969, except for BaS which is from Sillen and Martell, 1964).

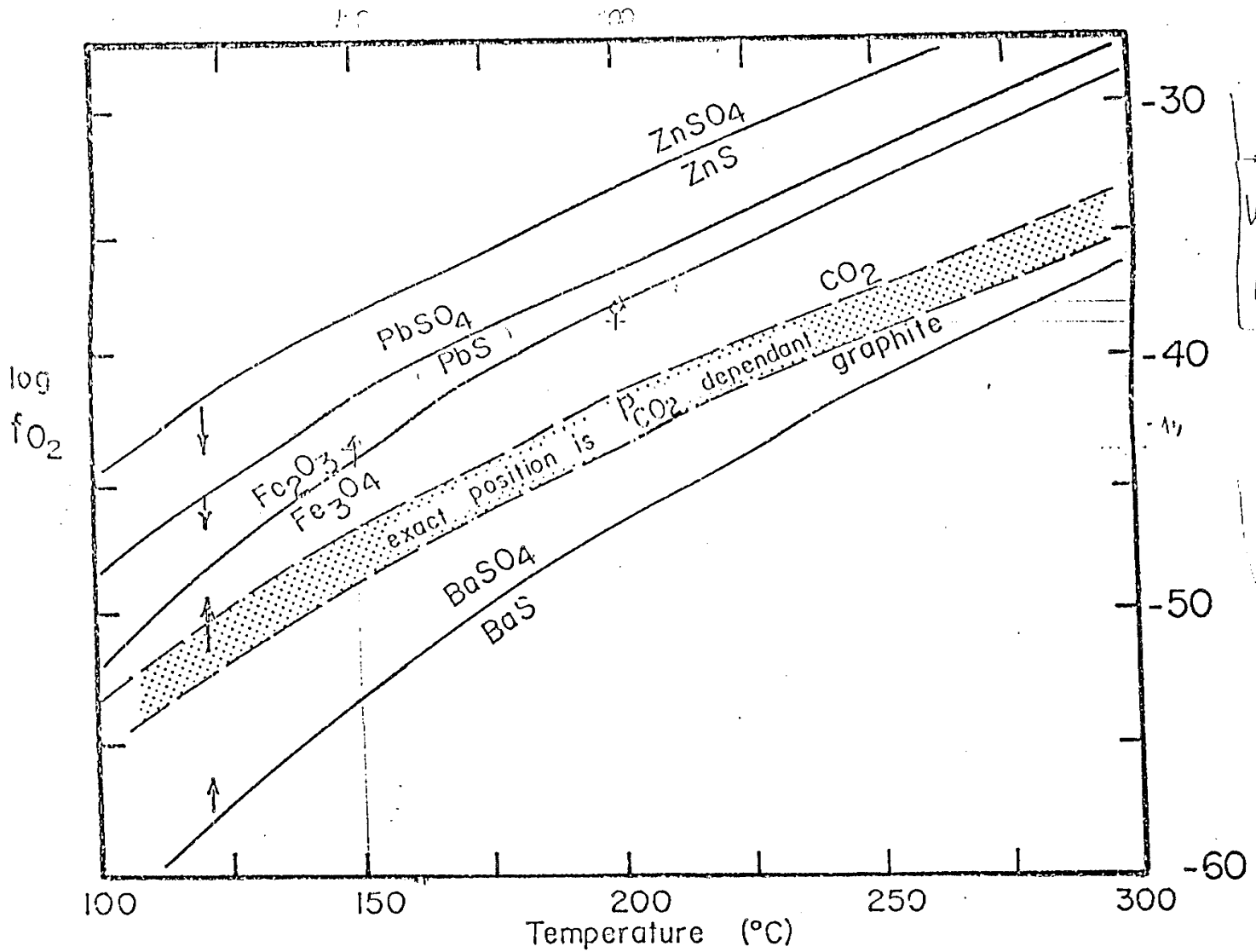

Pullman '66

$\log fO_{2\ 150} = -13.65$

$\log fO_{2\ 200} = -28.9$

Path '65

$\log fO_{2\ 150} = -43.43$

$\log fO_{2\ 200} = -38.0$

could cause the same type of alteration as noted in thin section, that is, albite stable-orthoclase destructive. It is almost certain that these modern waters vary in some details from Hansonburg fluids, but these are probably not important when temperature and hot-rock-interaction are considered. Table G shows the chemical compositions of fluids sampled below the playa surface at Lake Lucero and Figure 27 shows how increasing temperature shifts the fluid composition relative to the equilibrium boundaries of sodium and potassium silicates; at elevated temperatures the Lake Lucero brines would react with potassium feldspar but not sodium feldspar. In terms of these estimates it seems probable that the model proposed by Helgeson (1967) for origin of metals in Mississippi Valley-type deposits is valid for the Hansonburg district. Since the $^{a}Na^{+}/^{a}K^{+}$ ratios of the Lake Lucero waters are higher than the seawater composition used by Helgeson, it could be argued that more K-feldspar could be destroyed than Helgeson predicted for his model. The presence of kaolinite in only slightly altered orthoclase followed by abundant muscovite and albite in the intensely altered arkose suggests an even lower $^{a}K^{+}/^{a}H^{+}$ regime for the Hansonburg fluids than indicated in Figure 27. This argument will be developed in following sections.

As the solutions are known to be high chloride solutions it would be appropriate to consider the importance of chloride complexing. Helgeson (1969, p.762) predicted the dissociation constants of four lead-chloride complexes at 200° C:

Table G Compositions of Lake Lucero subsurface waters (mg/l) (From Allmendinger, 1971)

Species	Well Number								Average
	10	13	30	16	20	3	7	33	
Na	3300	2300	74000	28900	36500	21000	31500	41250	29840
K	230	201	2030	635	490	610	610	1125	741
Ca	600	510	385	595	585	600	595	667	567
Fe	.4	0	1.3	.5	.3	.3	.4	.7	.5
Mg	1100	1100	7900	2400	3260	3440	1880	5040	3260
SO_4	8640	9115	88610	38980	56860	30500	35440	33600	37700
Cl	7000	2055	102100	25137	23700	31500	35500	72000	37120
HCO_3	301	332	350	279	331	294	294	120	288
H_4SiO_4	33.76	33.36	16.92	33.33	5.53	11.93	15.15	4.92	19.36
F	1.20	2.78	.38	2.55	7.80	1.85	1.68	0.063	2.29
pH	7.36	7.93	7.36	7.75	7.94	7.66	7.76	7.50	7.66

Figure 27

Activity diagrams of log a_{Na^+}/a_{H^+} versus log a_{K^+}/a_{H^+} at 25°, 60°, 100°, and 125° C showing how increasing temperature shifts the field of equilibrium between the minerals shown and a fluid of Lake Lucero composition (Table G). Data are from Figures 8 and 9; fields were not shown for sodium or potassium montmorillonites for diagrammatic simplicity and because of the uncertainty in the thermodynamic data of these minerals. (From Beane and Allmendinger, 1974.)

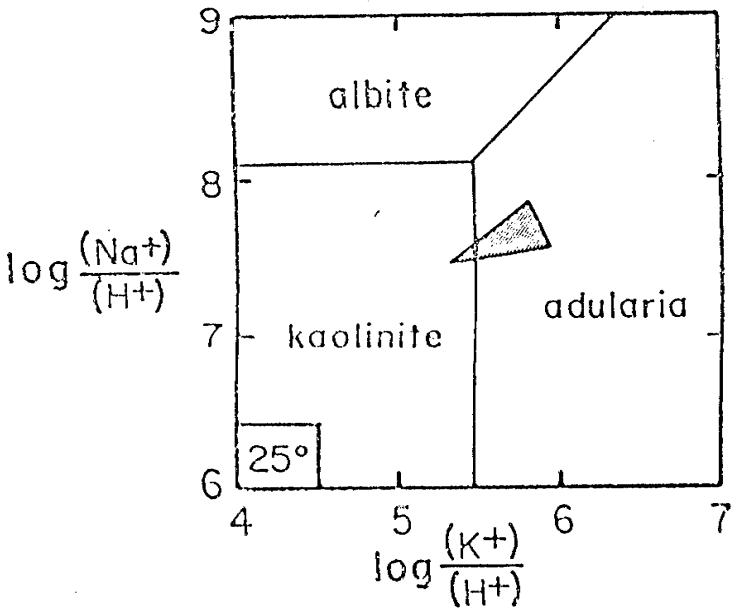
albite
kaolinite
adularia
25°
9
8
7
6
4
5
6
7
log (Na+)/(H+)
log (K+)/(H+)

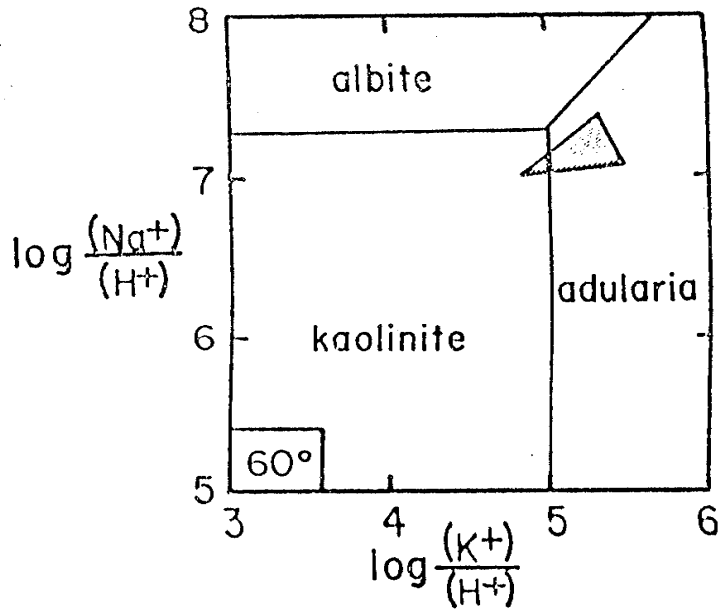
albite
kaolinite
adularia
60°
8
7
6
5
3
4
5
6
log (Na+)/(H+)
log (K+)/(H+)

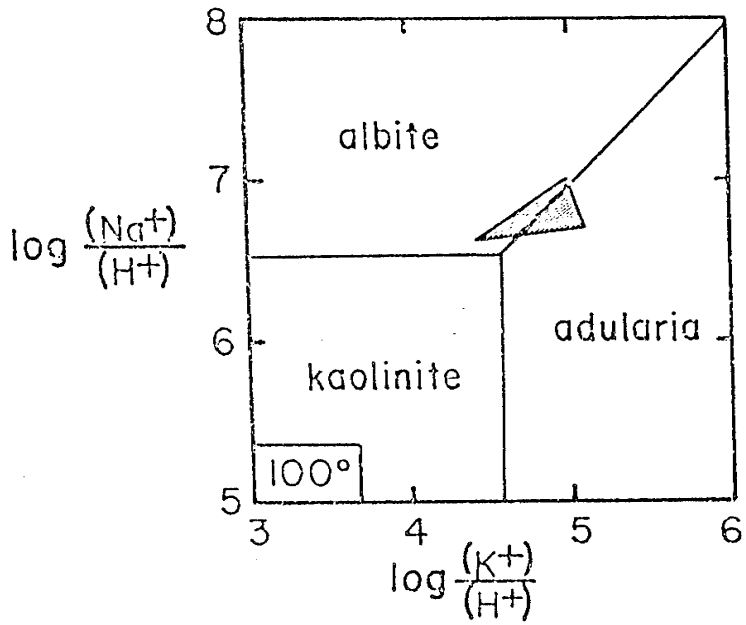
albite
kaolinite
adularia
100°
8
7
6
5
3
4
5
6
log (Na+)/(H+)
log (K+)/(H+)

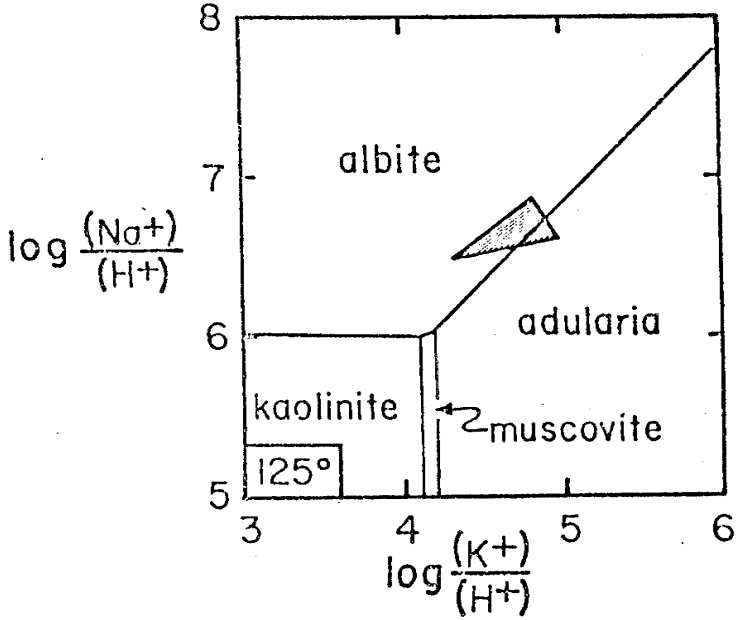
albite
kaolinite
muscovite
adularia
125°
8
7
6
5
3
4
5
6
log (Na+)/(H+)
log (K+)/(H+)

$$K_{d_1} = \frac{a_{Pb^{2+}} \cdot a_{Cl^-}}{a_{PbCl^+}} = 10.^{-2.1} \quad (PbCl^+ = Pb^{2+} + Cl^-) \qquad (35)$$

$$K_{d_2} = \frac{a_{Pb^{2+}} \cdot a^2_{Cl^-}}{PbCl^\circ_2} = 10^{-2.6} \quad (PbCl^\circ_2 = Pb^{2+} + 2Cl^-) \qquad (36)$$

$$K_{d_3} = \frac{a_{Pb^{2+}} \cdot a^3_{Cl^-}}{PbCl^-_3} = 10^{-3.0} \quad (PbCl^-_3 = Pb^{2+} + 3CL^-) \qquad (37)$$

$$K_{d_4} = \frac{a_{Pb^{2+}} \cdot a^4_{Cl}}{PbCl^{2-}_4} = 10^{-3.2} \quad (PbCl^{2-}_4 = Pb^{2+} + 4Cl^-) \qquad (38)$$

From the above equations, it can be seen that if the activity of chloride is greater than 10^{-2}, the ratio of uncomplexed lead to complexed lead ($Pb^{2+}/PbCl_x^{2-x}$) will be smaller than the dissociation constant of that complex. That is to say, when ($a_{Cl^-} > 10^{-2}$) the uncomplexed lead in solution is very small compared to the complexed lead. This is particularly true of multiple chloride complexes where the activity of the chloride ion is taken to the power of the multiple. As an example, assume the activity of chloride is 1.5 and consider the $PbCl_3^-$ complex:

$$\frac{a_{Pb^{2+}}}{a_{PbCl_3^-}} = \frac{10^{-3.0}}{(1.5)^3} = \frac{0.001}{3.375} = 2.96 \times 10^{-4} \qquad (39)$$

Under these conditions, the activity of $PbCl_3^-$ is 3.38×10^3 times greater than the activity of Pb^{2+}.

It is known from fluid inclusions that the chloride molality varied between two and three. Figure 28 shows the distribution of $^{m}Cl^-$, $^{\gamma}Cl^-$, $^{a}Cl^-$, and $^{a}Pb^{2+}/^{a}PbCl_x^{x-2}$ in paragenetic time. The activity coefficient ($^{\gamma}Cl^-$) was

Figure 28

Graphic representation of the variation of several chemical parameters of interest in "paragenetic time" as indicated by the fluid inclusion data. γ_{Cl^-} was calculated from the extended Debye-Huckel equation using the T and I values estimated from fluid inclusions. The activity ratios were determined from the log K of dissociation of the appropriate complex as given in Helgeson, 1969. The shaded region between the two dashed curves represents the uncertainly between considering or omitting the data from secondary inclusions in barite (see Figure 25, p. 90).

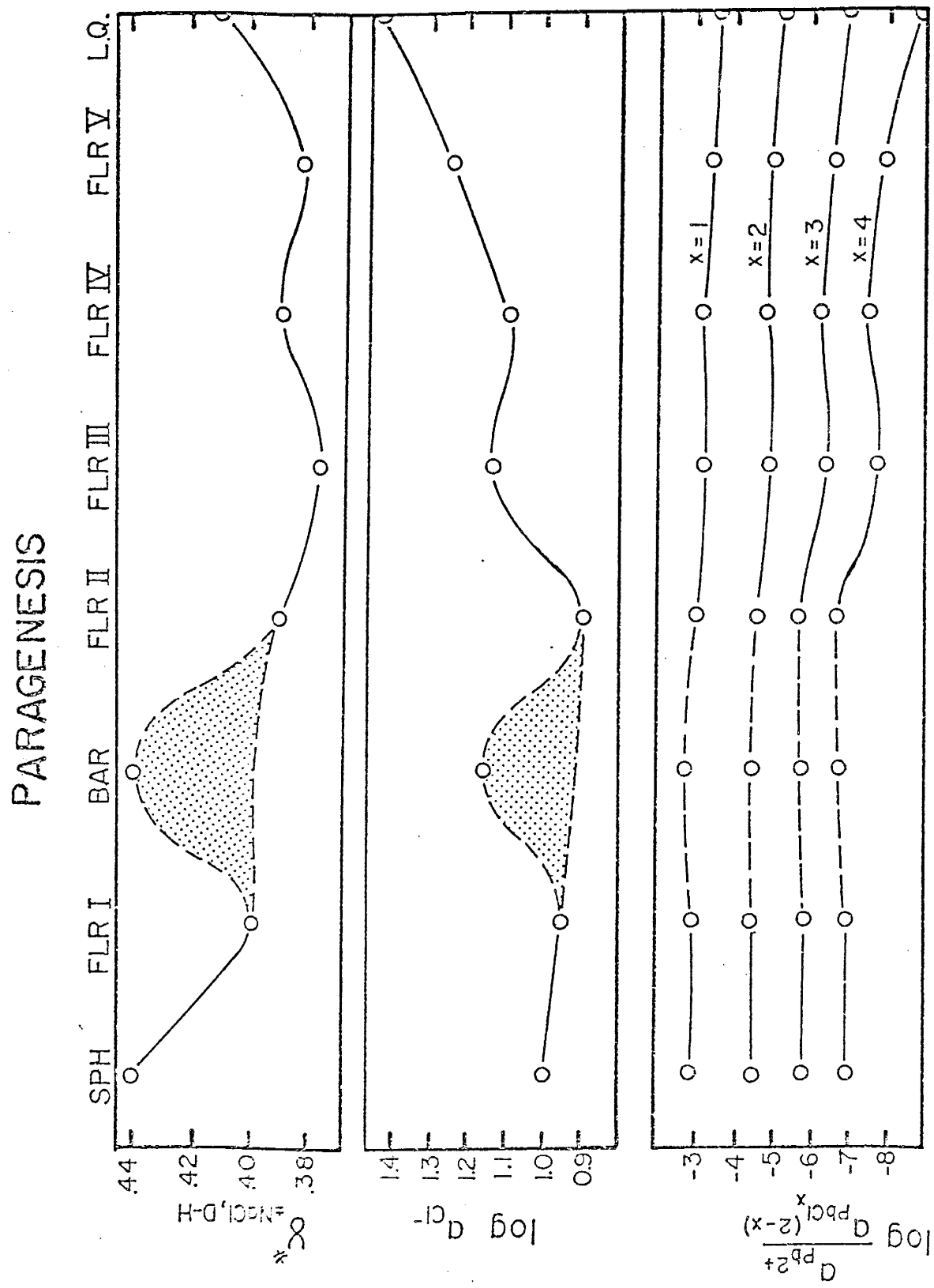
PARAGENESIS
SPH
FLR I
BAR
FLR II
FLR III
FLR IV
FLR V
L.Q.
$\gamma^*_{NaCl,D-H}$
.44
.42
.40
.38
log a_{Cl^-}
1.4
1.3
1.2
1.1
1.0
0.9
log $\frac{a_{Pb^{2+}}}{a_{PbCl_x^{(2-x)}}}$
-3
-4
-5
-6
-7
-8
x=1
x=2
x=3
x=4
CHEMICAL PARAMETERS

culated from the extended Debye-Huckel equation using
e temperature and ionic strength indicated for each
agenetic stage.

Other complexes which may be important are $ZnCl^+$, $ZnCl_2^\circ$, Cl_3^-, $ZnCl_4^{2-}$, $BaSO_4^\circ$, $CaSO_4^\circ$, KSO_4^-, $NaSO_4^-$, HSO_4^-, HCO_3^-, $BaCl^+$, d $CaCl^+$. Thermodynamic data for some of these species are cking and consequently they have been estimated (Figure 21). e importance of the carbonate species (CO_3^{2-} and HCO_3^-) may come significant in the immediate vicinity of mineralization ere dissolution of limestone is apparent. In this vironment, the amount of dissolved carbonate is a function pH, $a_{Ca^{2+}}$, and f_{CO_2}, i.e.

$$CaCO_3 + 2H^+ = Ca^{2+} + CO_2 + H_2O \qquad (40)$$

$$\log K = \log \frac{a_{Ca^{2+}}}{a^2_{H^+}} + \log f_{CO_2} = 8.95 \text{ at } 200^\circ \text{ C} \qquad (41)$$

Helgeson, 1969, Table 12). If $a_{Ca^{2+}}$ is controlled by the olubility of fluorite in a solution where a_{F^-} is 10^{-5} then:

$$CaF_2 = Ca^{2+} + 2F^- \qquad (42)$$

nd

$$\log K = \log a_{Ca^{2+}} - 10 = -10.26 \qquad (43)$$

herefore, $\log a_{Ca^{2+}} = -0.26$ and from equation (41)

$$\log f_{CO_2} - 2 \log a_{H^+} = 9.21 \qquad (44)$$

If f_{CO_2} is between 0 and 70 bars, $\log f_{CO_2}$ can vary from $-\infty$ to 1.5, and pH ($-\log a_{H^+}$) can vary from 3.86 upward. A change in the activity of the fluoride ion by an order of magnitude

shifts the pH by one unit. Arguing that the fluoride content of the mineralizing fluid was similar to fluoride contents of modern waters suggests a_{F^-} was between 10^{-5} and 10^{-4}. Tables H and I show the fluoride contents of some modern waters for comparison. The computed activities do not consider the effects of complexing; however, Table F (page 73) indicates these effects would be small. From these arguments it would appear that the probable pH range is above 3.9.

EVIDENCE FROM STABLE ISOTOPES

Table J shows the $\delta^{34}S$ values of minerals collected from the district, and Table K shows how these values relate to other sulfur species at 200° C, using the fractionation factors from Figure 12. The $\delta^{34}S$ values are very light isotopically; that is, they are very much depleted in the heavy isotope, sulfur-34. A likely source for such light sulfur is Permian evaporites as indicated by Figure 29 which shows the distribution of evaporites according to geologic age and their $^{34}S/^{32}S$ content.

With this in mind, two samples of gypsum from the Yeso Formation were collected, one from near the type section at Mesa del Yeso and another from Chupadera Mesa near Jones Camp; both yielded a value of $\delta^{34}S = +12.4$ relative to CDT. The similarity in values of $\delta^{34}S$ for the barite in the mineral deposits and the anhydrite in the Yeso Formation suggests that the latter may have been the source for the sulfate in the hydrothermal barite. The mean $\delta^{34}S$ of +10.8 for the barite is certainly within the range of 3 ‰ suggested as the maximum fractionation between aqueous sulfate and anhydrite

Table H Molalities of fluoride ion measured in Lake Lucero subsurface waters (Allmendinger, 1971) and corresponding activities calculated from the modified Stokes-Robinson equation:

$$-\log\gamma = \frac{AZ^2\sqrt{I}}{1.0 + \mathring{a}\, B\sqrt{I}} + B^{\circ} I$$

using the parameters A, B, and B° suggested by Helgeson (1969) and $\mathring{a}$ of 3.5 (Garrels & Christ, 1965). Average fluoride activity is 6.07×10^{-5}.

Molality ($\times 10^{-4}$)	Activity ($\times 10^{-5}$; at 200°C)
1.37	6.64
0.05	0.25
1.47	8.02
0.63	3.35
0.95	4.59
0.89	4.32
4.11	20.34
0.20	1.22
1.21	5.91

Table I Fluoride contents of some modern hot springs in New Mexico (from Summers, 1965). Most hot spring systems are sufficiently dilute so that molality is a good approximation to activity of the fluoride ion.

Spring Name or Location	ppm F	molality F ($\times 10^{-5}$)
Aragon Hot Springs	.4	2.1
	.6	3.2
Frisco Hot Springs	1.0	5.3
	1.6	8.4
	1.8	9.5
Radium Hot Springs & vicinity	4.6	24.2
	4.8	25.3
	5.7	30.5
	5.3	27.9
	2.2	11.6
	1.0	5.3
	5.2	27.4
	2.4	12.6
	3.4	17.8
	2.6	13.7
	3.2	16.8
	3	15.8
	3	15.8
	1.6	8.4
	2.8	14.7
	3.2	16.8
	3.2	16.8
	2.8	14.7
	3.3	17.4
	.6	3.2
	1.2	6.3
	1.2	6.3
Gila Hot Springs & vicinity	12	63.2
	9	47.3
	21	111
	.8	4.2
	8	42.1
	6	31.6
	1.1	5.8
	1.2	6.3
	.9	4.7
	5.2	27.4
Mimbres Hot Springs	16	84.2
	16	84.2
	16	84.2
Faywood Hot Springs	7	36.8
	6.8	35.8
	2.8	14.7

Table I (continued)

Spring Name or Location	ppm F	molality F ($\times 10^{-5}$)
Wells in Hidalgo Co. (Sec. 7, T. 25S., R. 19W.)	11	57.9
	9.9	52.1
Ojo Caliente	13	68.4
	16	84.2
	16	84.2
	16	84.2
	.8	4.2
	16	84.2
	16	84.2
	.5	2.6
	1.4	7.4
	.2	1.1
	.7	3.7
Soda Dam Springs	2.4	12.6
	3.2	16.8
	3.3	17.4
	3.2	16.8
	3.2	16.8
	3.6	19.0
	3.6	19.0
	3.6	19.0
	2.8	14.7
	3.5	18.4
	2.8	14.7
	4.0	21.0
Jemez Hot Springs	5.2	27.4
	.8	4.2
	.8	4.2
	.8	4.2
	7.1	37.4
	4.9	25.8
	4.9	25.8
	5.2	27.4

Table J Sulfur-34 compositions of hydrothermal minerals from Hansonburg mining district (°/oo).

Barite		Galena		Sphalerite	
A4-B	10.4	A7-G	-16.5	BL2-Sp	-10.6
B4-B	10.7	BL21-G	-16.4		
BL16-B	11.2	BL31-G	-15.8		
BL32-B	11.5	BL73-G	-15.5		
BL34-B	10.6	BL83-G	-15.9		
BL72-B	10.7	D3-G	-15.3		
BL82-B	11.6	D15-G	- 7.6		
D9-B	10.5	DR3-G	-15.1		
H2-B1	10.6	H5-G	-13.9		
H2-B2	10.4	H2-G	-14.6		
H4-B	11.0	K1-G	-15.0		
H12-B	10.3	K5-G	-14.7		
K7-B	11.2	L1N2	-15.3		
L1N1-B	10.3	LMT1-G	-17.1		
Mc-XB1	10.6	RB2-G	-15.2		
MC-XB2	11.1	RF3-G	-14.9		
MC-XB3	11.7	UMT3-G	-15.3		
MC4-B	10.5				
MC9-B	10.3				
MC13-B	11.1				
RB1-B	11.0				
RF4-B	10.9				
UMT2-B	11.0				
Mean	10.8	Mean	-15.0	Mean	-10.6

Table K Isotopic composition of sulfur-bearing aqueous species which would be in equilibrium with minerals having the mean isotopic composition listed in Table J (at 200° C and I = 2.0).

	Barite (+10.8 °/oo)	Galena (-15.0 °/oo)	Sphalerite (-10.6 °/oo)
H_2S°	-21.2	-10.5	- 9.4
HS^-	-22.8	-12.1	-11.0
S^{2-}	-28.3	-17.6	-16.5
SO_4^{2-}	+10.8	+21.5	+22.6

Figure 29

Variation of sulfur-34 contents of marine evaporites in geologic time. Data from:

- ● Ault, 1959
- ▲ Claypool et al., 1972
- ○ Adler, 1974

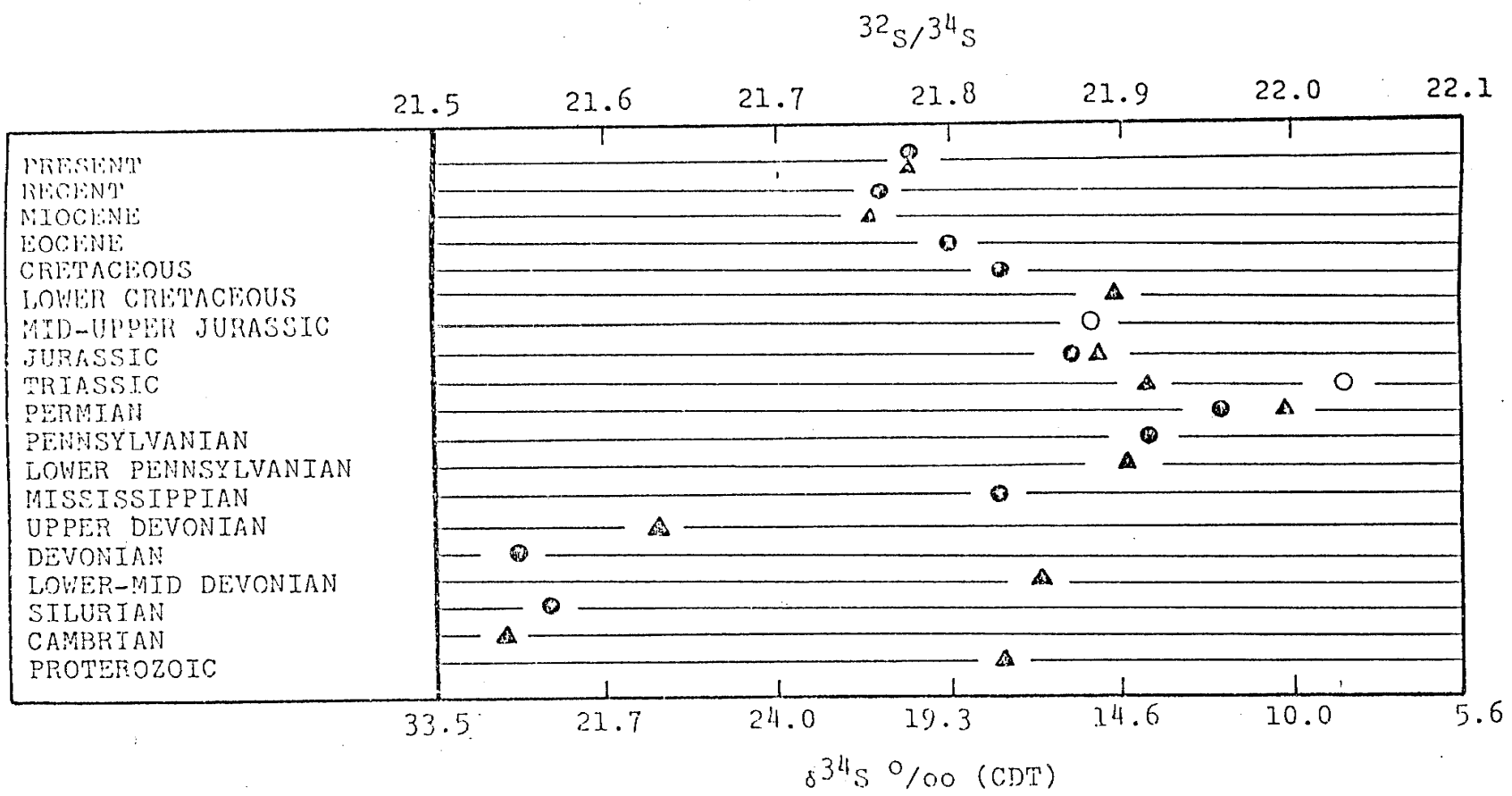
$^{32}S/^{34}S$
21.5
21.6
21.7
21.8
21.9
22.0
22.1
PRESENT
RECENT
MIOCENE
EOCENE
CRETACEOUS
LOWER CRETACEOUS
MID-UPPER JURASSIC
JURASSIC
TRIASSIC
PERMIAN
PENNSYLVANIAN
LOWER PENNSYLVANIAN
MISSISSIPPIAN
UPPER DEVONIAN
DEVONIAN
LOWER-MID DEVONIAN
SILURIAN
CAMBRIAN
PROTEROZOIC
33.5
21.7
24.0
19.3
14.6
10.0
5.6
$\delta^{34}S$ °/oo (CDT)

Figure 30

Distribution of $\delta^{34}S$ of various minerals analysed from Hansonburg mining district. Note the different scales used on the various horizontal axes.

(see page 46). Thus, the isotopic composition of the fluid from which barite precipitated may have originated by dissolution of anhydrite from the Yeso Formation, even at very low temperatures (i.e. 25° C).

The data of Table J have been plotted in Figure 30 which shows the close grouping of $\delta^{34}S$ values for barite and galena. The total variation in barite is less than $\pm$ 1.0‰ and is about $\pm$ 1.5‰ for galena with one exception. Comparison of the data from Hansonburg in Figure 30 with the theoretical fractionation factors in Figure 12 shows that barite and galena were not in isotopic equilibrium. The data in Figure 30 show that the difference in $\delta^{34}S$ of barite and galena is about 26‰ while Figure 12 predicts a fractionation of about 36.5‰ between these two species at 200° C. This is compatible with paragenetic observations which show that galena always precedes barite, and thus, there is no indication that the two minerals precipitated cogenetically. Two explanations for the apparent lack of chemical equilibrium between barite and galena exist. First, the chemistry of the hydrothermal fluid may have changed between precipitation of galena and barite. A change in temperature, pH, or f_{O_2} could have produced the observed variation. Figure 31 shows how a shift in pH or f_{O_2} at 200° C will change the isotopic composition of H_2S° in a fluid with $\delta^{34}S_{\Sigma S}$ equal to 10.3‰. It is quite possible that such a compositional shift could also explain the precipitation or lack of precipitation of some of the hydrothermal minerals. The total isotopic composition of

Figure 31

Plot of isodels (relative to H_2S) in pH-f_{O_2} space with $\delta^{34}S_{\Sigma S}$ = 10.8 °/oo for system similar to that responsible for mineralization of Hansonburg mining district (T=200° C, I=2.0).

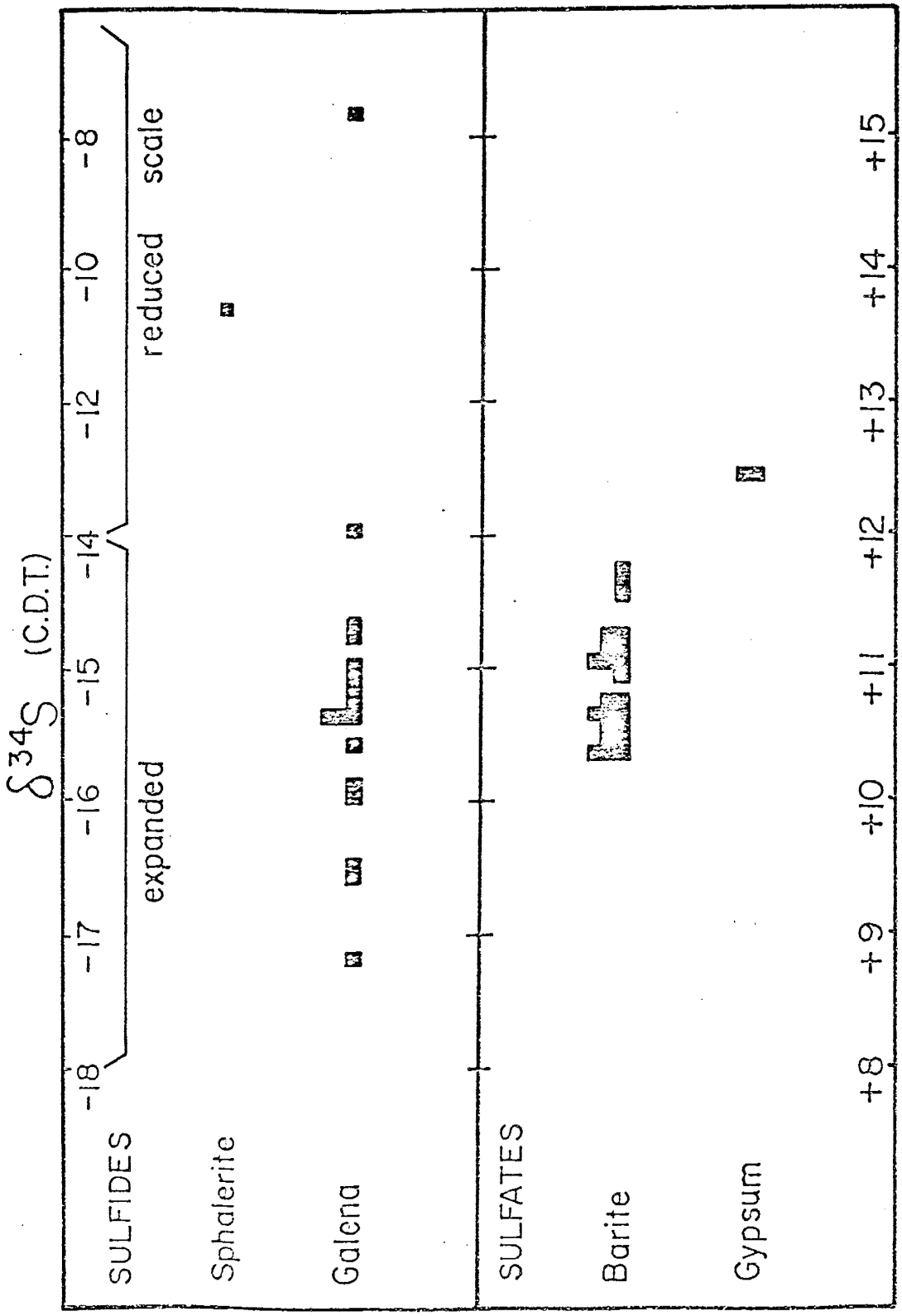
$\delta^{34}S$ (C.D.T.)
-18
-17
-16
-15
-14
-12
-10
-8
expanded
reduced scale
SULFIDES
Sphalerite
Galena
SULFATES
Barite
Gypsum
+8
+9
+10
+11
+12
+13
+14
+15

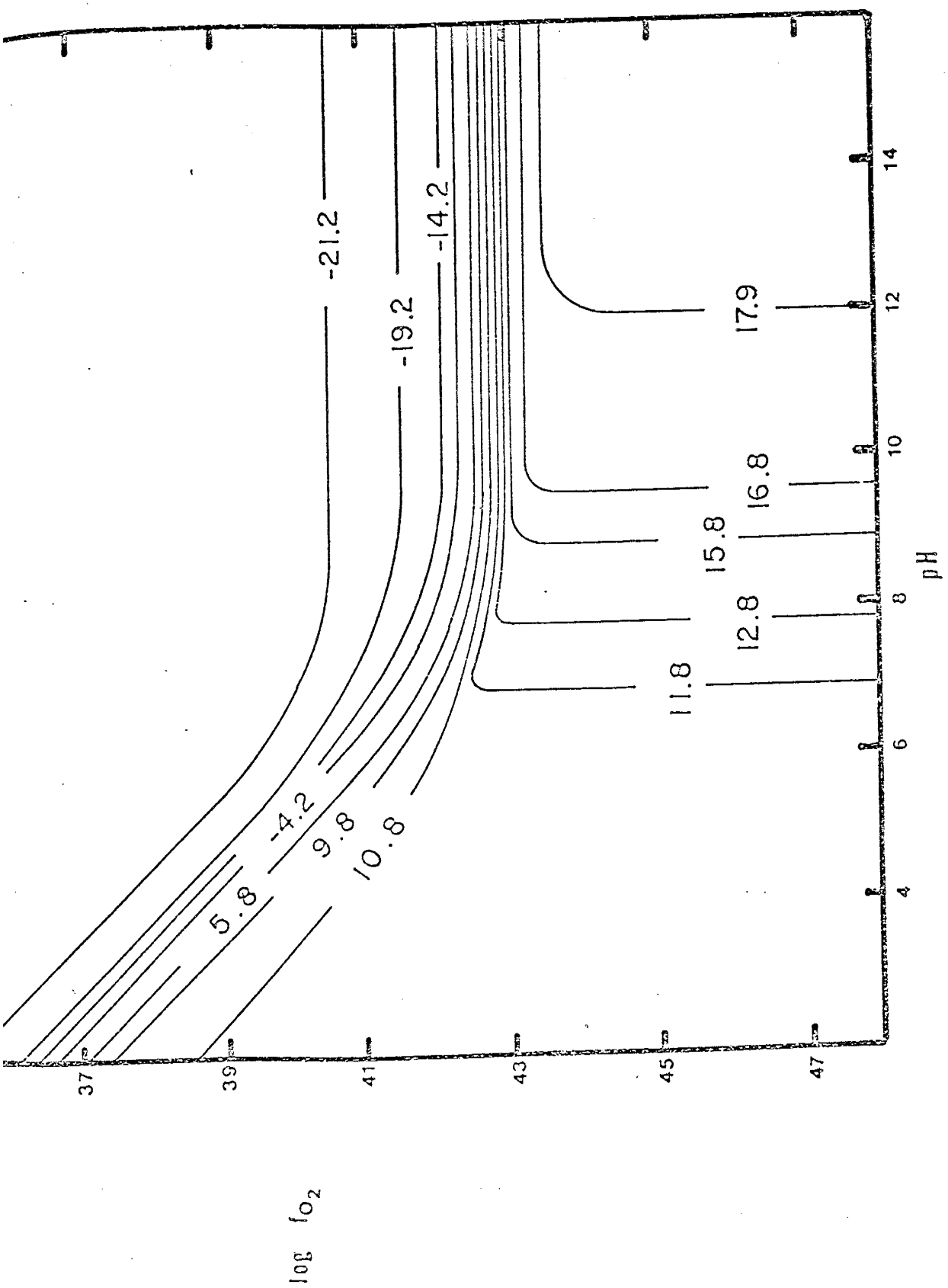
-21.2
-19.2
-14.2
-4.2
5.8
9.8
10.8
11.8
12.8
15.8
16.8
17.9
pH
4
6
8
10
12
14
37
39
41
43
45
47
log f_{O_2}

the fluid also may have changed between sulfide and sulfate mineralization. This could result from a change in source of sulfur. For instance, there may have been some small contribution from sedimentary sulfides during the earlier mineralization which was depleted before sulfate deposition.

A second explanation for the apparent lack of equilibrium may be that the $\delta^{34}S$ fractionation between barite and galena represents a relict equilibrium "frozen in" prior to mineralization. If the fractionation of 26‰ between galena and barite is considered a relict equilibrium fractionation then according to Figure 12, this would represent a temperature of about 300° C. It is possible that the hydrothermal fluids were considerably hotter prior to mineralization than the temperatures indicated by fluid inclusion filling temperatures. This possibility will be discussed in a later section concerning the genetic model.

A few carbon isotope analyses were made with the understanding that the results probably would relate to late stage hypogene processes. The results of these analyses are shown in Table L. The first four samples are limestones which might be considered as carbon sources for the CO_3^{2-} in hydrothermal calcite. The last four samples are hypogene (?) calcites collected from veinlets in mineralized limestones. These calcites are lighter than what would be expected for calcites precipitating in equilibrium from any of the analyzed limestones at 150° C. As it seems highly unlikely for there to be a carbon source other than the limestones in the immediate vicinity, it can be assumed that precipitation

Table L Isotopic composition of carbon in carbonates from Hansonburg district.

Sample Description	$\delta^{13}C$ (‰)
Yeso Limestone (SE1/4 Sec. 26, T. 5S., R. 6E.)	+2.86
Bursum Limestone (SE1/4 Sec. 32, T. 5S., R. 6E.)	-4.15
Council Spring Ls. (SW1/4 Sec. 30, T. 5S., R. 6E.)	-2.64
Council Spring Ls. (NE1/4 Sec. 36, T. 5S., R. 5E.)	-2.35
A-3 hydrothermal calcite N. Royal Flush	-7.30
A-2 hydrothermal calcite N. Royal Flush	-3.57
H-17 hydrothermal calcite N.W. Mex-Tex	-2.81
BL-64 hydrothermal calcite Blanchard Mine	-18.44

of calcite was a nonequilibrium process. Another possibility is that the calcites were contaminated with very light carbon derived from organic material. Almost all of the hypogene calcites are dark brown and appear to have countless dark inclusions. If these inclusions have a significant hydrocarbon content then contamination would appear unavoidable. It appears that carbon isotopes do not provide conclusive data regarding the paleogeochemical environment at Hansonburg.

SUMMARY OF CHEMICAL PARAMETERS

Figure 32 is a fence diagram in pH and log f_{S_2} space at 200° C. The shaded region was partioned by "fences" drawn between minerals present and minerals absent at the hypogene stage. The lines in this diagram represent equilibrium conditions between the separated mineral pairs and were constructed from published equilibrium constants (Helgeson, 1969). Contouring log f_{S_2} allows the region of mutual stability to be plotted in pH versus log f_{O_2} space (Figure 33). These figures show how even small changes in pH, f_{O_2} and/or f_{S_2} can create equilibrium or nonequilibrium conditions for the various phases at a fixed temperature.

Figure 34 is the same region of mutual mineral stabilities again plotted in terms of pH and log f_{O_2} at 200° C; however, the log f_{S_2} contours have been omitted and contours of mole fraction of total sulfate have been added. This has been done to show that all the minerals could have precipitated from a hydrothermal fluid which had its sulfur content dominated by a sulfate species. Only in the small region below the 0.5 contour could a sulfide species dominate.

Figure 32

Fence diagram in f_{S_2}-f_{O_2} space showing the boundaries of various phases important to the determination of the chemistry of mineralizing fluids. The shaded area represents the region of mutual stability for the phases present at Hansonburg.

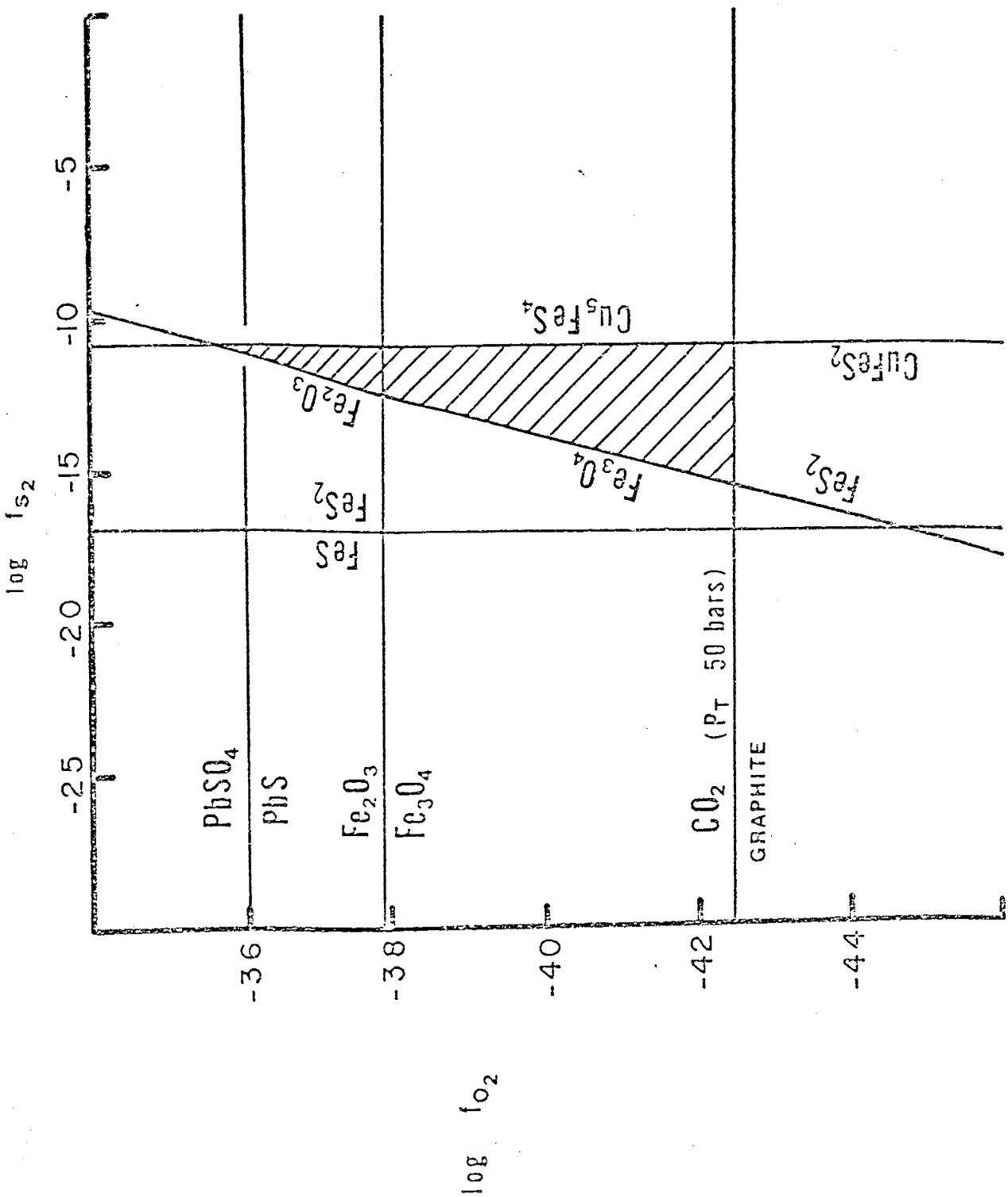
log f_{S_2}
-5
-10
-15
-20
-25
Cu_5FeS_4
$CuFeS_2$
Fe_2O_3
Fe_3O_4
FeS_2
FeS
$PbSO_4$
PbS
Fe_2O_3
Fe_3O_4
CO_2 (P_T 50 bars)
GRAPHITE
-36
-38
-40
-42
-44
log f_{O_2}

Figure 33

Region of mutual mineral stability plotted in f_{O_2}-pH space; contours are of log f_{S_2}.

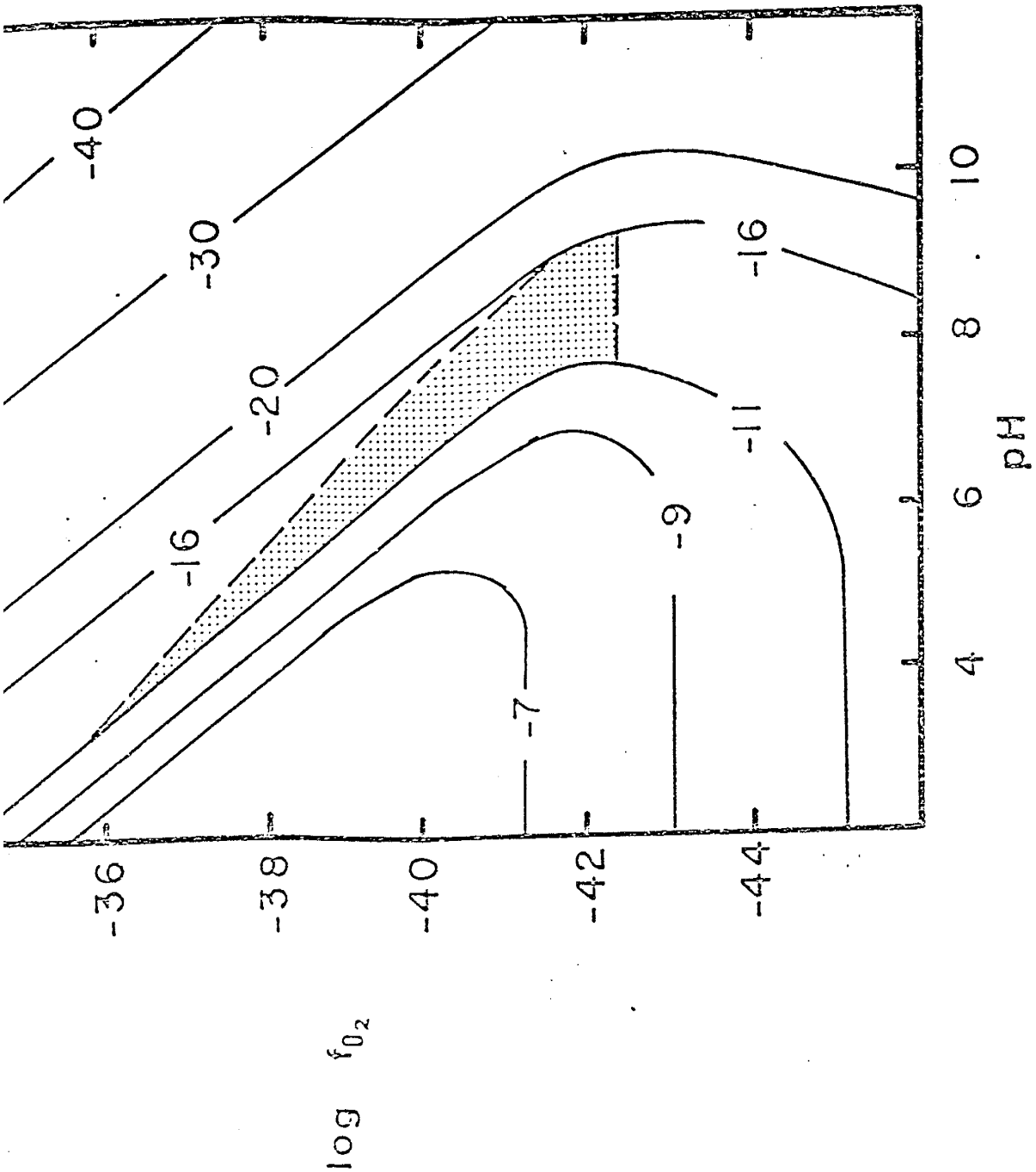
-40
-30
-20
-16
-16
-11
-9
-7
4
6
8
10
pH
-36
-38
-40
-42
-44
log f_{O_2}

Figure 34

Region of mutual mineral stability plotted in f_{O_2}-pH space; contours are of mole fraction total sulfate ($SO_4^{2-} + HSO_4^- + NaSO_4^- + KSO_4^- + CaSO_4^\circ + BaSO_4^\circ + H_2SO_4^\circ$). Note that the majority of the shaded region lies in the sulfate dominated region ($N_{\Sigma SO_4} > 0.5$).

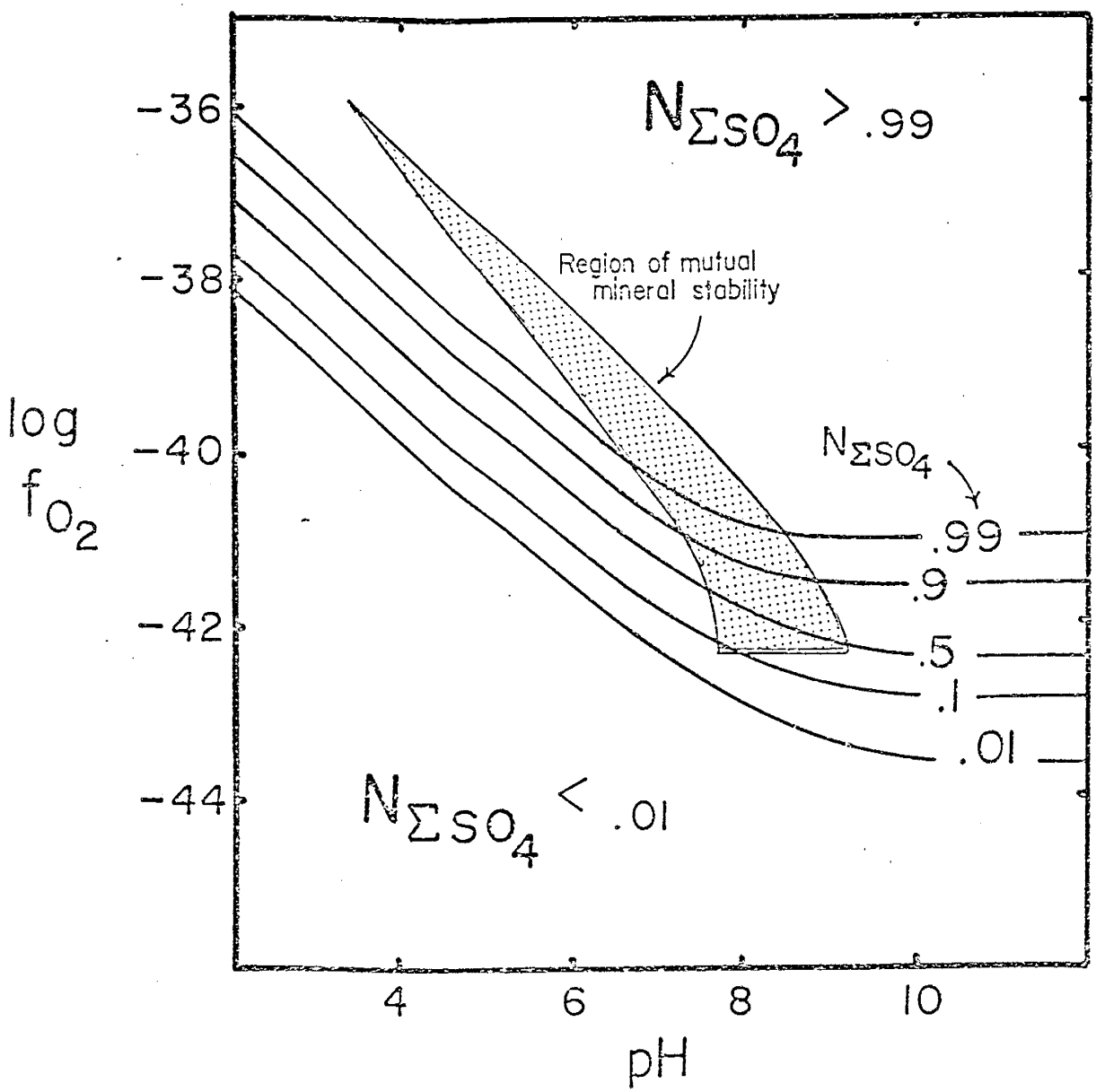
$N_{\Sigma SO_4} > .99$
Region of mutual mineral stability
$N_{\Sigma SO_4}$
.99
.9
.5
.1
.01
$N_{\Sigma SO_4} < .01$
-36
-38
-40
-42
-44
log f_{O_2}
4
6
8
10
pH

This figure supports the hypothesis that the sulfur isotopic composition of the hydrothermal fluid was controlled by the Yeso evaporites and thus, was very close to 10.8‰.

Figures 33 and 34 indicate f_{O_2} was between 10^{-36} and 10^{-42} bars, f_{S_2} was between 10^{-15} and 10^{-11} bars and that pH was greater than 4 but less than 9.5. Furthermore, if the f_{O_2} was near the magnetite-hematite boundary (Figure 37) as suggested by the mineralized dikes and sills in the area (Beane and Titus, 1973), then log f_{O_2} must have been near -38. It can be seen from Figures 33 and 34 that if log f_{O_2} were near -38, then pH would be about 5.0 or 5.5.

SOURCE AND LOCALIZATION OF ORE-FORMING CONSTITUENTS

The results of the sulfur isotope investigation suggested that Permian rocks were the source of at least one component (sulfur) of the ore-forming fluids. Helgeson (1967) presents some theoretical data which suggest the Mississippi Valley-type deposits formed from hot, saline waters which derived their lead contents from potassium feldspar upon altering host-rock arkoses. It is desired to investigate whether such a mechanism, coupled with the appropriate hydrologic model, may have provided the fluids responsible for mineralization of the Hansonburg district.

Country rock compositions

Samples of the Permian rocks were collected at 500 foot intervals along a four and one-half mile long, N 70 E traverse from Julian Arroyo past White Store to the crest of Chupadera Mesa (Figure 35). These samples are considered representative of the Permian section which may have acted as a source rock to the mineralization; however, preferential weathering and erosion of the shaley units may have biased the sampling. Later in the text, the section encountered in this traverse will be referred to as the "White Store Permian section". Table M is a compilation of chemical analyses obtained from the samples collected along the White Store Permian section. These analyses are similar, in most respects, to the compiled compositions of sandstones and shales listed by Pettijohn (1957, p. 283-380). The exception being that the Na_2O/K_2O ratios of the rocks listed by Pettijohn

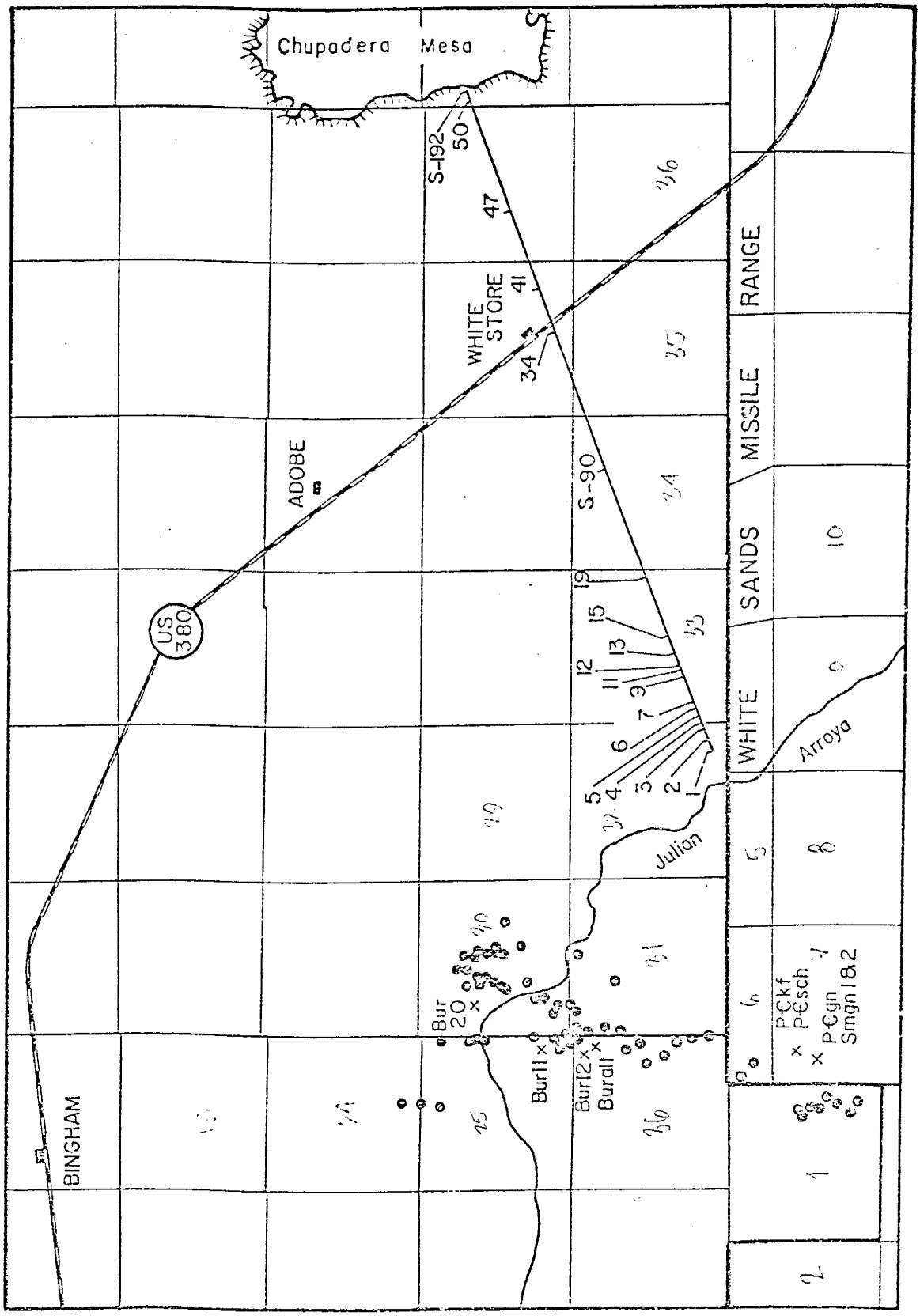
Chupadera Mesa
S-192
50
47
41
34
WHITE STORE
ADOBE
US 380
S-90
19
15
13
12
11
9
7
6
5
4
3
2
1
WHITE SANDS MISSILE RANGE
Arroya
Julian
BINGHAM
Bur 20
Burl1
Burl2
Burall
P€kf
P€sch
P€gn
Smgn182

Figure 55

Location map showing the White Store Permian section, sample locations and some geographic features for reference (taken from U.S. Geol. Survey, 15 minute, Bingham, New Mexico Quadrangle). Solid circles are locations where hydrothermal minerals were sampled for fluid inclusion, stable isotope, and paragenetic studies. Sample numbers along the White Store Permian section should be prefixed with Tl- to match the sample numbers in Table M. Samples in Table N are indicated with an x.

Table M Compositions of Permian rocks sampled along the White Store Permian section. High-CaO rocks are limestones or evaporites; weight percents do not add to 100.0 because H_2O and CO_2 were not measured and because of analytical error (discussed on pages 54-57). Sample locations are shown on Figure 35 beginning with T1-1 in the Bursum Formation and ending with S192 in the San Andres Formation.

	weight percent								parts per million			
Sample	K_2O	Na_2O	CaO	Al_2O_3	SiO_2	Fe_2O_3	MgO	SO_3	F	Pb	Ba	Sr	Sum %
T1-1	-	.1	52.1	2.6	.7	-	1.6	-	.08	12	54	470	57.2
T1-2	-	15.0	52.0	2.5	8.0	-	-	-	.09	32	72	113	77.6
T1-3	-	.1	52.7	1.3	.6	-	1.6	-	.09	36	105	530	56.4
T1-4	-	11.7	9.0	18.	55.0	2.4	-	-		24	310	9	96.1
T1-5	-	10.2	4.1	17.2	63.5	2.5	-	-					97.5
T1-6	-	7.8	7.8	12.6	56.0	1.5	4.0		.09	-	223	64	89.8
T1-7										16	108	20	-
T1-9	-	10.5	5.5	16.9	61.0	-	2.5	-	.22	32	340	60	96.6
T1-11										36	1240	104	-
T1-12									.08	20	553	29	-
T1-13	-	8.8	5.0	15.5	59.0	1.5	-	-					89.8
T1-15										60	816	96	-
T1-19										24	553	56	-
S-90	-	11.2	5.7	16.8	59.0	2.0	.5	-		14	126	33	95.2
T1-34	-	-	56.0	1.6	5.7	-	-	-		32	72	111	63.3
T1-41	.4	.7	31.0	3.5	10.0	.5	23.0	-		14	67	69	69.1
T1-47	-	1.3	27.0	1.8	.5	-	11.8	26.0		-	54	182	68.4
T1-50	-	3.3	55.2	2.2	5.5	-	1.0	-	.08	24	126	87	67.3
S-192											162	120	-

- Below detection

are about 1.0 or less; the ratios indicated by Table M are all much greater than one. Chemical compositions of samples from the Bursum Formation which were described above as being hydrothermally altered and samples of Precambrian rocks are tabulated in Table N for comparison. Lewchalermvong (1973, Appendix II) estimated the total amounts of proven, probable and potential ore in the Hansonburg mining district north of T. 6S. From his estimates it was determined that the total amounts present in the entire district would be about: 1.0×10^6 kg PbS, 1.6×10^8 kg $BaSO_4$, and 5.0×10^6 kg CaF_2. To these values must be added 3.2×10^7 kg barite (Williams et al., 1964, p. 34) and 5.00×10^6 kg lead (Howard, 1967, p. 103) already produced. Thus, about 5.9×10^6 kg lead, 1.1×10^8 kg barium, 2.4×10^6 kg fluorine and 2.2×10^7 kg sulfur are required to produce the deposits in the Hansonburg mining district. Using Table M as a reference and mean values of 23.5 ppm lead, 281 ppm barium, and 10,000 ppm fluorine, the required amounts of source rock would be 2.5×10^{11} kg, 3.9×10^{11} kg and 2.4×10^8 kg respectively. Assuming all of the sulfur was derived from a rock of composition similar to sample T1-47 (Yeso evaporite), 2.2×10^8 kg rock would be required.

Assuming a bulk density of 2.25 g/cc for an arkose, a total volume of rock required to supply the elements is calculated to be between 0.011 and 53.0 km^3. The barium budget requires the largest volume of source rocks while the fluorine budget requires the smallest volume. These figures can be revised somewhat, assuming that barium and

Table N Compositions of altered Bursum Formation and Precambrian rocks sampled in the vicinity of the Hansonburg mining district. Samples were not analyzed for H_2O or CO_2, but the sums for BUR11 and BURalt indicate that total analytical errors are at least about 5%. Sample locations are on Figure 35.

BURSUM ROCKS

	weight percent									parts per million			
Sample	K_2O	Na_2O	CaO	Al_2O_3	SiO_2	Fe_2O_3	MgO	SO_3	F	Pb	Ba	Sr	Sum %
BUR11	-	11.8	-	22.8	68.3	1.6	-	-	.14	-	993	-	104.7
BUR12	-	5.3	1.5	20.6	60.0	3.7	-	-	.71	-	4670	11	92.3
BUR20	.1	10.5	.7	23.7	50.0	1.5	-	-	.16	-	36	4.4	86.7
BURalt	-	10.4	-	21.0	72.0	.4	-	-	-	18	1580	6.7	104.2

PRECAMBRIAN ROCKS

PCkf	7.7	4.3	-	24.8	45.5	.8	-	-	.14	40	-	3.6	83.2
PCsch	2.5	1.4	4.5	24.8	42.5	2.2	7.2	-	.20	-	450	6.7	85.3
PCgn	5.0	2.3	.7	30.0	58.5	.4	-	-	.21	20	388	89	97.2
Smgn1	1.8	2.6	5.5	22.3	48.1	8.6	8.7	-	.18	20	470	116	97.8
Smgn2	1.3	4.8	5.9	20.0	49.0	8.5	10.1	-	.09	.8	350	102	99.7

- Below detection

lead were derived from feldspars and micas in arkoses (Levinson, 1974, p. 46). The average lead and barium values in the arkoses (25 ppm and 452 ppm respectively) are higher than the above averages for the whole Permian section. The amount of arkose required to satisfy the budget would be 2.36×10^{11} and 2.44×10^{11} kg for lead and barium respectively.

It is reasonable to assume that sufficient amounts of each of the ore-forming elements could be contained in less than 2.5×10^{11} kg source rock, although not neccessarily the same rock. Barium and lead were most likely derived from the Permian redbed arkoses while the source of the sulfur appears to be Yeso evaporites. Derivation of the sulfur probably resulted from dissolution of the rock; thus about 1.1×10^{5} m^3 (bulk density = 2.0 g/cc) of gypsum would have to be dissolved to supply the necessary sulfur. This amount is trivial when it is realized from conservative estimates that 3.2×10^{10} m^3 of gypsum are available. From Table M it can be seen that the 2.2×10^{8} kg of rock necessary for the sulfur would also yield 1.7×10^{5} kg of fluorine.

Derivation of the lead, barium and remainder of the fluorine from arkoses requires a much greater volume of rock. It is necessary to determine the mechanism by which these elements are derived from the source before any quantitative estimates can be made regarding the required mass. The above estimate of 2.5×10^{11} kg assumes that the necessary element (i.e. Pb, Ba or F) is completely leached from the source rock. However, in terms of these

Figure 36

Calculation for estimating amount of albitization of potassium feldspar and resulting concentration of lead in solution (from Beane, 1974).

estimates it seems probable that Helgeson's model is valid for the Hansonburg district. Because $^{a}Na^{+}/^{a}K^{+}$ is higher and $^{a}K^{+}/^{a}H^{+}$ is lower in Lake Lucero waters than the seawater composition used by Helgeson, it could be argued that more potassium feldspar could be destroyed than Helgeson predicted for his model.

Beane (1974) has used the data from modern Lake Lucero water compositions in conjunction with measured ratios of sodium and potassium in fluid inclusions to estimate how much lead was leached during the albitization of microcline. These estimates are summarized in Figure 36 and can be briefly reviewed as follows. The mole ratio of sodium to potassium measured in fluid inclusions from the Hansonburg district averaged about six. By letting the mole ratio of sodium to potassium in modern Lake Lucero waters represent the initial ratio of hydrothermal fluids, a value, x, could be calculated which, when subtracted from sodium and added to potassium, would make this ratio equal to the observed ratio in fluid inclusions. The value determined for x in this manner represents a necessary number of moles (per 1000 g H_2O) of potassium feldspar destroyed by albitization to produce the observed mole ratio of six. This value (0.1-0.4) indicates that between 5 and 20 ppm Pb could be leached from the arkose. The range of 0.1 to 0.4 moles is equivalent to about 28 to 111 grams of potassium feldspar. If the arkose were 5 to 10 weight percent microcline this would indicate a water-to-rock mass ratio of 0.3 to 2.0. These ratios are similar to ratios found by Taylor (1973,

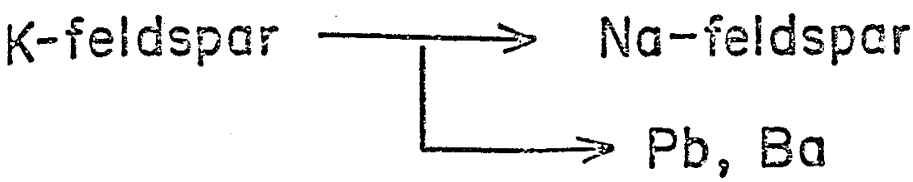

from leaching of fluid inclusions:

$$\frac{\text{moles Na}}{\text{moles K}} = 6.0$$

using water of Lake Lucero composition,

$$\frac{Na_{init} - X}{K_{init} + X} = 6.0$$

X = moles of K-feldspar albitized

$$= 0.1 \rightarrow 0.4 \ \frac{\text{moles K-feldspar}}{1000 \text{ gm } H_2O}$$

50 ppm Pb in K-feldspar

$\longrightarrow$ 5-20 ppm Pb in solution

p. 7-8) for another meteoric-hydrothermal mineral deposit.

The trend of this study has been to keep the numbers conservative; therefore, it will be assumed that a fluid containing 1 ppm Pb can be derived from the destruction of feldspar (Helgeson, 1967, p. 337). As the ratio of Pb:Ba is about 1:18 in the arkoses, it can be expected that the fluid would also contain about 18 ppm Ba. This is based on the assumption that most of the lead and barium are in the K-feldspar. Helgeson (op. cit.) assumed equilibrium was reached between fluid and rock phases in the course of alteration and that in doing so each 1000 grams of water destroyed 40 grams of potassium feldspar, producing 1 ppm lead in solution. If the fluid contains 1 ppm lead and the deposit contains about 6×10^6 kg lead then the minimum amount of fluid necessary is 6×10^{15} g or (assuming 1 g = 1 cc) 6×10^{15} cc. Darcy's law in its simplist form indicates what amount of time and permeability are required to move this much water through the mineralized area:

$$Q = KA \frac{dh}{dl} .$$

This equation states that the flow rate, Q is equal to the product of the cross sectional area, A, through which flow occurs, the hydrologic gradient dh/dl, and the hydrologic conductivity of the sediments K. Table O shows some representative values of K for different aquifers. Letting $A = 2.5 \times 10^{10}$ cm^2, $K = 10^2 \frac{cc/day}{cm^2}$, and dh/dl = 0.01, yields a flow rate of 2.5×10^{10} cc/day. This statement indicates that hydrologically, the Hansonburg mining district may

Table O Permeabilities which may be expected for different aquifers (modified from Davis and DeWiest, 1966; p. 164).

Aquifer	K, cm/sec	k, darcy's	k, gpd/ft^2	K, $\frac{cc/day}{cm^2}$
Gravel	$1 - 10^2$	$10^3 - 10^5$	$10^4 - 10^6$	$10^5 - 10^7$
Clean Sand (good aquifer)	$10^{-3} - 1$	$1 - 10^3$	$10^1 - 10^4$	$10^2 - 10^5$
Clayey sand, fine sand (poor aquifer)	$10^{-6} - 10^{-3}$	$10^{-3} - 1$	$10^{-2} - 10^1$	$10^{-1} - 10^2$

have formed in about 600 to 700 years. Beane (pers. comm., 1974) calculates that magnetite mineralization associated with nearby dikes and sills required a period of about seven to eight hundred years.

Regional hydrologic considerations

Hubbert (1940) presented the first comprehensive picture of regional ground-water motion but little else was published in this field until Toth's (1962) study of small groundwater basins. Toth (op. cit.) shows the effect which the distance to the lower impermeable boundary (i.e. depth of the basin) has on the flow pattern and modified the model to account for basins of variable extent and influence (1963). Figure 37 shows how basins of local and intermediate rank can be superimposed on the regional system. Note that in Figure 37 ground-water divides are not vertical and discontinuous but rather are curved, generally convex downward and begin and end at the water table. One feature which can be pointed out is that this treatment does not allow for the presence of connate water, "connate" implying water which was buried with the rocks and remained trapped in the pore space. This model indicates that as long as the water table is inclined anywhere within a basin, all of the water within the basin will be in motion.

Freeze and Witherspoon (1966, 1967, and 1968) show the influences of water-table irregularities and basin anisotropy and inhomogeniety on flow patterns. This series of papers considers a number of different geometries and variable permeabilities; one example appears in Figure 38.

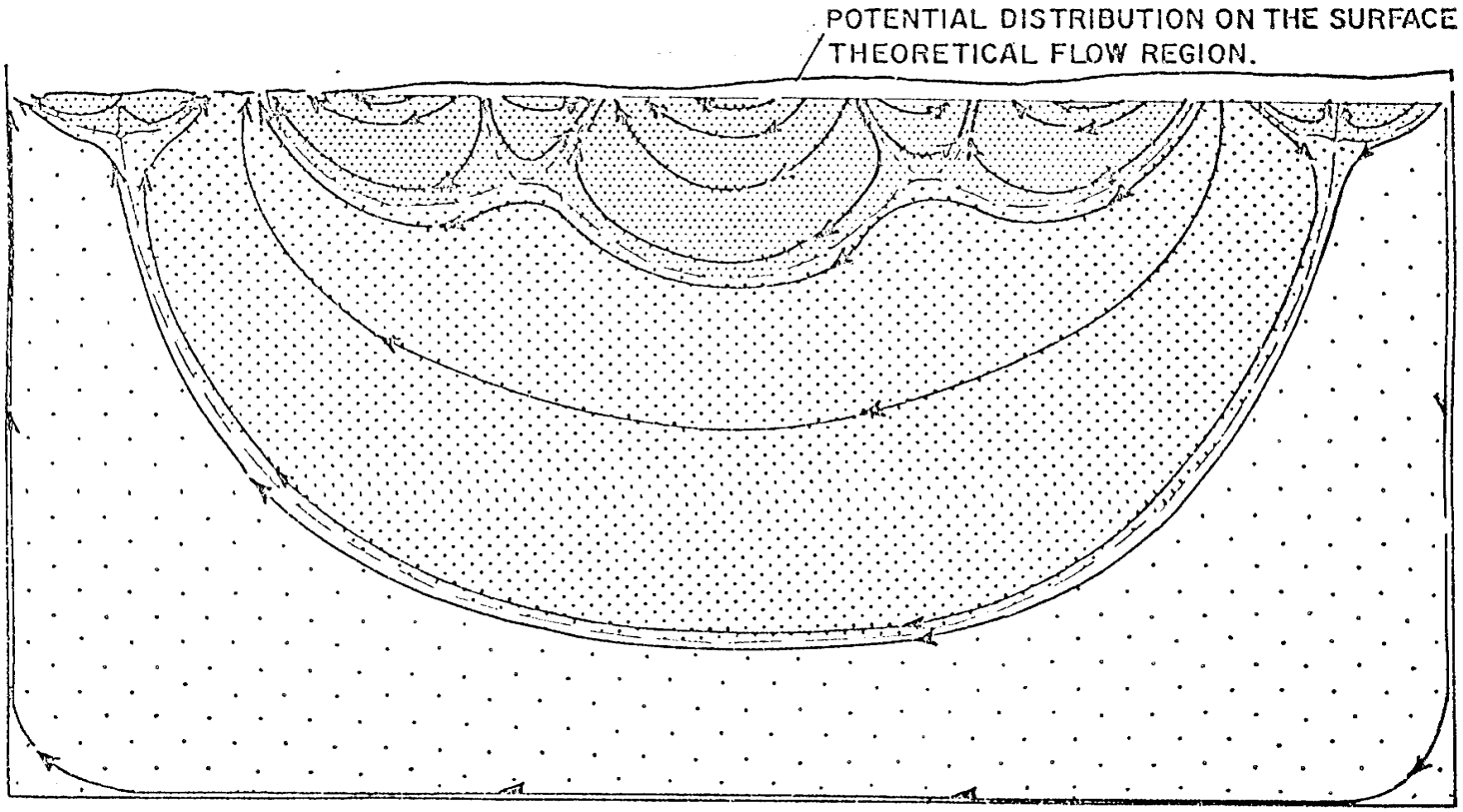
POTENTIAL DISTRIBUTION ON THE SURFACE OF THE THEORETICAL FLOW REGION.
BOUNDARY BETWEEN FLOW SYSTEMS OF A DIFFERENT ORDER
BOUNDARY BETWEEN FLOW SYSTEMS OF A SIMILAR ORDER
LINE OF FORCE
REGION OF LOCAL SYSTEM OF GROUNDWATER FLOW
REGION OF INTERMEDIATE SYSTEM OF GROUNDWATER FLOW
REGION OF REGIONAL SYSTEM OF GROUNDWATER FLOW

Figure 37

Theoretical flow pattern for a series of superimposed flow systems. Note how boundaries between flow systems are continuous and curvilinear. (from Toth, 1963).

Figure 38

chematic diagram showing the effects layering and
nisotropy on regional flow patterns. Note how
ischarge is concentrated in a very small region
elative to the total basin. (from Freeze and Witherspoon,
967).

K_h = permeability in horizonal direction

K_v = permeability in vertical direction

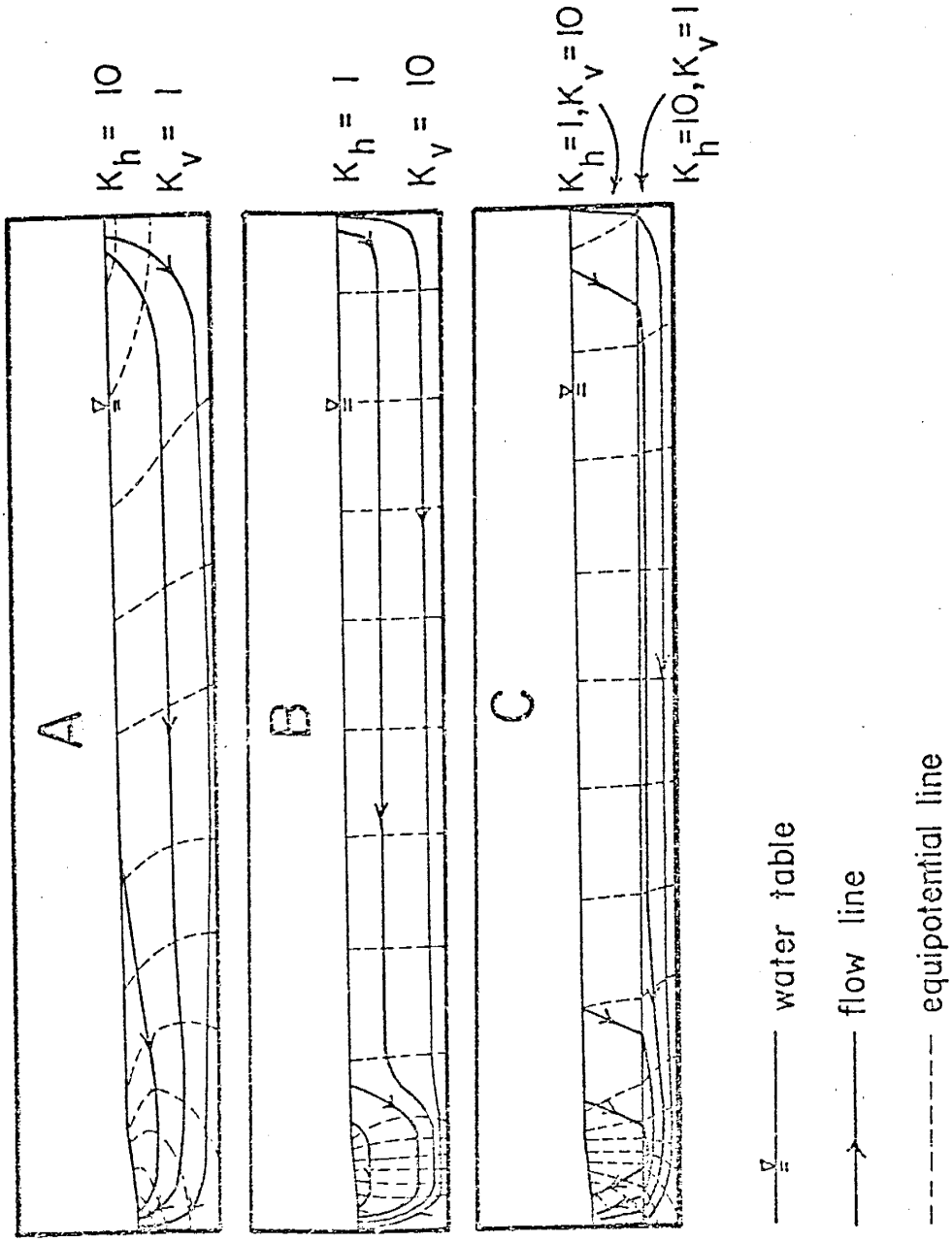
A
$K_h = 10$
$K_v = 1$
B
$K_h = 1$
$K_v = 10$
C
$K_h = 1, K_v = 10$
$K_h = 10, K_v = 1$
water table
flow line
equipotential line

The relative amount of movement is indicated by the spacing of the equipotential lines: the closer these lines - the higher the rate of ground-water flow. Many of their models show interesting patterns and should be of interest to studies involved with ground water, basin brines, petroleum geology, hydrogeochemistry and hydrothermal processes. The quantitative patterns they have derived will be used in a qualitative sense here to approximate hypothetical flow patterns for mid-Tertiary times in the vicinity of the Hansonburg mining district. Qualitative estimates are the best which can be made, because it is impossible to accurately determine the attitude and shape of the mid-Tertiary water table. Consequently the following model is not rigorously defined, but instead, is intended to represent, in a general way, mid-Tertiary flow patterns areally related to the Hansonburg mining district.

Hypothetical model of mid-Tertiary flow patterns

There are serious uncertainties in the direction of regional ground-water motion which may never be accurately known. It is possible that regional groundwater movement would be from west to east at the onset of Tertiary times because of the regional Laramide uplift to the west. This flow pattern may have been significantly modified during late Eocene erosion and very certainly by later Tertiary extension and faulting. Thick accumulations of Sierra Blanca volcanics may have caused regional ground-water movement to be reversed relative to the Laramide flow regime in the vicinity of Carrizozo and westward. It is equally

difficult to evaluate the north-south vector of ground-water flow; however, Beane (pers. comm., 1974) believes that the asymmetry of magnetite mineralization around mid-Tertiary dikes suggests a strong south-to-north component.

Thus, there is much uncertainty in the hydrologic model which is related to a poor knowledge of how paleotopography responded to changing tectonic conditions. Figure 39 is a schematic cross-section drawn approximately east-west through central New Mexico and represents a possible interpretation of mid-Tertiary flow patterns related to the Hansonburg district. For simplicity, Paleozoic rocks and Precambrian rocks are considered to be homogenous within themselves. A considerable permeability contrast between these two units is indicated by the refraction and spacing of flow lines. The complexities of fluid flow through fractures was eliminated by considering fault zones as tabular bodies of high anisotropic permeability.

Thus, the hot ascending fluids at Hansonburg may be explained in terms of discharging meteoric waters heated by passage through hot rocks in a high geothermal gradient. Similar flow patterns have been suggested as being responsible for the accumulation of high dissolved solids in groundwaters and even for the accumulation of evaporite deposits (Williams, 1970; Allmendinger, 1971). Therefore it is not unreasonable to assume that part of the high dissolved-solids content of the fluids was genetically related to this model.

Figure 39 shows that the White Store Permian section was located in a recharge area east of the mining district.

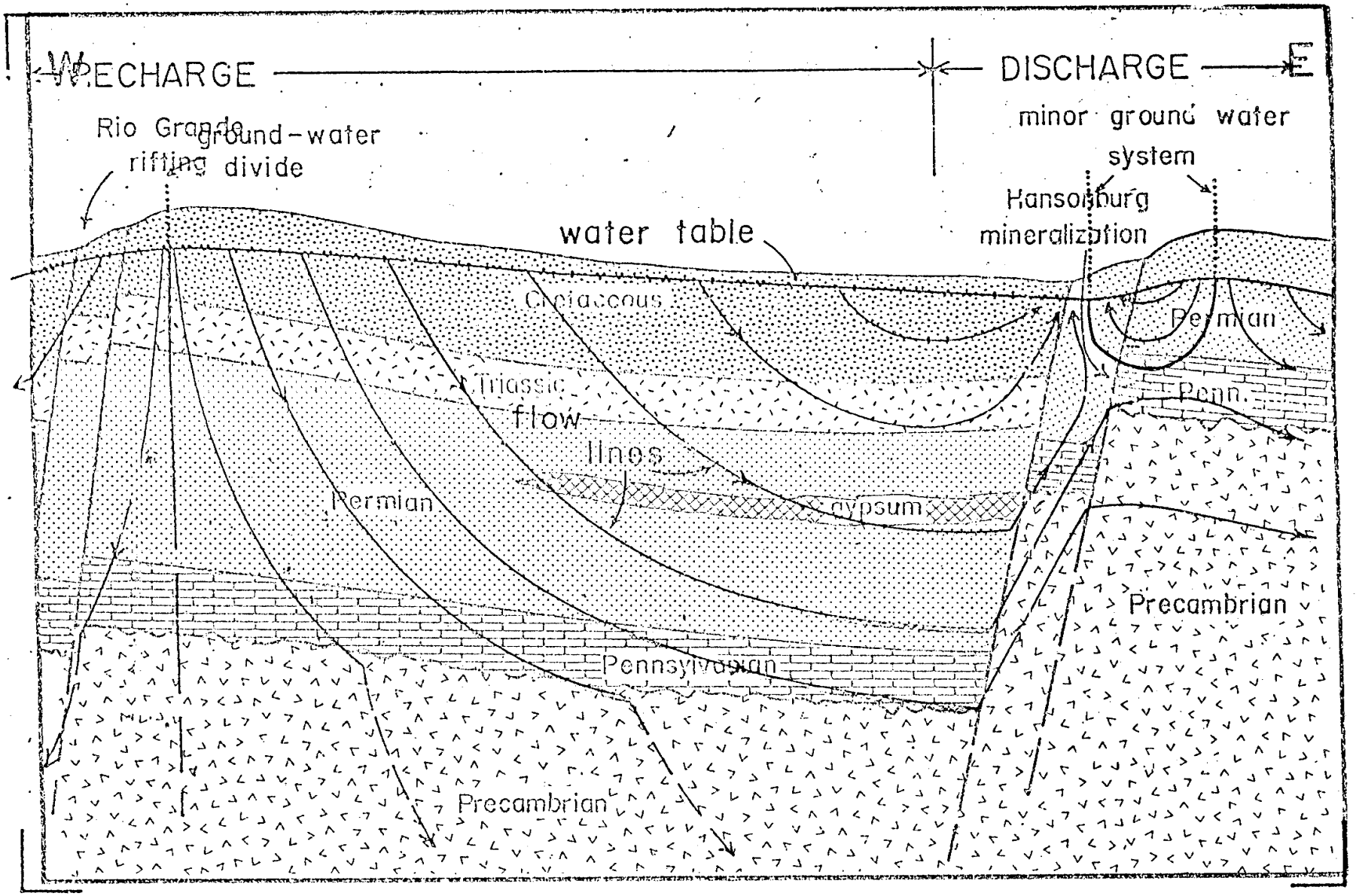
W
RECHARGE
DISCHARGE
E
Rio Grande rifting
ground-water divide
minor ground water system
Hansonburg mineralization
water table
Cretaceous
Permian
Triassic
Penn.
flow lines
gypsum
Permian
Precambrian
Pennsylvanian
Precambrian

Figure 39

Generalized cross section (east-west) through central New Mexico showing the relationship between a theoretical flow pattern and a reconstructed stratigraphic section. Flow patterns incorporate the ideas illustrated in Figures 37 and 38 and show how the discharge area is concentrated in a small region. Note how flow lines originating from widely separated regions are localized by a high vertical permeability in the fault zone. Flow lines are dashed where flow rates are very low or uncertain.

Figure 40

Qualitative illustration showing how a dynamic regional groundwater flow system may affect the distribution of the geothermal gradient. Isotherms are depressed and compressed in the recharge zone where cold ground water is migrating downward. A "thermal plume" results where hot ground water is migrating rapidly upward in the fault zone. This "plume" is elongated in the direction of high permeability.

This recharge area is shown as being part of a local system because Figure 39 depicts a regional movement from west to east. If the regional component were from east to west then the same recharge area would be part of a regional system and there would exist a minor system on the westward side of the faulting. In both instances; however, the discharge area would be located above the faults where the water table is concave upwards. In either instance, it appears likely that the rocks sampled across the White Store Permian section did in fact interact to some degree with waters which eventually became incorporated into the hydrothermal system. One might assume, then, that these rocks were somewhat higher in the ore-forming constituents prior to mineralization.

The influence of regional ground-water patterns on the geothermal gradient may be significant. Figure 40 is a qualitative representation of how the movement of ground water may alter isotherms in saturated permeable portions of the Earth's crust. This qualitative model has some validity if it can be demonstrated that the amount of heat transported by ground water is of the same order of magnitude or greater than the amount of heat conducted towards the Earth's surface per unit area. Four or five heat flow units (10^{-6} cal/cm^2 - sec) represents an abnormally high heat flow. Table O indicates the amounts of ground-water flow which might be expected in certain types of aquifers; column four shows the metric equivalent of column three and allows comparison of ground-water flow data with heat flow

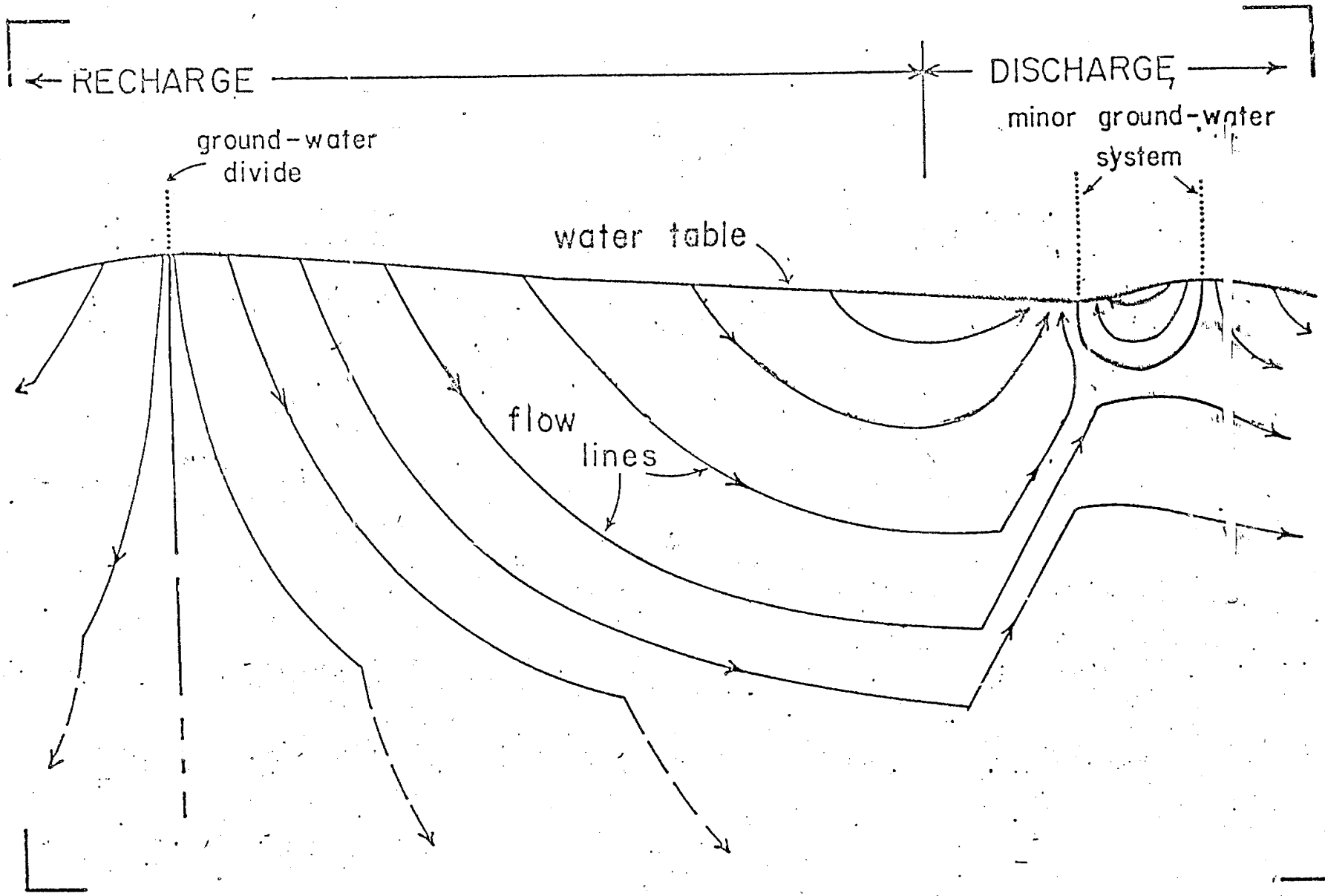
RECHARGE
DISCHARGE
ground-water divide
minor ground-water system
water table
flow lines

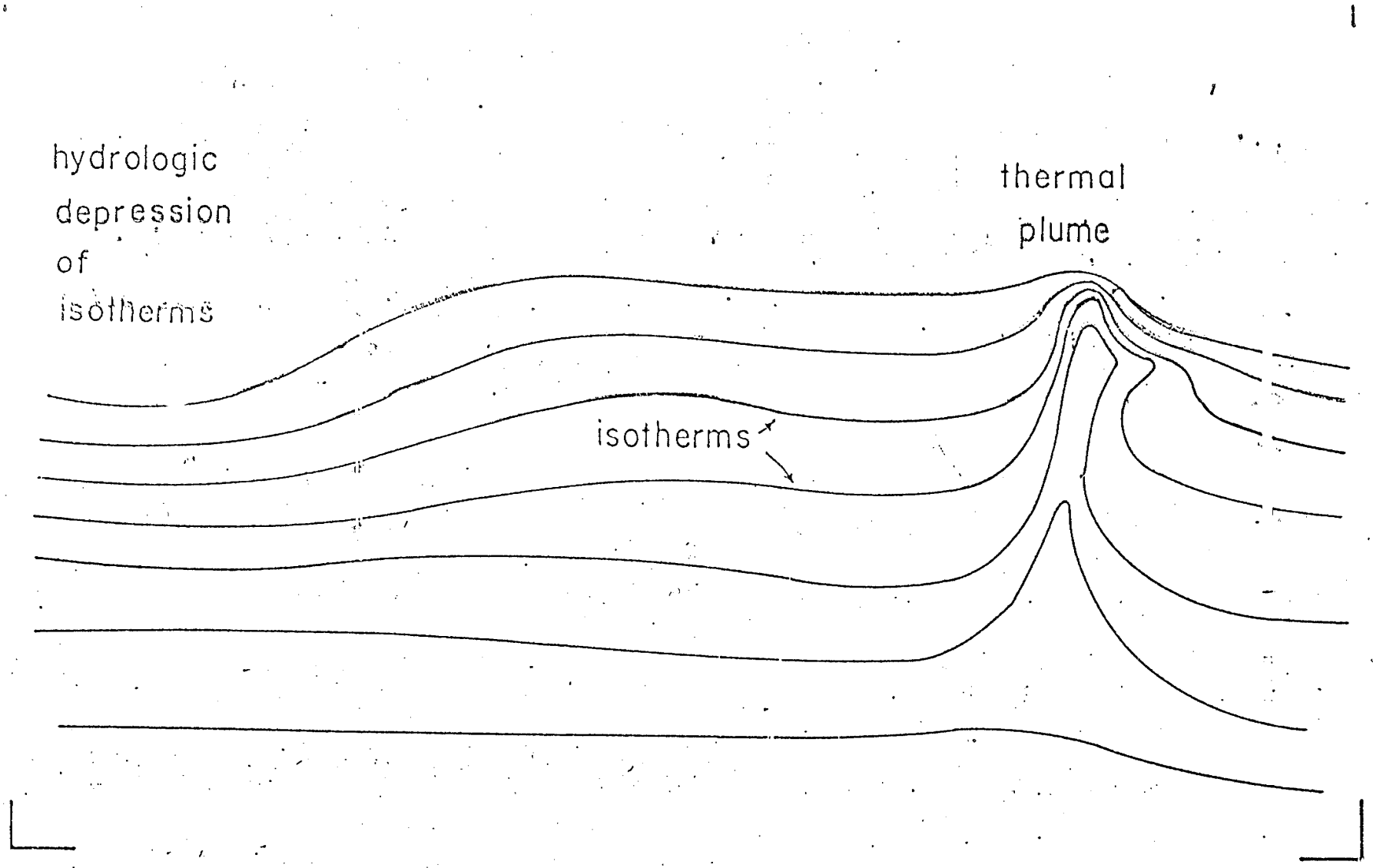
hydrologic
depression
of
isotherms
thermal
plume
isotherms

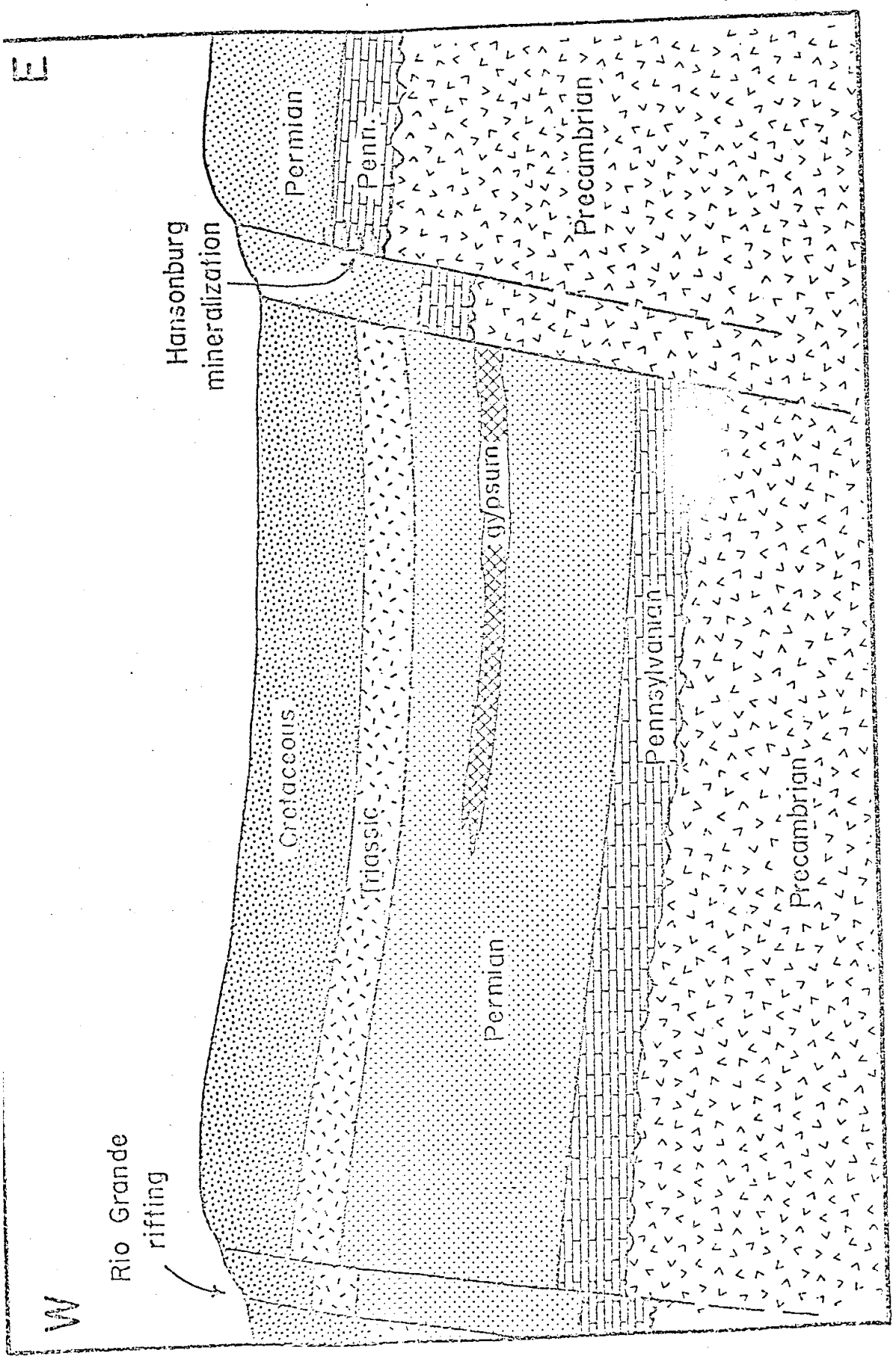
W
E
Rio Grande rifting
Hansonburg mineralization
Permian
Penn.
Precambrian
Cretaceous
Triassic
gypsum
Permian
Pennsylvanian
Precambrian

data. Using the lowest values in Table O and assuming that water has a heat capacity of 1 cal/g, it can be seen that the heat transfer by moving ground water is comparable to that of normal conductive heat flow across the geothermal gradient. Areas of faulting and open channels, such as those observed in mineralized zones throughout the Hansonburg district, should be expected to have very high vertical permeabilities and thus, heat transfer in these zones could be orders of magnitude higher than the regional heat flow. Such a process could result in a thermal plume similar to those observed in modern geothermal systems (c.f. Olmstead and Van Denburgh, 1974; Wallenburg, 1974; and Dutcher et al., 1972). Figure 40 shows a thermal plume in the vicinity of the fault zone at the Hansonburg mining district. This plume allows high temperatures and low gradients upward and along the fault zone but steep gradients across the zone and near the top of the system.

Evidence from lead isotopes

Slawson and Austin (1960, 1962) studied the isotopic composition of leads from a number of deposits within and outside the Hansonburg district. The locations of these deposits are shown in Figure 41. These deposits were classified as anomalous lead deposits, old lead deposits, and modern lead deposits (op. cit., 1962), and $^{206}Pb/^{204}Pb$ vs. $^{207}Pb/^{204}Pb$ relative isotope abundances are plotted on Figure 42. Figure 42 shows a linear relationship with a small degree of scatter, which indicates an age of about 1515 million years for the radiogenic lead (Slawson &

Figure 41

Index map of New Mexico showing location of lead isotope studies made by Slawson and Austin (1962).

Roman numerals - old leads
Arabic numerals- modern leads
Letters - anomalous leads

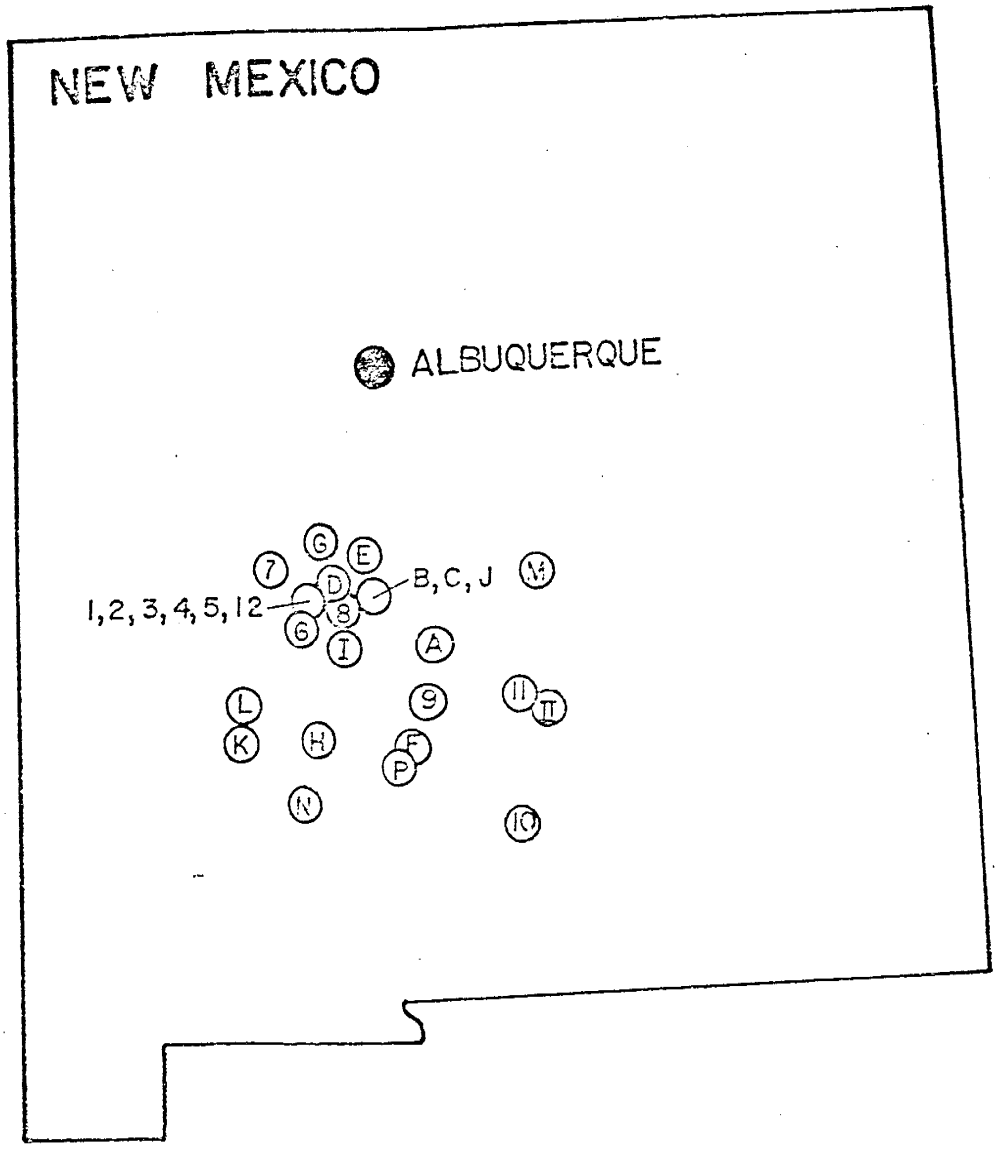

ROMAN NUMERALS - OLD LEADS

ARABIC NUMERALS - MODERN LEADS

LETTERS - ANOMALOUS LEADS

Figure 42

$^{206}Pb/^{204}Pb$ versus $^{207}Pb/^{204}Pb$ for deposits shown in Figure 41. Modern leads are those clustered around the zero isochron, anomalous leads are those shifted toward the right, and those shifted to the left are the old leads.

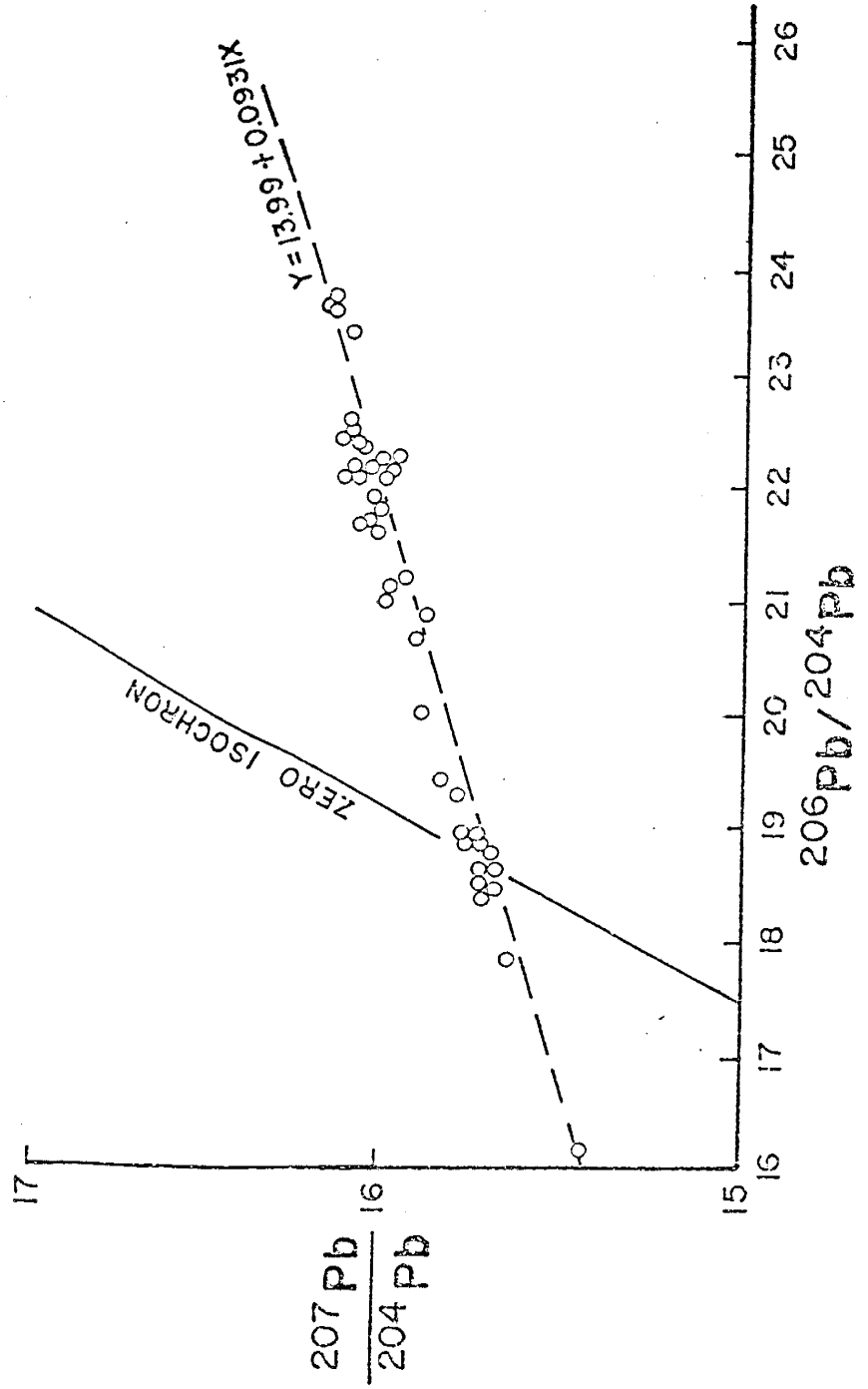
Y=13.69+0.0931X
ZERO ISOCHRON
$\frac{207Pb}{204Pb}$
$206Pb/204Pb$
17
16
15
16
17
18
19
20
21
22
23
24
25
26

Austin, 1962). The "zero isochron" line of Figure 42 is defined by meteoric leads and is used to indicate the location of modern leads. Samples which lie far to the right of this line are defined as anomalous leads. These leads contain abnormally high amounts of radiogenic leads, are not datable, and indicate a multistage origin (compare with Figure 16).

Doe (1970, p. 55) states that lead isotopic composition of sediments is a function of the source areas for the sediments because the source rocks contain significant amounts of uranium and thorium relative to lead. Also, well-mixed sediments tend to be isotopically uniform but radiogenic, even if the source is Precambrian in age. Further (and of considerable consequence to this study),

> "the isotopic composition in the insoluble residues of these sediments, all roughly of the same sedimentation age, appears to be more a function of grain size but which may in reality be more a function of K-feldspar content. The coarse fractions are less radiogenic than the silt- or clay-sized fractions, and the lead isotope ratios still reflect the Precambrian ancestry of the detritus (Muffler and Doe, 1968). The finer fractions of detritus approach more closely the isotopic composition of the HCl-soluble fraction."

The above statement from Doe is support for an earlier statement made by Austin and Slawson (1961) who suggest that radiogenic lead is interstitial and hence more mobile than the common leads trapped in feldspars. It is suggested here that these anomalous leads in central New Mexico resulted from mixing of interstitial radiogenic lead (from

uranium-bearing, Permian arkoses) with normal leads which were hydrothermally leached from the feldspars in the arkose. Furthermore Austin and Slawson (1961, p. 1135) noted that the isotopic composition of lead in selected galena cubes from the Hansonburg district decreased from the core outwards. They concluded

> ". . . that the lead isotope composition of the ore fluids definitely underwent measurable changes with time. The mineralizing solutions contained somewhat less radiogenic lead as time progressed, thus causing a decrease in the radiogenic content of the lead deposited."

Slawson and Austin (1960) note a consistent variation in the areal distribution of isotopic compositions; radiogenic lead was found to increase from west to east. This asymmetry may reflect the asymmetry of the flow patterns shown in Figure 39.

These observations appear to support the hypothesis that the lead was derived from the Permian arkose and is compatible with the proposed hydrologic model. This model would supply the mineralized region with the more mobile, radiogenic leads first, followed by progressively less radiogenic leads derived from the alteration of potassium feldspars. Thus, both the sulfur isotope data described earlier and the lead isotope data support a sedimentary source for these elements. Further, the isotopic composition of the lead in galena crystals supports the dynamic aspects of a regional hydrologic model.

Thus, about 4 to 7.6 km^3 of dike rock, cooling by 300° C, is required to produce the calories needed to heat the hydrothermal fluids to 200° or 300° C. This is equivalent to 80 to 150 dikes or sills having dimensions of 10 m x 1 km x 5 km distributed through the basin. Although this estimated volume of rock necessary to fulfill the temperature requirements is about an order of magnitude higher than that observed in the field, it is apparent that some significant quantities of heat could be added to the system in this manner. It is likely that the presence of a thin crust and (or) nearby batholiths were a more significant heat source. Chapin (pers. comm., 1975) notes that central New Mexico was underlain by a batholith in the Oligocene. Although the eastward extent of this batholith is unknown, it must have extended at least as far east as the Magdalena Range because of the major cauldron there and the abundance of the stocks in the Magdalena area (Chapin, op. cit.). In addition, another batholith existed to the east in the Sierra Blanca area where regional extension, beginning at about 29 million years ago, broke the roofs of these batholiths with abundant normal faults.

Thus, it seems probable that ground water entering the hydrologic regime in the vicinity of the Rio Grande rift would migrate through approximately 2650 meters of sediments and a high geothermal gradient. Thermal gradients might have been 2 or 3 times higher than "normal" gradients (0.33×10^{-3} °C/cm) thus causing temperatures near the bottom of the system to be as high as 195° to 280° C. A

A "normal" geothermal gradient would maintain temperatures at about 107° C at this depth. Transfer of some of this heat would occur as ground water moved from recharge to discharge area and thus add to high heat flows in the vicinity of the Hansonburg mining district.

Mechanisms of precipitation

A source for the ore-forming constituents has been suggested and a model described which would bring these constituents together in a hydrothermal environment. To complete the model, it is necessary to show that sufficient means existed to induce precipitation of the constituents from the transporting fluid. Figures 39 and 40 show two changes which an increment of fluid would encounter upon entering the proposed ore zone. First, the host rock composition changes abruptly from a silicate assemblage to a carbonate sequence and, second, temperatures rapidly decrease across the mineralized region. A third change which may be important but which is not illustrated in the figures is that fluid flow in the undisturbed and unmineralized regions is primarily laminar flow through a porous medium. This is probably not true in the faulted, mineralized zones where open spaces are common; in these zones it is likely that fluid movement was primarily tubular or fracture flow. These three parameters could, individually or collectively, cause precipitation of the minerals observed in the ore zones.

The effect of temperature has already been mentioned at several points. First, Figures 29, 20, and 21 were

Source of the energy

Using the estimates (p. 125) of a solution containing 1 ppm lead and 18 ppm barium together with the estimates of 5.9×10^6 kgs lead and 1.1×10^8 kgs barium in the ore deposit, it was calculated that the amount of ore fluid which produced the mineralization was about 6.0×10^{12} liters (assuming that all of the barium and lead were precipitated). Thus, at least 6.0×10^{12} liters of fluid must have been heated from about 20° C (at surface) to at least 200° C prior to mineralization and possibly 300° C to 400° C. This change in temperature would require on the order of 10^{18} calories. Present-day thermal gradients are too low to account for this temperature increase in the immediate vicinity of the mining district. As Figure 40 shows, however, the fluids were moving upward in the vicinity of the mineralization.

As discussed previously the mineralization probably occurred at shallow depths owing to its position on a Laramide anticline. Overburden thickness increases westward for three reasons: 1) the Baca Formation was deposited in an early Tertiary basin; 2) downwarping of this basin preserved the Mesozoic section; and 3) the thickness of Datil volcanic rocks increases to the west. As noted earlier Baca sediments may be from 1000 to 2000 feet thick in the Carthage area. In addition, it seems likely that Datil rocks may have been on the order of 2000 feet thick (Sanford, p. 10). It appears likely, then, that the total section thickness increased from about 1100-1800

meters near Hansonburg to 2650 meters in the Carthage area. As indicated in Figure 40, the thicker sections lie in the recharge area of the model, which is marginal to the main structural zone of the Rio Grande trough. Proximity to the trough is significant, because there is evidence that it was (and indeed is) associated with high heat flow (Reiter et al., 1975). Lipman (1969, p. 1350) working with volcanic rocks in southern Colorado and northern New Mexico states that the ". . . Rio Grande rift may have been a locus of high heat flow and possibly an upward protrusion of the mantle, allowing fractionation of basalt to take place at an unusually high crustal level." Chapin (1971, Figure 4) presents a similar conceptual model where a bulge in the mantle would be expected to produce abnormally high heat flows.

Some physical constraints may be placed on the hydrothermal system to evaluate the importance of dikes and sills as a significant source of heat. A basin of two kilometers average depth, having a "normal" geothermal gradient of 33° C/km will have a base temperature of 86° C. This is about 115° C less than the maximum temperature indicated by fluid inclusions and about 215° C less than the equilibrium temperature indicated by sulfide-sulfate fractionation (see page 112). Thus, another $.7 \times 10^{18}$ to 1.3×10^{18} calories are required to bring the solution to 200° or 300° C, respectively. A typical igneous rock having a density of 2.75 g/cc, and a specific heat of 0.21 cal/g-°C will lose 173 cal/cc upon cooling from 600° to 300° C.

constructed to show the effect of temperature on the stability of a number of aqueous complexes. The multiple chloride complexes of lead and zinc rapidly become more stable with increasing temperature. Thus, if these metals were precipitating as sulfides from an aqueous chloride-rich solution with fixed sulfide (S^{2-}), it would be possible that even a small increase in temperature would cause the solution to be undersaturated with respect to those sulfides as the metal ions become partitioned into the complexed state. Figure 28 was used to show how lead complexes would respond to the conditions indicated by fluid inclusion analyses.

Figure 43 demonstrates that even the paragenesis is compatible with a thermally controlled precipitation mechanism. Curve 1 is a plot of the equilibrium constant (K) for the reaction:

$$PbS + Zn^{2+} = ZnS + Pb^{2+}$$

which is equivalent to the activity ratio: $^{a}Pb^{2+}/^{a}Zn^{2+}$. Curve 2 is a plot of the stoichiometric ion activity coefficient ratio $\dot{\gamma}Zn^{2+}/\dot{\gamma}Pb^{2+}$ along the same temperature axis, and Curve 3 is the algebraic product of these two curves or simply, the mole ratio ($^{m}Pb^{2+}/^{m}Zn^{2+}$) necessary for equilibrium between galena and sphalerite in a two molar NaCl solution. This last curve decreases with increasing temperature, indicating that for a solution with a fixed lead-zinc mole ratio, increasing temperature could cause galena to be stable relative to sphalerite. Curve 3 in Figure 43 can be used to

Figure 43

Plots of log $a_{Pb^{2+}}/a_{Zn^{2+}}$, log $\gamma_{Zn^{2+}}/\gamma_{Pb^{2+}}$, and log $m_{Pb^{2+}}/m_{Zn^{2+}}$ as a function of temperature at some fixed sulfide activity. The activity ratio corresponds to the equilibrium curve between galena and sphalerite; the stoichiometric activity coefficient ratio is for a 2.0 m NaCl solution. Multiplying these two ratios gives the mole ratio of lead and galena (curve 2) necessary to maintain equilibrium between sphalerite and galena in a 2.0 m NaCl solution. (Data from Helgeson, 1969.)

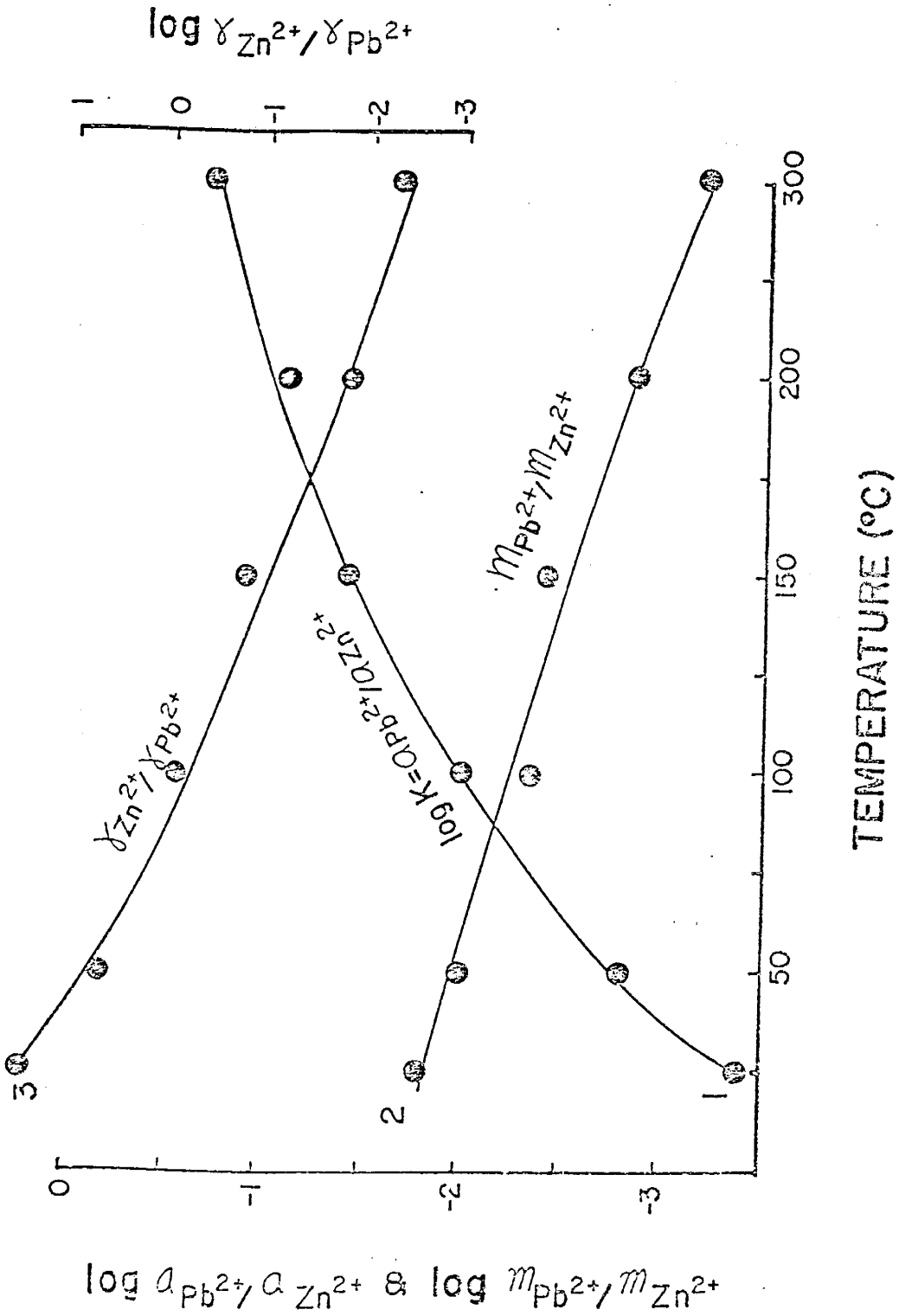
log $\gamma_{Zn^{2+}}/\gamma_{Pb^{2+}}$
1
0
-1
-2
-3
300
200
150
100
50
TEMPERATURE (°C)
$m_{Pb^{2+}}/m_{Zn^{2+}}$
$\gamma_{Zn^{2+}}/\gamma_{Pb^{2+}}$
$\log K = \log a_{Pb^{2+}}/a_{Zn^{2+}}$
3
2
1
0
-1
-2
-3
log $a_{Pb^{2+}}/a_{Zn^{2+}}$ & log $m_{Pb^{2+}}/m_{Zn^{2+}}$

.timate the permissable range of mole ratios of Pb^{2+}/Zn^{2+} ıring precipitation of galena or sphalerite from a 2 m NaCl)lution.

Aside from its effects on aqueous complex stabilities, :mperature also has a direct effect on the solubility of :nerals. Figure 24 illustrates the effect of temperature ı SiO_2 solubility and Figure 44 shows the solubility roducts for barite and fluorite at varying ionic strengths $_{m_{NaCl}}$).

The change in host-rock types probably also played an mportant role in the precipitation of the ore minerals. t is quite possible that hydrocarbons in the carbonates elped to maintain reducing conditions for the precipitation f the sulfides. Certainly, dissolution of calcite would ncrease dissolved calcium which is necessary for precipitation f fluorite. Thus, the interaction with a different rock ype could create a new chemical environment favorable to ıineral precipitation. Figure 5 indicates how pH and f_{O_2} :an influence mineral precipitation. A shift in pH or $_{O_2}$ toward the S^{2-}-dominated field could result in precipitation of a metal sulfide if sufficient quantities of :he metal were present.

Thus, any number of mechanisms or combination of nechanisms may have caused precipitation of the hydrothermal minerals. It seems likely that the decreasing temperatures predicted from Figure 40 and the change in rock type were sufficient to effect one or several of these mechanisms.

Figure 44

Fluorite and barite solubilities at various NaCl concentrations as a function of temperature (from Holland, 1967). The solubility of fluorite is plotted as milligrams CaF_2 per kilogram H_2O at several NaCl normalities. Barite solubility is plotted as the square root of the "apparent solubility product" of barite at several NaCl molalities. The apparent solubility product of barite (K'_{Bar}) is defined as:

$$K'_{Bar} = (M_{Ba^{2+}})(M_{SO_4^{2-}}).$$

BARITE
SOLUBILITY

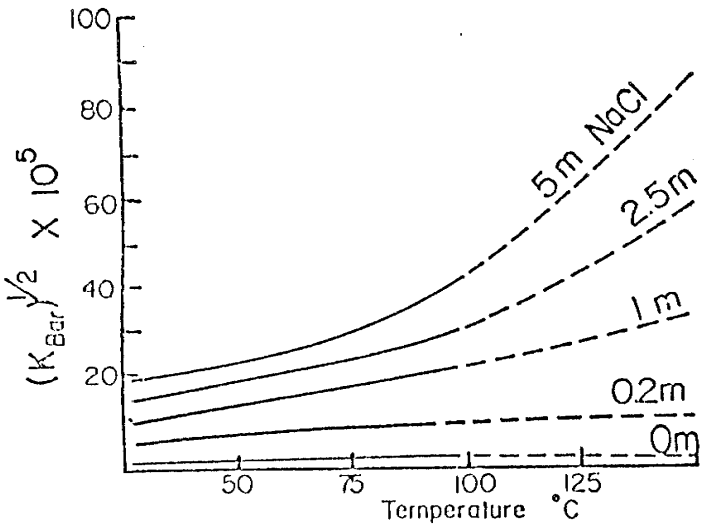

FLUORITE
SOLUBILITY

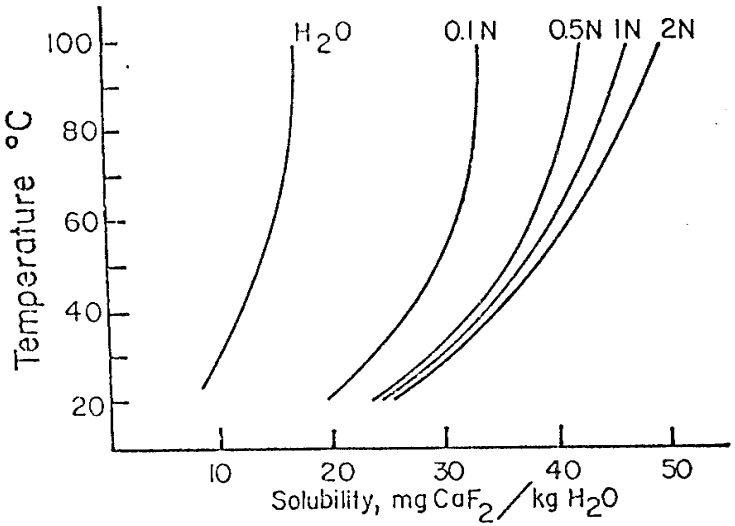

One special case might also have been important in the Hansonburg model. This is again related to the change in rock type which fluids moving from arkose to limestone would encounter. Since flow lines can not cross on a regional basis, it is unlikely that waters which derived lead, barium, and some fluorine from lower Permian arkoses as described earlier, intermingled with waters which contained high sulfate and some fluoride from middle or upper Permian evaporites. At the discharge end of this system mixing of the two waters would be much more probable as the flow lines are converging and laminar flow may give way to turbulent flow in the fault zones. Large "solution-type channels" in the limestone within which mineralization has taken place is suggestive of an open system. Communication between the two fluids was probably aided by limestone dissolution and faulting.

The 18 ppm barium is at least an order of magnitude greater than that required for saturation with barite in a solution with similar sulfate contents as those observed at Lake Lucero. This includes the fact that about 99.99% of the total barium occurs as the $BaSO_4^\circ$ complex (see Figure 11). Thus, mixing of a high-sulfate solution with the arkose-derived solution would result in precipitation of barite. It appears that a mixing model similar to one speculated upon by Roedder et al. (1968, p. 345-347), may well be responsible for much of the barite mineralization. The model presented above may explain the drop in temperature and the increasing salinity indicated by the fluid inclusion

data (Figure 25). Precipitation of barite would decrease the concentration of SO_4^{2-} in solution slightly, resulting in dissociation of some $CaSO_4^{\circ}$ complex; this would increase Ca^{2-} in solution and thus, aid in precipitation of fluorite during the final stages of mineralization. If mixing of the two fluids in a fault zone is acceptable, then zoning of a high barite-fluorite ratio in the north relative to the south may indicate fluid movement from north to south. As described earlier (p. 82), barite at the Royal Flush mine is primarily massive whereas, barite at the Blanchard mine is primarily as individual crystals or aggragates of crystals protruding into open space. A north to south component of flow could create this zoning because the first-mixed waters would precipitate the most barite while "downstream" fluids would be more depleted in the necessary constituents. However, this direction of flow is not compatible with that found by Beane (pers. comm., 1974) for the Jones Camp and Iron Horse magnetite deposits (loc. on Figure 2).

Summary of hydrothermal model

In summary then, mineralization can be related to a sequence of typical, geologic events which, together, produced the anomalous concentrations of elements in the Hansonburg district. Deeply circulating groundwater obtaining a high dissolved-solids content from Permian evaporites were heated by a high geothermal gradient. These hot brines hydrothermally altered potassium feldspars in arkosic units thus releasing ore-forming constituents

into solution where they could be transported (at high temperatures) as stable complexes. At the discharge end of the hydrologic system, these fluids would be moving upward through a decreasing temperature gradient. At this point, zinc and lead chloride complexes would become decreasingly stable thus increasing the activities of the free metal ions.

The activity of the various sulfur species would be controlled by pH and f_{O_2} as well as temperature; changes in any of these parameters could thus cause precipitation or dissolution of sulfur-bearing species. It is possible that sulfide mineralization occurred as the activities of both the metals and the sulfide increased. This stage of mineralization might have yielded to the barite stage when movement within the fault zone introduced a stratigraphically higher, cooler, and more saline fluid to the system. Mixing with the high-sulfate fluid would shift the overall fluid chemistry toward high oxygen fugacities more suited for barite precipitation. Fluorite precipitation which occurred during this mixing and later stages was influenced to a large degree by low pressures which allowed dissolution of limestone necessary for the high calcium activities. Precipitation of quartz would result throughout the mineralization sequence as a consequence of the negative temperature gradient occurring along flow lines in the mineralized zone.

COMPARISON WITH SIMILAR DEPOSITS ELSEWHERE IN NORTH AMERICA

New Mexico

There exist a number of hydrothermal deposits in central New Mexico which have physical characteristics remarkably similar to the deposits within the Hansonburg mining district, although they are of considerably smaller size. Figure 45 shows the locations of the New Mexico deposits which will be discussed in this section and Figure 46 shows the results of some preliminary fluid inclusion analyses for comparison between the deposits. The filling temperatures of these fluid inclusions show a surprisingly narrow range considering the geographic and geologic diversity of the deposits which they represent.

The Gonzales deposits are fracture fillings in Precambrian granites which have been faulted upward into contact with Pennsylvanian limestones. The similarities in mineralogy, paragenesis, fluid inclusion temperatures of the individual minerals, lithologic associations, and sulfur isotope compositions suggest a similar mode of origin for these deposits as proposed for the Hansonburg deposits. Some of these features are shown in Table P which compares several of the deposits. Figures 39 and 40 are generalized models which could be modified significantly by local structural and topographic variations. Figure 38 illustrates the importance of small-scale permeability and topographic variability to the modification of the regional system.

DEPOSIT NAME	MINERAL OCCURRENCE	HOST ROCKS	INTRUSIVE ASSOCIATIONS
HANSONBURG	open-space filling, limestone replacement	Pennsylvanian limestone and arkose	dikes and sills in vicinity
GONZALES	vein filling minor replacements	Precambrian granite	none exposed nearby
JOYITA HILLS	vein filling	Precambrian granite Tertiary volcanics	volcanic plugs in vicinity
MAGDALENA MTS.	open-space filling limestone replacement	Mississippian limestones	many stocks and dikes in vicinity
FLUORITE RIDGE	vein filling	Tertiary volcanics agglomerates basalt dikes monzonite porphyry	basalt dike, monzonite porphyry
GILA	vein filling	Tertiary volcanics	none exposed nearby
LADRON MTS.	vein filling limestone replacement	Pennsylvanian limestones	monzonite dike

DEPOSIT NAME	MINERALOGY	FLUID INCLUSION FILLING TEMP. (°C)	$\delta^{34}S$
HANSONBURG	sphalerite, barite galena, quartz fluorite, calcite	145 → 200	barite = 10.8 galena = -15.0 sphalerite= -10.6
GONZALES	sphalerite, barite galena, quartz fluorite, calcite	160 → 200	barite = 8.0 galena = -9.8 sphalerite = -10.6
JOYITA HILLS	barite, fluorite galena, quartz	190 → 205	
MAGDALENA MTS.	barite, fluorite galena, quartz	145 → 190	barite = 12.6
FLUORITE RIDGE	fluorite, quartz	155 → 165	
GILA	fluorite, quartz	130 → 250	
LADRON MTS.	barite, calcite	145 → 190	

Figure 46

Results of some preliminary fluid inclusion homogenization studies for several deposits mentioned in text. Only five to ten good primary inclusions were studied from each deposit, and therefore this preliminary work should not be considered definitive but rather a first approximation to the actual temperature of formation. No freezing temperature determinations were made and no pressure corrections have been applied.

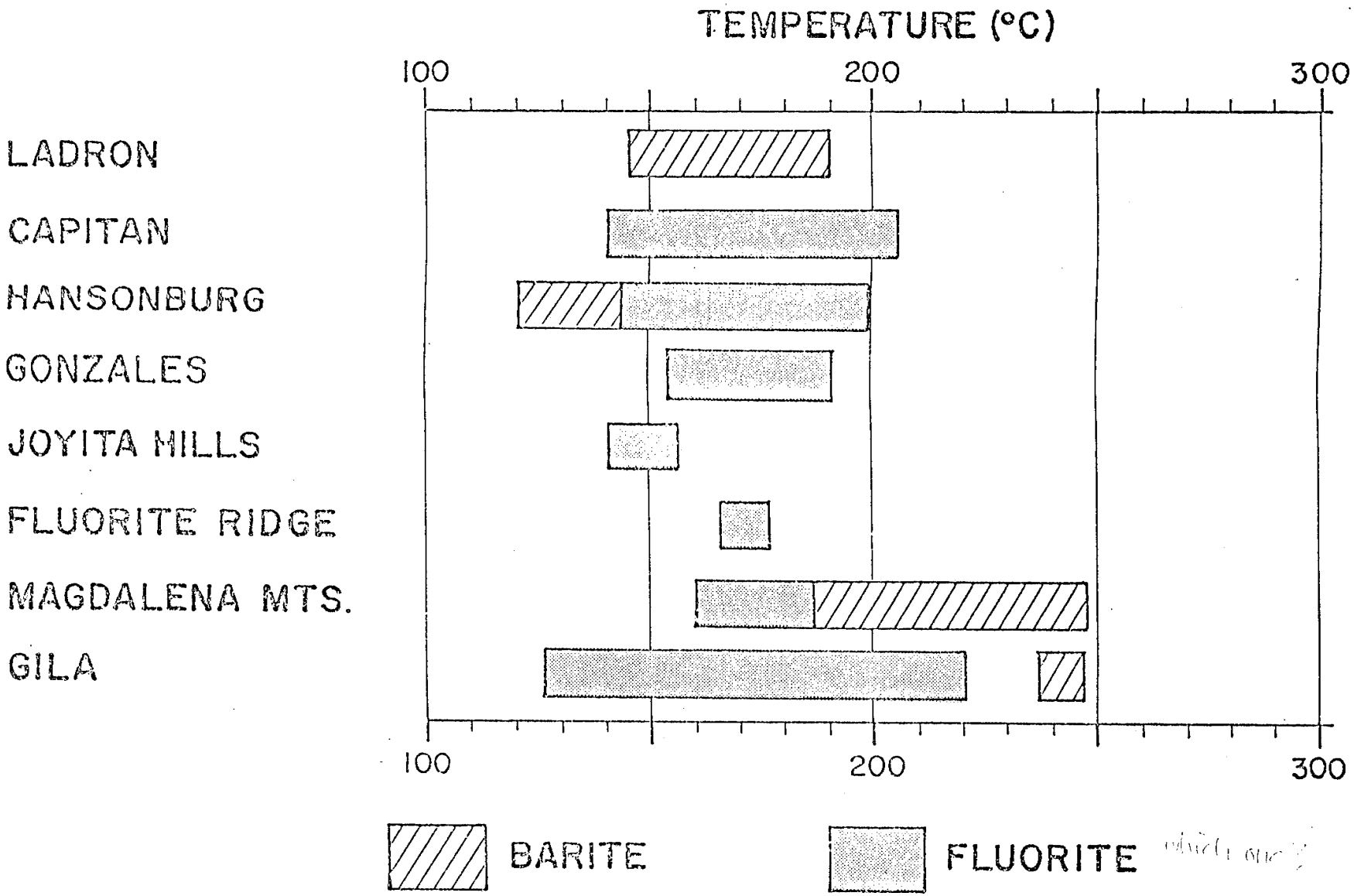
TEMPERATURE (°C)
100
200
300
LADRON
CAPITAN
HANSONBURG
GONZALES
JOYITA MILLS
FLUORITE RIDGE
MAGDALENA MTS.
GILA
100
200
300
BARITE
FLUORITE

It appears reasonable from structural evidence to suggest that the east border region of the rift zone, at the latitude of Socorro, has had a topography of small basins and ranges since rifting began, and that there were many local hydrologic basins superimposed on the regional model in this area of high heat flow. Such local basins were instrumental in the formation of small deposits such as the Gonzales hydrothermal system.

The same arguments apply to the small deposits scattered throughout the Joyita Hills about ten to fifteen miles northward in the same structural-tectonic zone. In the Joyita Hills local thermal anomalies may have been more important than at Hansonburg or Gonzales since there are a few plugs and sills in the area (Arendt, 1971, p. 56). However, all deposits in the district are areally related to Precambrian granitic rocks. Lasky (1932, p. 58-59) states that

> "No ore has been found in either the sedimentary or volcanic rocks more than a few feet distant from the contact with the pre-Cambrian. So far as could be determined this relationship seems to be due to structural control. Mineralization apparently occurred in Tertiary time contemporaneously with and also slightly following the faulting which exposed the granite core."

Lasky's description could be applied to the general features of the Gonzales prospect as well.

The Hansonburg, Gonzales and Joyita Hills districts may represent one end-member type of hydrothermal mineral deposits common to central New Mexico. This "type" deposit is characterized as the end result of a large hydrothermal fluid

system which acquired its heat and chemical constituents from a large volume of permeable rocks. The effects of such a system are not obvious in the source or recharge area. The effects do become obvious in the discharge region where flow lines are converging and the results of "abnormal" temperatures and solution chemistries become more pronounced. Such is the case at Hansonburg where the Bursum Formation has been hydrothermally altered by the hot, NaCl-rich basin waters where they were discharging upward along the permeable fault zone(s).

Obviously, a number of prerequisites must be met to make this a viable model for ore deposition. These are: 1) a source rock, 2) an energy source, 3) chemical and physical interaction between source rock and fluid, 4) a fluid chemistry capable of transporting the ore constituents, 5) a hydrologic system capable of directing the fluid to the host rock, and 6) an appropriate environment for mineral precipitation. This combination of requirements does not seem so improbable when all the possibilities of the basin and range province are considered. Many such systems exist today but are lacking one or more of the requirements; however, saline lakes and playas are evidence that the appropriate hydrologic systems exist. Socorro Hot Spring and the Salton Sea as described earlier are a step closer in that both have the energy source, but the Socorro Spring system lacks interaction with the appropriate source rock and the Salton Sea lacks the necessary "plumbing" at the discharge end. Indeed, wells which have been drilled for

geothermal power in the Salton Sea area are complicated by deposition of material which if present in sufficient amounts would constitute an ore deposit. Skinner and others (1967, p. 318) indicate that 5 to 8 tons of metal-rich scale precipitated inside casing and discharge pipes in one test well during a three-month period. Table Q is reproduced from their communication and indicates the potential that system has as an ore-producer.

Although the hydrologic system proposed above for a few deposits in central New Mexico seems valid, it is not intended to suggest that all hydrothermal barite-fluorite-sulfide deposits were formed by the same mechanism. As stated previously, this model is considered to be only one end-member of a series of possible mechanisms which are capable of producing similar deposits. Figure 47 and 48 show the location of most of New Mexico's barite and fluorite occurrences relative to outcrops of Precambrian rocks and Chapin's (1971) concept of the extent of the Rio Grande rift zone. Both minerals seem to follow the rift zone quite well and fluorite shows a stronger correlation with Precambrian rocks than does barite. Part of this correlation may exist because the rifting with which many of these deposits are associated has been the mechanism for exposing the Precambrian rocks.

The good correlation with Precambrian rocks and the rift zone is compatible with the model proposed for Hansonburg. Precambrian rocks are the source of the sediments which are the source of the lead, barium, and fluorine while the rift

Table Q Quantitative X-ray fluorescence analyses and mineralogical contents of sulfide-rich scale from No. 1 IID well. asp=arsenopyrite, bn=bornite, cc II=dense Cu_2S, cp=chalcopyrite, dg=digenite, py=pyrite, strm=stromeyerite, td=tetrahedite. (from Skinner et al., 1967).

Weight Percent

Sample No.	Cu	Ag	Fe	As	Sb	S
W-769 (1) 220±30°C	10.0	1.3	3.8	0.23	1.05	6.6
W-769 (2) "	43.6	5.8	7.1	0.15	0.69	22.5
W-767 (1) 170±30°C	14.0	1.2	15.7	0.20	0.52	10.2
W-767 (2) "	27.5	3.1	8.6	0.13	0.66	13.4
W-767 (3) "	23.6	1.0	10.6	0.13	0.57	12.8
W-768 (1) 130±20°C	10.1	1.0	25.4	0.30	0.55	9.9
W-768 (2) "	13.4	1.2	18.8	0.23	0.53	10.8
W-768 (3) "	19.2	1.6	11.3	0.15	0.56	12.2
W-768 (4) "	12.4	1.6	14.0	0.15	0.53	10.9
W-768 (5) "	11.5	2.1	12.0	0.14	0.45	11.6
W-768 (6) "	28.2	3.4	9.8	0.11	0.55	14.2

Weight Ratios

Sample No.	Metals/S	Cu/Ag	Sb/As	Mineral Content
W-769 (1) 220±30°C	2.47	8.9	4.6	bn, cp, Ag
W-769 (2) "	2.55	7.5	4.6	bn, cp, cc II, asp, Ag
W-767 (1) 170±30°C	3.10	11.7	2.6	dg, py
W-767 (2) "	2.98	8.9	5.1	bn, cc II, Ag
W-767 (3) "	2.80	23.6	4.4	dg, bn
W-768 (1) 130±20°C	3.78	10.1	1.8	dg, trace td
W-768 (2) "	3.17	11.2	2.3	dg, trace td
W-768 (3) "	2.69	12.0	3.7	dg, bn, py
W-768 (4) "	2.63	7.8	3.5	dg, bn
W-768 (5) "	2.26	5.5	3.2	dg, strm
W-768 (6) "	2.96	8.3	5.0	bn, cp, cc II, strm, Ag

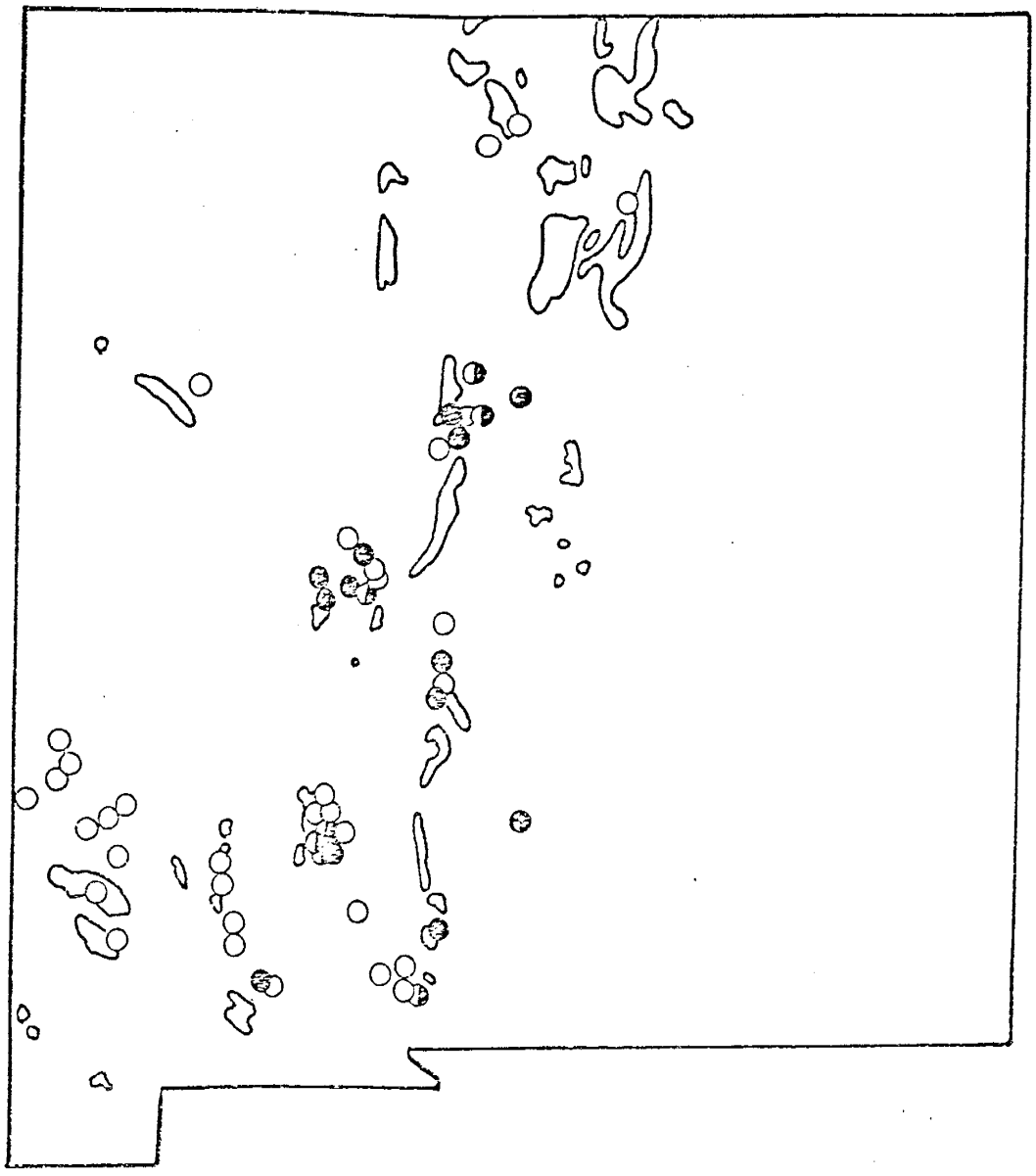

) FLUORITE ⓕ BARITE-FLUORITE ● BARITE

Figure 47

Location of most of New Mexico's barite and fluorite occurrences relative to outcrop patterns of Precambrian rocks in the state.

Figure 48

Location of most of New Mexico's barite and fluorite occurrences relative to the outline of the Rio Grande rift zone as defined by Chapin (1971).

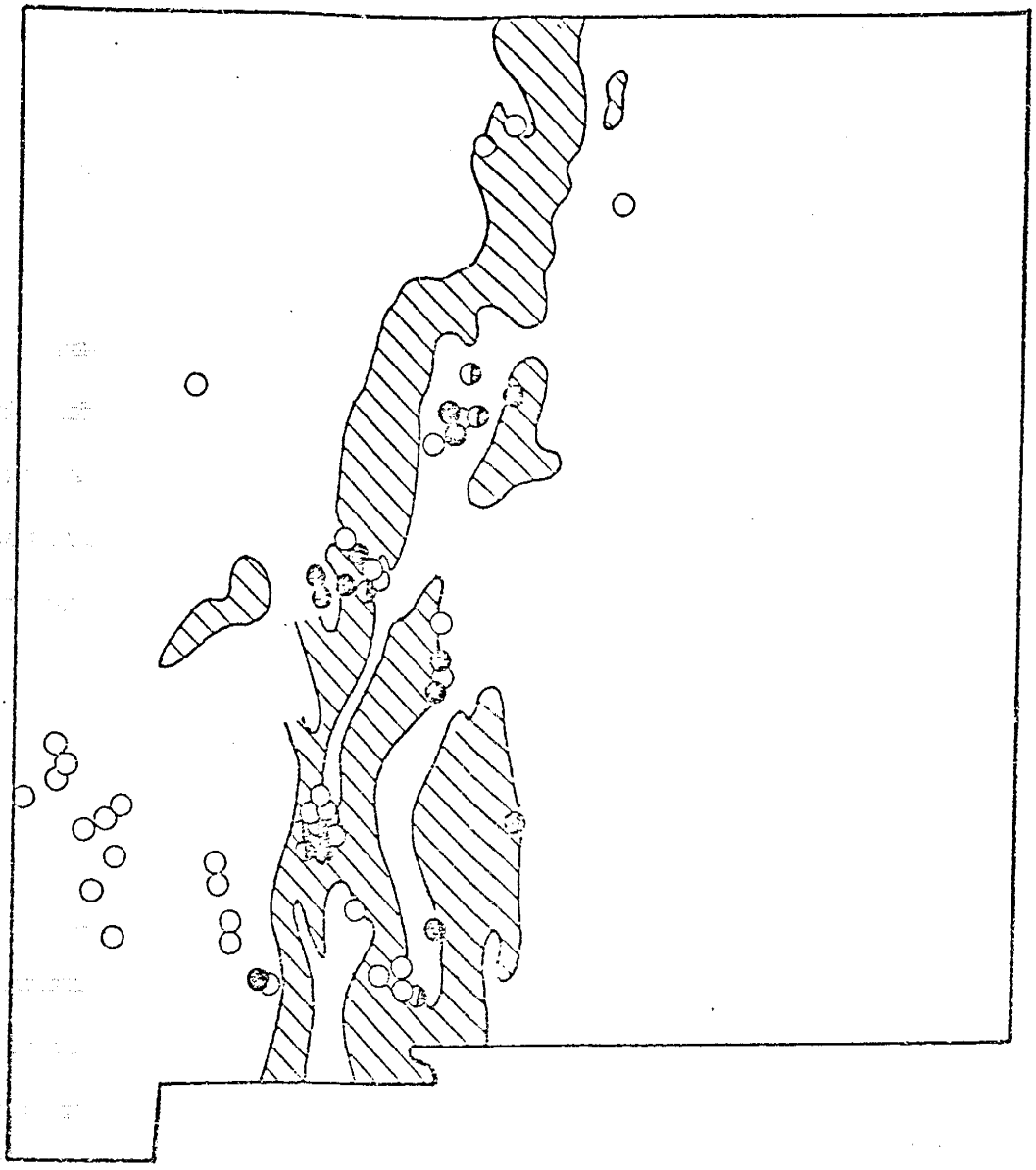

FLUORITE ◐ BARITE-FLUORITE ● BARITE

the stratigraphic section in the southwestern part of New Mexico lacks the abundant late Paleozoic arkose and evaporite facies which occur in central New Mexico. Because barium and lead substitute in potassium feldspars of the permeable arkosic rocks and because these rocks are not abundant in southwestern New Mexico, it is not surprising that galena and barite are less common in the fluorspar deposits of this part of the state. Also lacking in this region is a sulfur source for barite and sulfides. Thus these deposits might be the end product of a hydrothermal system similar to that proposed for the central New Mexico deposits with the primary difference being the lack of a sedimentary sulfur and metal source.

An alternative explanation would be that these deposits precipitated from a fluid of magmatic origin. The Zuni Fluorspar District is also lacking in sulfides (Goddard, 1966, p. 1) but lies in Precambrian granites and gneisses. Goddard (op. cit.) proposed a magmatic source for the hydrothermal fluids but a meteoric hydrothermal system could also be argued. The Gallinas district may be an example where pluton-driven convection was an effective means of localizing meteoric fluids. At the Red Cloud mine, barite and fluorite occur with quartz, calcite, iron, copper, and lead sulfides; and iron, copper, and lead oxides. Perhac (1970, p. 47) concludes that "their proximity to the igneous contact strongly suggests a magmatic affinity, but they were almost certainly derived from hydrothermal fluids released from the trachyte magma." The fluorite

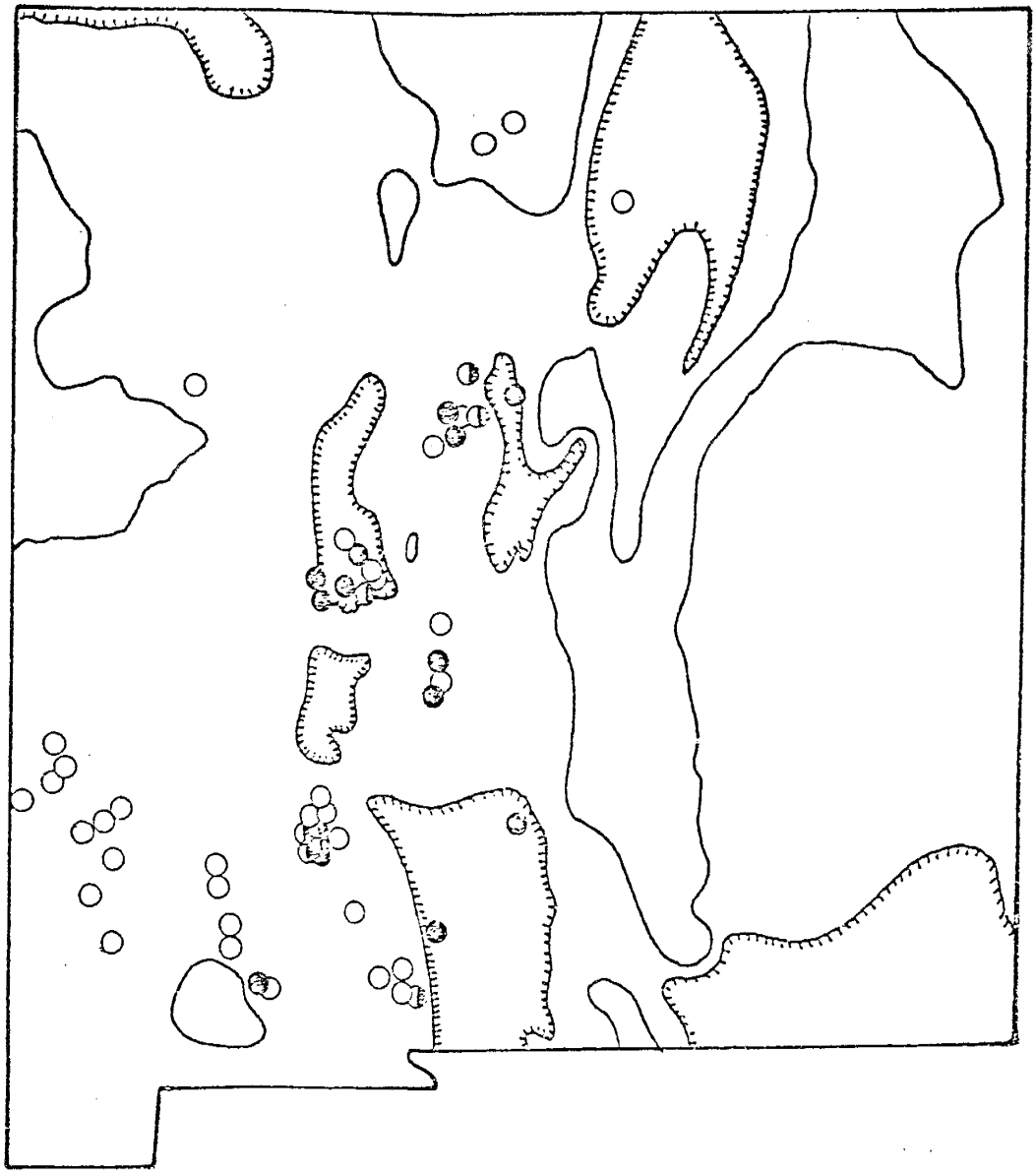

) FLUORITE ◐ BARITE-FLUORITE ● BARITE

UPLIFT

BASIN

Thus, there may be several genetic mechanisms resulting deposition of hydrothermal barite, fluorite, and galena. h individual deposit must be studied as an entity and .1 compared with existing models to determine their licability. This study has developed one such model ch should prove useful in terms of analyzing existing osits as well as exploring for new deposits in New Mexico.

sissippi Valley-type

The expression "Mississippi Valley-type" refers to a ss of low temperature hydrothermal mineral deposits ch are common, but not limited, to central, cratonic th America. This type of deposit has been referred to stratabound and stratiform; however, secondary structures ear to be important in many deposits and it is believed t most are epigenetic. Although each deposit has its 1 peculiarities which distinguish it from others, they do ve many features in common with one another. Heyl et al. 974) have recently listed some of these similarities.

The Hansonburg mining district has previously been npared to Mississippi Valley deposits (Roedder, 1967a; edder et al., 1968; Heyl, 1967, 1968). Certain similarities exist which suggest a common genesis for these "cratonic" posits and the hydrothermal deposits of New Mexico. rtain comparisons can be drawn between Mississippi Valley- pe and New Mexico deposits based on published data on e former. This comparison will be limited to the deposits ove, which show anomalous leads. The deposits shown Figure 41 which are characterized by normal leads could

nd barite deposits occur in breccia zones in Yeso and
lorieta sands, which suggest the possibility of evaporite-
erived sulfur and fluorine. A sulfur isotope study of
he district would be a useful aid in proposing a genetic
odel for these deposits.

Two sulfur isotope analyses made on a small barite-
luorite-galena deposit at the head of Jordan Canyon in the
agdalena Mountains (Figure 45 and Table P) suggest a
ermian evaporite source for sulfur at that location.
his was not expected in light of the large amount of
agmatic activity and the apparent lack of Permian evaporites
in the immediate area. Two analyses however, cannot rule
ut a magmatic source, not even the sulfur alone, although
it would be very unlikely that two samples of magmatic
origin would give identical values equal to Permian sulfur
values.

A stable isotope study of larger base metal deposits
in the Magdalena Mountains, which are more directly associated
with magmatic activity, may help to identify the origin of
some of the ore-forming constituents. A small, peripheral(?)
deposit was sampled for this study because of its similarity
with the other deposits considered herein (see Table P).
The sulfur isotope composition of this Jordan Canyon
mineralization is similar to those found at Hansonburg and
Gonzales; however, lead isotopes in the Magdalena vicinity
were described as "old leads" while those at Hansonburg and
Gonzales were described as anomalous by Slawson and Austin
(see Figure 41).

Figure 50

ssociation of Mississippi Valley-type deposits (shaded) in orth America with structural highs (modified from Hanor, 966). Large arrows have been added to suggest what direc- ion regional groundwater motion would have been if it is ssumed that this motion was responsible for the asymmetry etween the mineral deposits and structural highs.

be genetically related to magmatic activity and hence are not strictly controlled by the hydrodynamic model.

Many Mississippi Valley-type districts (Upper Mississippi Valley, Southern Illinois, S.E. Missouri, Tri-state) are spatially related to a structural dome, or arch which has elevated the Precambrian to the surface or near surface (Figure 50). Snyder (1967, p. 12) states that in the southeast Missouri district, the ore fluid was a brine which derived its metal content and radiogenic character from nearby sedimentary basins. Recently, Carpenter et al. (1974) have described modern oil field brines which contain high concentrations of lead and barium. Snyder (1967) describes how similar fluids could have moved out of basins along unconformities and bedding planes until basement topography channelled them upward into ore-bearing horizons.

This type of fluid movement could be responsible for the asymmetric spacial relationship between ore bodies and Precambrian uplifts. If the Precambrian rocks were essentially low permeability islands in a large, regional flow system, and the ore deposits formed as described by Snyder (1967) then they would be expected to be located on the "upstream" side of the Precambrian high relative to the direction of regional ground water flow. Similar hydrologic flow patterns have been suggested as the cause of asymmetric relationships between "contact metasomatic" iron deposits and causal igneous rocks in central and south central New Mexico (Beane and Titus, 1973; Beane and Allmendinger, 1974).

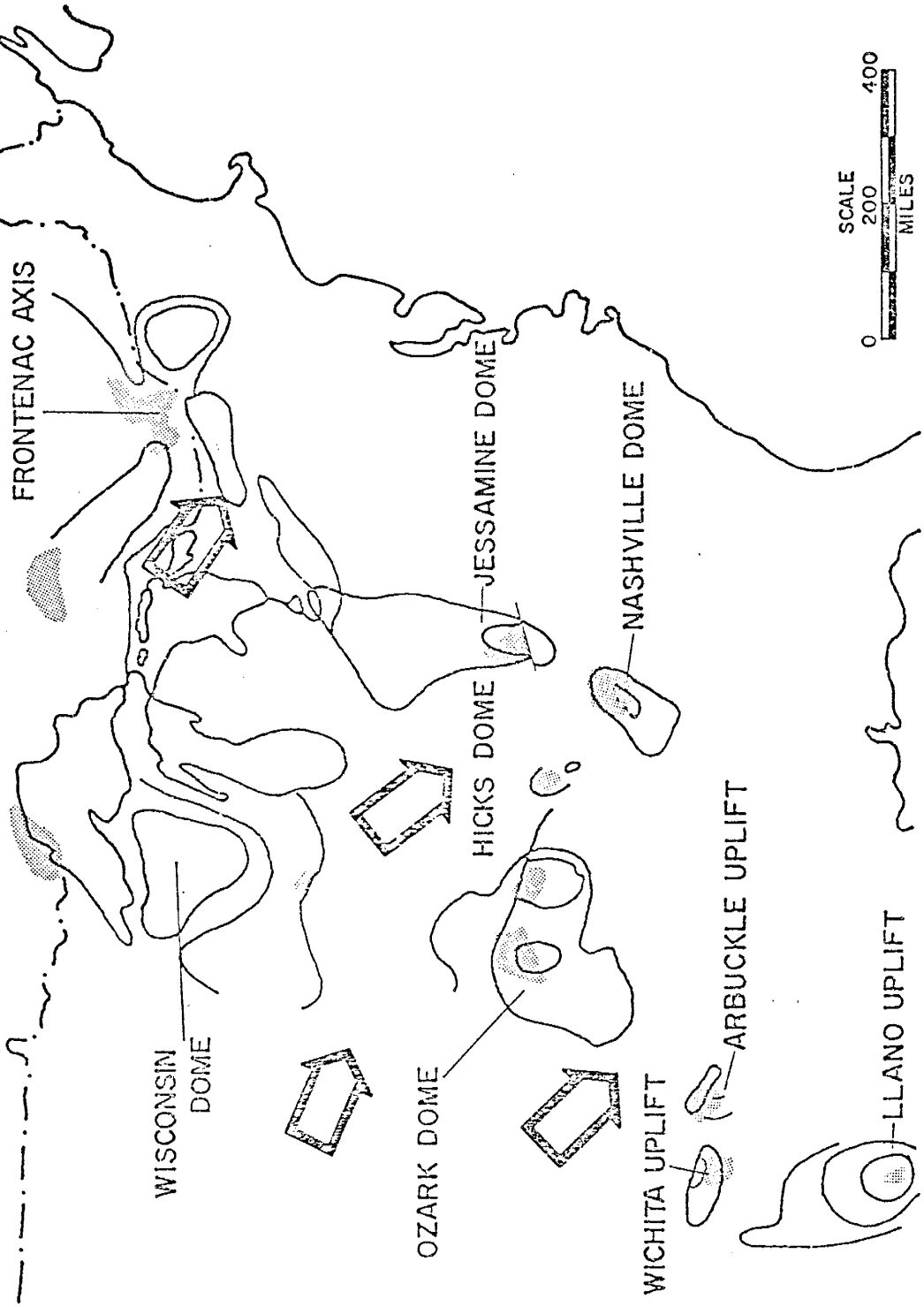
FRONTENAC AXIS
WISCONSIN DOME
OZARK DOME
HICKS DOME
JESSAMINE DOME
NASHVILLE DOME
WICHITA UPLIFT
ARBUCKLE UPLIFT
LLANO UPLIFT
SCALE
0
200
400
MILES

The possibility that Mississippi Valley-type deposits are genetically related to regional hydrologic movement was suggested above. Certainly the structural complexity of the associated domal features enhances the secondary permeability, especially in the vertical direction. Snyder (1967) states: "Ground preparation (intense fracturing of indurated rock) is one of the most impressive epigenetic features of the district." in reference to the southeast Missouri district. The New Mexico deposits are similarly characterized by a structural complexity which strongly influences the permeability (and hence, ore) distribution.

The major difference between the New Mexico deposits and the Mississippi Valley-type is probably the size of the system. The major hydrothermal barite-fluorite districts in New Mexico are on the order of a few square miles in area, where the southeast Missouri and Tri-state districts are 500 and 700 square miles respectively (Ohle, 1967, p. 34).

Such a size difference can be explained as a function of two factors in terms of a hydrodynamic model. First, and probably of most importance, is that the basins and domes of the central continental region are much larger than the basins and ranges of New Mexico. Therefore, the hydrologic systems of the central United States contained a much greater volume of rock and fluid. In addition, the discharge area would be spread out over a larger region because of the subdued structure. Secondly, the relatively stable tectonics of the craton would allow a hydrothermal system, once set up, to remain active for considerable

periods of time.

It seems very possible that if movement within the fault zone at Hansonburg had not occurred, precipitation of galena and sphalerite would have continued for a considerably longer period of time. However, it appears as though some movement did take place which allowed the introduction of cooler, more saline and more oxidizing, sulfate-bearing fluids into the Hansonburg system. Thus, it may be that the areal extent of the mineral deposits are closely related to size of the hydrologic system, specifically the discharge region, while tenor is more closely related to length of time involved in mineral deposition (other factors constant).

Another characteristic of the Mississippi Valley-type ore deposits is the association of hydrocarbons found in both the host rocks and in fluid inclusions (Hall and Friedman, 1963; Roedder, 1967a). Several writers have discussed the role of hydrocarbons in a depositional model for the Mississippi Valley deposits (c.f. Skinner, 1967; Barton, 1967). Regardless of the genetic consequences, the presence of organic matter is nearly universal in Mississippi Valley-type deposits, and is usually associated with a carbonate rock facies. This is analagous to the methane-bearing Pennsylvanian and Permian carbonates in the Oscura anticline. The organic material observed in fluid inclusions at Hansonburg indicates its presence in the ore-forming fluids.

From the work of previous investigators, it would appear that the Mississippi Valley-type deposits have many features in common with the Hansonburg mining district. Heyl et al. (1974) listed the common characteristics of the eight principal Mississippi Valley-type deposits. These 12 characteristics will be used to summarize the similarities which the Hansonburg and other central New Mexico deposits have in common with the Mississippi Valley-type. Of the twelve Heyl et al. (op. cit.) list, nine directly apply to the New Mexico deposits.

(1) Most deposits are structurally controlled, largely open-space fillings.

(2) Although the deposits may favor certain carbonate beds for major commercial deposits, they are not strictly stratabound nor stratiform.

(3) The mineralogy of the ore bodies and associated trace element patterns can no longer be called unusually simple but is subtly complex, especially locally, within parts of districts.

(4) Fluid inclusion data, including homogenization temperatures, D values, and chemical compositions, indicate that the hydrothermal solutions were mainly heated basin brines (evolved connate waters) with salinities in excess of 20 weight percent. Temperatures of ore deposition were about 200° C or less.

(5) All deposits contain markedly radiogenic J-type lead with $^{206}Pb/^{204}Pb$ ratios that are 20 or greater. A shallow crustal source for nearly all the lead is indicated.

(6) $\delta^{34}S$ indicates a crustal source for most of the sulfur in the sulfides and sulfates in the deposits.

(9) The mineral zonation in each district is distinctive and districtwide; the vertical mineral zonation is present in

places but much less widespread.

> (11) Data available on districtwide solution patterns suggest the ore fluids spread laterally through sandstone aquifers, . . . to form unified districtwide solution-flow systems.
>
> (12) Silver is present in most districts.

Although silver is not abundant in any of the New Mexico deposits described, it is present in most galena-bearing deposits.

The three other characteristics listed are:

> (7) Each district has distinctive regional isotopic patterns in lead and sulfur isotopes that reflect directions of solution flow, buried heat sources, and areas of localization of ore fluids.
>
> (8) Oxygen isotope data from wall rocks outside of the alteration halos surrounding ore deposits show that those wall rocks were never exposed to abnormally high fossil geothermal gradients.
>
> (10) Post-Precambrian igneous rocks are sparse except in two districts.

Although a district isotopic pattern was noted (p. 140) for lead, none was noted for sulfur. The lack of high geothermal gradients mentioned in (8) above may indicate a deeper environment for the Mississippi Valley-type mineralization. Finally, the lack of post-Precambrian igneous rocks in the Mississippi Valley deposits suggests that sufficient heat was derived from deep circulation in large basins to account for the fluid inclusion filling temperatures without the input of additional magmatic heat.

The smaller, shallower basins in New Mexico may require this magmatic heat to accomplish the same results.

SUMMARY AND CONCLUSIONS

A source-bed origin for the ore-forming constituents is proposed for the hydrothermal mineralization in the Hansonburg mining district. Total sulfur during both the sulfide and sulfate stages appears to have been dominated by isotopically light sulfur derived from Permian evaporites. Lead isotope studies of other workers in the district are of the anomalous J-type. This is interpreted as indicating an originally Precambrian lead, which was eroded and incorporated into Permian arkosic and red-bed deposits prior to mobilization and incorporation into the hydrothermal system. This lead is probably a mixture of lead which was trapped in microcline or other potassium feldspar and lead which resulted from the decay of interstitial uranium. Analyses of the arkosic and red-bed deposits suggests that these units contained sufficient quantities of barium and fluorine, in addition to lead, necessary to account for the quantities estimated in the hydrothermal mineralization.

A comparison of fluid inclusion compositions with modern basin fluids suggests a mechanism for both mobilizing and transporting these constituents. A regional flow system would provide natural groundwater with the physical and chemical properties necessary for leaching the essential elements from the arkosic units. A high Na/K ratio would result from interaction with the same evaporites which supplied the isotopically light sulfur. Farther along the flow lines dikes and sills, supported by a high geothermal

gradient, would add heat to the fluid. This hot, NaCl-rich fluid would be an ideal medium for leaching lead and barium from potassium silicates. In addition, the high chloride solutions could transport metals as multiple-chloride complexes. The regional flow system would then transport the constituents to a discharge region where a rapdily decreasing thermal gradient would be encountered as the fluids discharged upward. This is analogous to many modern geothermal systems. Such a hydrologic system would be capable of supplying the necessary volumes of fluid within about 600-700 years.

Fluid inclusion filling temperatures, corrected for pressure, specify a temperature range of 150° to 200° C for most of the primary mineralization. It seems unlikely that pressure could have exceeded 100 bars at this depth throughout Tertiary time. Composition of the fluid was dominated by the approximately 3.0 molar NaCl content. The probable ranges of f_{O_2} and pH are 10^{-36} to 10^{-32} and about 4.0 to 5.5 respectively, based on stability ranges of the observed hydrothermal mineralization. Initial mineral precipitation apparently was effected by a change in both aquifer composition and thermal regime down flow lines. The hydrologically steepened geothermal gradient would dramatically reduce the stability of metal chloride complexes as they move toward the surface, such that metal ions would be "partitioned" from the complexed state into the free ionic state where they could combine with the small quantities of reduced sulfur ion available and precipitate the metal sulfides. Sulfide mineralization may have come

to an end as tectonic movement shifted the deposits relative to the hydrothermal fluids. These new waters would be cooler, more saline and more oxidizing than the earlier fluid with which they mixed and gradually replaced. This is a consequence of their prior circulation through the shallower Permian evaporite sequence. This mixing model is compatible with the sudden decrease in temperature associated with barite precipitation followed by a more gradual cooling trend associated with increasing salinity. Barite precipitation may therefore, be the result of mixing of a "high"-barium fluid with a high-sulfate fluid. Fluorite precipitation probably occurred in much the same manner but could also have been related to decreasing temperature (and hence solubility) with time. Addition of Ca^{2+} to the fluid by interaction with limestone was likely an important factor in fluorite precipitation.

The mid-Tertiary age assigned to this district, although compatible with the hydrologic model, is not certain. It is probable that the mid-Tertiary dikes and sills contributed significant amounts of heat to the hydrothermal system. Also, the mid-Tertiary tectonic regime could have produced the tension responsible for the normal faults with which the mineralization is presently associated.

Several deposits occur in central New Mexico which are mineralogically and texturally very similar to the Hansonburg deposit. Not only do they occur in the same or equivalent stratigraphic and tectonic environments but

they also contain isotopically similar sulfur and lead. Further, fluid inclusion analyses indicate that mineralization took place in nearly the same temperature range as Hansonburg. These similarities are shown to be more than coincidental and it is likely that these deposits lying several tens of miles from one another, have a common genetic history. Differences in mineralogy among the various individual deposits can be attributed to variations in chemistry and degree of interaction of the source rocks with regionally heated, subsurface waters which eventually became the ore-forming fluids. A review of the literature indicates that Mississippi Valley-type deposits have many features in common with the Hansonburg mining district, and it is suggested that some or all of the processes believed responsible for mineralization at Hansonburg may have played an important role in the formation of the Mississippi Valley-type deposits.

LIST OF REFERENCES

Adler, Hans H. (1974) Sulfur-isotope compositions of Jurassic and Triassic marine sulfates of the United States, in; Geol. Soc. Am., Abstracts with programs, v. 6, n. 7, p. 630.

Allmendinger, Roger J. (1971) Hydrologic control over the origin of gypsum at Lake Lucero, White Sands National Monument, New Mexico, M.S. thesis, New Mexico Inst. Min. & Tech., Socorro, New Mexico, 82 p.

Ames, L. L., Jr. (1958) Chemical analysis of the fluid inclusions in a group of New Mexico minerals, Econ. Geol., v. 53, p. 473-480.

Anonymous (1963) Baca Formation in the area around Socorro, N.M., in; N.M. Geol. Soc., 14th Field Conf. Guidebook, p. 100-101.

Arendt, Ward W. (1971) The geology of La Joyita Hills, Socorro, Co., N.M., M.S. Thesis, Univ. New Mex. 75 p.

Ault, Wayne W. (1959) Isotopic fractionation of sulfur in geochemical processes, in; Researches in Geochemistry, Abelson, (ed.), John Wiley and Sons, 511 p.

Ault, W. W. and Jensen, M. L. (1963) Summary of sulfur isotope standards, in; Biogeochemistry of sulfur isotopes, Jensen M. L., (ed.), Natl. Sci. Found. Symp. Proc., Yale Univ., p. 16-29.

Austin, C. F. and Slawson, W. F. (1961) Isotopic analyses of single galena crystals: a clue to history of deposition, Am. Mineralogist, v. 46, p. 1132-1140.

Barnes, H. L. and Kullerud, O. (1961) Equilibria in sulfur-containing aqueous solutions in the system Fe-S-O, and their correlation during ore deposition, Econ. Geol., v. 56, p. 648-688.

Barton, Paul B., Jr. (1967) Possible role of organic matter in the precipitation of the Mississippi Valley ores, in; Genesis of stratiform lead-zinc-barite-fluorite deposits (J. S. Brown, ed.), Econ. Geol. Mon. 3, p. 371-378.

Bates, R. L., Wilpolt, R. H., MacAlpin, A. J., and Vorbe, G. (1947) Geology of the Gran Quivira Quadrangle, New Mexico, N.M.B.M.M.R., Bull. 26, 57 p.

ane, Richard E. (1974) Barite-fluorite-galena deposits in south-central New Mexico: A product of shallow intrusions, groundwater, and epicontinental sediments, (abs.), in; Geol. Soc. Am., Abstracts with programs, v. 6, n. 7, p. 646-647.

ane, R. E. and Allmendinger, R. J. (1974) Shallow intrusives, groundwater, and ore deposits (abs.), in; Base metal and fluorspar districts of New Mexico, Symposium sponsored by: N. M. Geol. Soc., and New Mex. Bur. Mines & Min. Res., p. 5-6.

ane, R. E., Bloom, M. S. and Jaramillo, L. (1974) Skarn and disseminated mineralization in the Jicarilla Mountains, Otero County (abs.), in; Base metal and fluorspar districts of New Mexico, Symposium sponsored by: N. M. Geol. Soc. and New Mex. Bur. Mines & Min. Res., p. 6.

ane, R. E. and Titus, F. B., Jr. (1973) Thermal control of magnetite deposition in central New Mexico (abs.), in; Geol. Soc. Am., Abstracts with programs, v. 5, p. 543-542.

lding, A. J. (1964) Geologic outline of the Jicarilla Mountains, Lincoln County, New Mexico, in; N. M. Geol. Soc., 15th Field Conf. Guidebook, p. 82-86.

ahnell, Hugh P. (1955) Mesozoic stratigraphy of south-central New Mexico, in; N. M. Geol. Soc., 6th Field Conf. Guidebook, p. 81-87.

lek, J., Vesely, J., and Sulcek, Z. (1971) Formation of fluoride complexes with metals of alkaline earths, Collect. Czech. Chem. Commun., v. 36, n. 9, p. 3377-3381.

mon, R. S. and Pierce, A. P. (1967) Isotopic varieties of lead in stratiform deposits, in; Genesis of stratiform lead-zinc-barite-fluorite deposits, J. S. Brown (ed.), Econ. Geol. Mon. 3, 443 p.

penter, A. B., Trout, M. L., Pickett, E. E. (1974) Preliminary report on origin and chemical evolution of lead- and zinc-rich oil field brines in central Mississippi, Econ. Geol., v. 69, p. 1191-1206.

pin, Charles E. (1971) The Rio Grande Rift, Part I: Modifications and additions, in; N. M. Geol. Soc., 22nd Field Conf. Guidebook, p. 191-201.

ypool, G. E., Holser, W. T., Kaplan, I. R., Sakai, H., and Zak, I. (1972) Sulfur and oxygen isotope geochemistry of evaporite sulfates, (abs.), in; Geol. Soc. Am., Abstracts with programs, v. 4, p. 473.

Cobble, James W. (1953) Empirical considerations of entropy. I. The entropies of oxy-anions and related species, Jour. Chem. Phys., v. 21, p. 1443-1446.

Cobble, James W. (1953a) Empirical considerations of entropy. II. The entropies of inorganic complex ions, Jour. Chem. Phys., v. 21, p. 1446-1450.

Craig, Harmon (1963) The isotopic geochemistry of water and carbon in geothermal areas, in; Nuclear Geology on Geothermal areas, Consiglio Nazional Delle Ricerche, Pisa, p. 17-53.

Craig, H. (1966) Isotopic composition and origin of the Red Sea and Salton Sea geothermal brines, Science, v. 154, p. 1544-1548.

Craig, Harmon (1969) Discussion source fluids for the Salton Sea geothermal system, Am. Jour. Sci., v. 267, p. 249-255.

Culberson, O. L. and McKetta, J. J., Jr. (1951) The solubility of methane in water at pressures to 10,000 psia, Tech Pub. 3032, Trans. Amer. Inst. Min. Met. Engrs., v. 192, p. 223-226.

Dane, C. H. and Bachman, G. O. (1965) Geologic map of New Mexico, U.S. Geol. Survey, New Mex. Bur. Mines & Min. Res., and Univ. of New Mexico Geol. Dept.

Davis, S. N. and DeWiest, R. J. M. (1966) Hydrogeology, John Wiley and Sons, Inc., 463 p.

Doe, B. R., Hedge, C. E., and White, D. E. (1966) Preliminary investigation of the source of lead and strontium in deep geothermal brines underlying the Salton Sea geothermal area, Econ. Geol., v. 61, p. 462-483.

Doe, B. R. (1970) Lead isotopes, in; Minerals rocks, and inorganic materials, v. 3, Berlin-Heidelberg-New York, Springer-Verlag, 137 p.

Dutcher, L. C., Hardt, W. F., and Moyle, W. R., Jr. (1972) Preliminary appraisal of ground water in storage with reference to geothermal resources in the Imperial Valley area, California, U.S. Geol. Surv., Circ. 649, 57 p.

Freeze, R. A. and Witherspoon, P. A. (1966) Theoretical analysis of regional groundwater flow: 1. Analytical & numerical solutions to the mathematical model, Water Res. Res., v. 2, p. 641-656.

Freeze, R. A. and Witherspoon, P. A. (1967) Theoretical analysis of regional groundwater flow: 2. Effect of water-table configuration and subsurface permeability variation, Water Res. Res., v. 3, p. 623-634.

Freeze, R. A. and Witherspoon, P. A. (1968) Theoretical analysis of regional groundwater flow: 3. Quantitative Interpretations, Water Res. Res., v. 4, p. 581-590.

Garrels, R. M. and Christ, C. L. (1965) Solutions, minerals, and equilibria, Harper and Row, New York, 450 p.

Goddard, Edwin H. (1966) Geologic map and sections of the Zuni Mountains fluorspar district, Valencia County, New Mexico, U.S. Geol. Survey, Misc. Inv. Map I-454.

Haas, John L., Jr. (1971) The effect of salinity on the maximum thermal gradient of a hydrothermal system at hydrostatic pressure, Econ. Geol., v. 66, p. 940-946.

Hall, F. R. (1963) Springs in the vicinity of Socorro, New Mexico, in; N. M. Geol. Soc., 14th Field Conf. Guidebook, p. 160-170.

Hall, W. E. & Friedman, Irving (1963) Composition of fluid inclusions, Cave-in-Rock fluorite district, Illinois, and Upper Mississippi Valley lead-zinc district, Econ. Geol., v. 58, p. 886-911.

Hanor, Jeffrey S. (1966) The origin of barite, PhD. Thesis (copyright 1966) Harvard Univ.

Heath, R. L. (1973) Table of the isotopes, in; Handbook of Chemistry and Physics, Weast R. C. (ed.), 54th Ed., CRC Press.

Helgeson, Harold C. (1966) Solution chemistry and metamorphism, in; Researches in Geochemistry, Volume II, P. H. Abelson (ed.), Wiley, New York, p. 362-404.

Helgeson, Harold C. (1967) Silicate metamorphism in sediments and the genesis of hydrothermal ore solutions, in; Genesis of stratiform lead-zinc-barite, fluorite deposits, J. S. Brown (ed.), Econ. Geol. Mon. 3, 443 p.

Helgeson, Harold C. (1968) Evaluation of irreversible reactions in geochemical processes involving minerals and aqueous solutions. I. Thermodynamic relations. Geoch. et Cosmoch. Acta., v. 32, p. 853-877.

Helgeson, Harold C. (1969) Thermodynamics of hydrothermal systems at elevated temperatures and pressures, Am. Jour. Sci., v. 267, p. 729-804.

Helgeson, H. C., Brown, T. H., and Leeper, R. H. (1969) Handbook of theoretical activity diagrams depicting chemical equilibria in geologic systems involving an aqueous phase at ore atmosphere and 0° to 300° C., Freeman, Cooper & Co., San Francisco.

Helgeson, H. C., Brown, T. H., Nigrini, A., & Jones, T. A. (1970) Calculation of mass transfer in geochemical processes involving aqueous solutions, Geoch. et Cosmoch. Acta., v. 34, p. 569-592.

Heyl, A. V. (1967) Some aspects of genesis of stratiform zinc-lead-barite-fluorite deposits in the United States, in; Genesis of stratiform lead-zinc-barite-fluorite deposits, J. S. Brown (ed.), Econ. Geol. Mon. 3, p. 410-425.

Heyl, Allen V. (1968) Minor epigenetic, diagenetic, and syngenetic sulfide, fluorite, and barite occurrences in the central United States, Econ. Geol., v. 63, p. 585-594.

Heyl, A. V., Landis, G. P., and Zartman, R. E. (1974) Isotopic evidence for the origin of Mississippi Valley-type mineral deposits: a review, Econ. Geol., v. 69, p. 992-1006.

Holland, Heinrich D. (1967) Gangue minerals in hydrothermal deposits, in; Geochemistry of hydrothermal ore deposits, Barnes, H. L. (ed.), Holt, Rinehardt, and Winston, Inc., 670 p.

Hubbert, M. King (1940) The theory of ground-water motion, Jour. Geol., v. 48, p. 785-944.

Huheey, James E. (1972) Inorganic chemistry: principles of structure and reactivity, Harpar & Row, Publ., 737 p.

Kajiwara, Yoshimichi (1971) Sulfur isotope study of the Kurobo-ores of the Shakanai, No. 1 deposits, Akita Prefecture, Japan, Geoch. Jour., v. 4, p. 157-181.

Kelley, V. C. and Thompson, T. B. (1964) Tectonics and general geology of the Ruidoso-Carrizozo region, central New Mexico, in; N. M. Geol. Soc., 15th Field Conf. Guidebook, p. 110-121.

Kopicki, Robert J. (1962) Geology and ore deposits of the Northern part of the Hansonburg mining district, Bingham, New Mexico, M.S. Thesis, New Mex. Inst. of Min. & Tech.

Kottlowski, Frank E. (1953) Geology and ore deposits of a part of the Hansonburg mining district, Socorro County, New Mexico, New Mex. Inst. of Min. & Tech., New Mex. Bur. of Mines & Min. Res., Circ. 23, 9 p.

Kottlowski, Frank E. (1962) Reconnaissance of commercial high-calcium limestones in New Mexico, New Mex. Bur. Mines & Min. Res., Circ. 60, 77 p.

Kottlowski, Frank E. (1963) Paleozoic and Mesozoic strata of southwestern and south-central New Mexico, New Mex. Bur. Mines & Min. Res., Bull. 79, 100 p.

Kottlowski, F. E. and Stewart, W. J. (1970) The Wolfcampian Joyita uplift in central, New Mexico, New Mex. Bur. Mines & Min. Res., Mem. 23, pt. 1, 31 p.

Kvenvolden, K. A. and Roedder E. (1971) Fluid inclusions in quartz crystals from South-West Africa, Geoch. et Cosmoch. Acta., v. 35, p. 1209-1229.

Landis, Gary P. (1972) Geologic fluid inclusion and stable isotope studies of a tungsten - base metal ore deposit: Pasto Bueno, Northern Peru, PhD Thesis, Univ. Minn.

Lasky, Samual G. (1932) The ore deposits of Socorro County, New Mexico, New Mex. Bur. of Mines and Min. Res., Bull. 8, 139 p.

Levinson, A. A. (1974) Introduction to exploration geochemistry, Applied Publishing Ltd., Calgary, 612 p.

Levorsen, A. I. (1967) Geology of petroleum, W. H. Freeman and Co., 724 p.

Lewchalermvong, C. (1973) Investigation and evaluation of the Royal Flush and Mex-Tex mines, adjacent area, Hansonburg mining district, Socorro County, New Mexico, M.S. Thesis, New Mex. Inst. of Min. & Tech.

Lipman, P. W. (1969) Alkalic and tholeiitic basaltic volcanism related to the Rio Grande depression, southern Colorado and northern New Mexico, Geol. Soc. Am., Bull., v. 80 p. 1341-1354.

Macnamara, J. and Thode, H. G. (1950) Comparison of the isotopic constitution of terrestrial and meteoric sulfur, Phys. Rev., v. 78, p. 307-308.

McCrea, J. M. (1950) On the isotopic chemistry of carbonates and a paleotemperature scale, Jour. Chem. Phys., v. 18, p. 849-857.

McLean, J. S. (1970) Saline ground-water resources of the Tularosa Basin, New Mexico, U.S. Dept. Int., Office of Saline Water Res. and Dev. Prog. Rep. No. 561.

Muffler, L. J. P. and Doe, B. R. (1968) Composition and mean age of detritus of the Colorado River Delta in the Salton Trough, southeastern California, Jour. Sed. Pet., v. 38, p. 384-399.

Ohle, Ernest M. (1967) The origin of ore deposits of the Mississippi Valley-type, in; Genesis of stratiform lead-zinc-barite-fluorite deposits, J. S. Brown (ed.), Econ. Geol. Mon. 3, p. 33-39.

Ohmoto, Hiroshi (1968) The Bluebell Mine, British Columbia, Canada: Pt. 2 Chemistry of the hydrothermal fluids, PhD. Thesis, Princeton Univ.

Ohmoto, Hiroshi (1971) Fluid inclusions and isotope study of the lead-zinc deposits at the Bluebell mine, British Columbia, Canada, Soc. Mining Geol. Japan, Spec. issue 2, p. 93-99. (Proc. IMA-IAGOD Meetings, 1970, Joint Symp. Vol.)

Ohmoto, Hiroshi (1972) Systematics of sulfur and carbon isotopes in hydrothermal ore deposits, Econ. Geol., v. 65, p. 551-578.

Ohmoto, Hiroshi and Rye, R. O. (1970) The Bluebell Mine, British Columbia, I. Mineralogy, Paragenesis, fluid inclusions, and the isotopes of hydrogen, oxygen, and carbon, Econ. Geol., v. 65, p. 417-437.

Ohmoto, H. and Shettel, D. L. (1974) Effect of f_{O_2} on the hydrogen and oxygen isotopic compositions of minerals at high temperatures and pressures, in: Geol. Soc. Am., Abstracts with programs, v. 6, n. 7, p. 898.

Okamoto, G., Okura, T., and Goto, K. (1957) Properties of silica in water, Geoch. et Cosmoch. Acta., v. 12, p. 123-132.

Olmstead, F. H. and Van Denburgh, A. S. (1974) Leach Hot Springs geothermal area, Nevada, (abs.), in; Geol. Soc. Am., Abstracts with programs, v. 6, n. 7, p. 899-900.

Pettijohn, F. J. (1957) Sedimentary rocks, 2nd ec., Harper and Bros., 526 p.

Perhac, Ralph M. (1970) Geology and mineral deposits of the Gallinas Mountains, Lincoln and Torrance Counties, New Mexico, New Mex. Bur. Mines and Min. Res., Bull. 95, 51 p.

Powell, R. E. and Latimer, W. M. (1951) The entropy of aqueous solutes, Jour. Chem. Phys., v. 19, p. 1139-1141.

Reiter, M., Edwards, C. L., Hartman, H., and Weidman, C. (1975) Terrestrial heat flow along the Rio Grande rift, New Mexico and southern Colorado, Geol. Soc. Am. Bull., v. 86, p. 811-818.

Robie and Waldbaum (1968) Thermodynamic properties of minerals and related substances, U.S. Geol. Surv., Bull. 1259, 256 p.

Robinson, B. W. and Ohmoto, H. (1973) Mineralogy, fluid inclusions, and stable isotopes of the Echo Bay U-Ni-Ag-Cu deposits, Northwest Territories, Canada, Econ. Geol., v. 68, p. 635-656.

Robinson, R. A. and Stokes, R. H. (1970) Electrolyte Solutions, London, Butterworths and Co., Ltd., 571 p.

Roedder, Edwin (1958) Technique for the extraction and partial chemical analysis of filled fluid inclusions from minerals, Econ. Geol., v. 53, p. 235-269.

Roedder, Edwin (1967) Fluid inclusions as samples of ore fluids, in; Geochemistry of hydrothermal ore deposits, Barnes, H. L. (ed.), Holt, Rinehardt, and Winston, Inc., 670 p.

Roedder, Edwin (1967a) Environment of deposition of stratiform (Mississippi Valley-type) ore deposits from studies of fluid inclusions, in; Genesis of stratiform lead-zinc-barite-fluorite deposits, J. S. Brown (ed.), Econ. Geol. Mon. 3, 443 p.

Roedder, Edwin (1971) Fluid inclusion evidence on the formation of mineral deposits of the southern Appalachian Valley, Econ. Geol., v. 66, p. 777-791.

Roedder, Edwin (1972) Composition of fluid inclusions, U.S. Geol. Surv., Prof. Paper, 440-JJ, 164 p.

Roedder, E., Heyl, A. V., and Creel, J. P. (1968) Environment of ore deposition at the Mex-Tex deposits, Hansonburg district, New Mexico, from studies of fluid inclusions, Econ. Geol., v. 63, p. 336-348.

Roedder, E., Ingram, B., and Hall, W. E. (1963) Studies of fluid inclusions III: Extraction and quantitative analysis of inclusions in the milligram range, Econ. Geol., v. 58, p. 353-374.

Rossini, F. D., Wagman, D. D., Evans, W. H., Levine, S., and Jaffe, I. (1969) Selected values of chemical thermodynamic properties, U.S. Dept. of Comm. N.B.S. Tech. Note 270-4, 264 p.

Rothrock, H. E., Johnson, C. M., and Hahn, A. D. (1946) Fluorspar resources of New Mexico, New Mex. Bur. Mines and Min. Res., Bull. 21, 245 p.

Rye, R. O. (1966) The carbon, hydrogen and oxygen isotopic composition of the hydrothermal fluids responsible for the lead-zinc deposits at Providencia, Zacatecas, Mexico, Econ. Geol., v. 61, p. 1399-1427.

Rye, R. O. (1974) A comparison of sphalerite-galena sulfur isotope temperatures with filling temperatures of fluid inclusions, Econ. Geol., v. 69, p. 26-32.

Rye, R. O. and Haffty, J. (1969) Chemical composition of the hydrothermal fluids responsible for the lead-zinc deposits at Providencia, Zacatecas, Mexico, Econ. Geol., v. 64, p. 629-643.

Rye, R. O. and Sawkins, F. J. (1974) Fluid inclusion and stable isotope studies on the Casapalca Ag-Pb-Zn-Cu deposits, central Andes, Peru, Econ. Geol., v. 69, p. 181-205.

Sakai, Hitoshi (1968) Isotopic properties of sulfur compounds in hydrothermal processes, Geoch. Jour., v. 2, p. 29-49.

Sanford, A. R. (1968) Gravity survey in central Socorro County, New Mexico, New Mex. Bur. Mines and Min. Res., Circ. 91, 14 p.

Sawkins, F. S. (1966) Ore genesis in the north Pennine ore field, in the light of fluid inclusion studies, Econ. Geol., v. 61, p. 385-401.

Sawkins, F. J. (1968) The significance of Na/K and Cl/SO_4 ratios in fluid inclusions and subsurface waters, with respect to the genesis of Mississippi Valley-type ore deposits, Econ. Geol., v. 63, p. 935-942.

Sheppard, S. M. F., Nielsen, R. L., and Taylor, H. P., Jr. (1969) Oxygen and hydrogen ratios of clay minerals from porphyry copper deposits, Econ. Geol., v. 64, p. 755-777.

Siebenthal, C. E. (1916) Origin of the zinc and lead deposits of the Joplin region Missouri, Kansas, and Oklahoma, U.S. Geol. Surv. Bull. 606, 283 p.

iebert, Robert M. (1974) The stability of $MgHCO_3^+$ and $MgCO_3^\circ$ ion-pairs from 10° C to 90° C, Phd. Thesis, Univ. Missouri, 107 p.

illen, L. G. and Martell, A. E. (1964) Stability constants of metal-ion complexes, London Chem. Soc., 745 p.

inclair, Patricia D. (1972) Bicarbonate and carbonate complexes as potential transporting agents for lead in hydrothermal solutions, (abs.), in; Geol. Soc. Am., Abstracts with programs, v. 4, p. 666.

kinner, Brian J. (1967) Precipitation of Mississippi Valley-type ores: A possible mechanism, in; Genesis of stratiform lead-zinc-barite-fluorite deposits, J. S. Brown (ed.), Econ. Geol. Mon. 3, p. 363-370.

kinner, B. J., White, D. E., Rose, H. J., and Mays, R. E. (1967) Sulfides associated with the Salton Sea geothermal brine, Econ. Geol., v. 62, p. 316-330.

lawson, W. F. and Austin, C. F. (1960) Anomalous leads from a selected geological environment in west-central New Mexico, Nature, v. 187, p. 400-401.

lawson, W. F. and Austin, C. F. (1962) A lead isotope study defines a geological structure, Econ. Geol., v. 57, p. 21-29.

nith, Clay T. (1964) Geology of the Little Black Peak Quadrangle, Socorro, and Lincoln Counties, New Mexico, in; N. M. Geol. Soc., 15th Field Conf. Guidebook, p. 92-99.

nyder, Frank G. (1967) Criteria for origin of stratiform ore bodies with application to southeast Missouri, in; Genesis of stratiform lead-zinc-barite-fluorite deposits, J. S. Brown (ed.), Econ. Geol. Mon. 3, 443 p.

tacey, J. S., Zartman, R. E., and Nkomo, I. T. (1968) A lead isotope study of galenas and selected fedspars from mining districts in Utah, Econ. Geol., v. 63, p. 796-814.

train, William S. (1969) Late Cenozoic strata of the El Paso area, in; Border stratigraphy symposium, Kottlowski, F. E. and Lemone, W. W. (eds.), New Mex. Bur. Mines and Min. Res., Circ. 104, p. 122-123.

ull, D. R. (ed.) (1965, 1966) JANAF Thermochemical tables, Thermal Res. Lab., Dow Chem. Co.

gisaki, R. and Jensen, M. L. (1971) Oxygen isotopic studies of silicate minerals with special reference to hydrothermal mineral deposits, Geoch. Jour., v. 5, p. 7-21.

mers, W. K. (1965) A preliminary report on New Mexico's geothermal energy resources, New Mex. Bur. Mines and Min. Res., Circ. 80, 41 p.

mage, S. B. and Wootton, T. P. (1937) The non-metallic mineral resources of New Mexico and their economic features, New Mex. Bur. Mines & Min. Res., Bull. 12, 159 p.

ylor, H. P., Jr. (1967) Oxygen isotope studies of hydrothermal mineral deposits, in; Geochemistry of hydrothermal ore deposits, Barnes H.L. (ed.), Holt, Rinehardt, and Winston, Inc., 670 p.

ylor, Hugh P., Jr. (1973) O^{18}/O^{16} evidence for meteoric-hydrothermal alteration and ore deposition in the Tonopah, Comstock Lode, and Goldfield mining districts, Nevada, Econ. Geol., v. 68, p. 747-764.

mpson, M. L. (1942) Pennsylvanian system in New Mexico, New Mex. Bur. Mines and Min. Res., Bull. 17, 92 p.

railkill, John (1968) Chemical and hydrologic factors in the excavation of limestone caves, Geol. Soc. Am. Bull., v. 79, p. 19-46.

th, J. (1962) A theory of groundwater motion in small drainage basins in central Alberta, Canada, Jour. Geophys. Res., v. 67, p. 4375-4387.

th, J. (1963) A theoritical analysis of ground-water flow in small drainage basins, Jour. Geophys. Res., v. 68, p. 4795-4812.

ruijt, A. (1970) Theory of groundwater, Gorden & Breach Sci. Publ., 190 p.

ber, Robert H. (1963) Cenozoic rocks of Socorro County, in; N. M. Geol. Soc., 14th Field Conf. Guidebook, p. 132-143.

ber, Robert H. (1964) Geology of the Carrizozo Quadrangle, New Mexico, in; N. M. Geol. Soc., 15th Field Conf. Guidebook, p. 100-109.

eir, James E. (1965) Geology and availability of ground water in the northern part of the White Sands Missile Range and vicinity, New Mexico, U.S. Geol. Surv., Water-Supply Paper 1801, 78 p.

nite, D. E. (1957) Magmatic, connate, and metamorphic waters, Geol. Soc. Am. Bull., v. 68, p. 1659-1682.

ite, D. E. (1968a) Hydrology activity and heat flow of the Steamboat Springs thermal system, Washoe Co., Nev., U.S. Geol. Surv. Prof. Paper 458-C, 109 p.

ite, D. E. (1968b) Environments of generation of some base-metal ore deposits, Econ. Geol., v. 63, p. 301-335.

lliams, Frank E. (1966) Fluorspar deposits of New Mexico, U.S. Bur. Mines, Inf. Circ. 8307, 143 p.

lliams, F. E., Fillo, P. V., and Bloom, P. A. (1964) Barite deposits of New Mexico, New Mex. Bur. Mines and Min. Res., Circ. 76, 46 p.

lliams, Roy E. (1970) Ground water flow systems and accumulation of evaporite minerals, Am. Assoc. Petrol. Geol., v. 54, p. 1290-1295.

lpolt, R. H., MacAlpin, A. J., Bates, R. L., and Vorbe, G. (1946) Geologic map and stratigraphic sections of Paleozoic rocks of Joyita Hills, Los Pinos Mountains, and Northern Chupadera Mesa, Valencia, Torrance, and Socorro, Counties, New Mexico, U.S. Geol. Surv. Oil and Gas Inv., Prelim. Map 61.

lpolt, R. H. and Wanek, A. A. (1951) Geology of the region from Socorro and San Antonio east to Chupadera Mesa, Socorro County, New Mexico, U.S. Geol. Surv. Oil and Gas Investigations Map M121 (2 sheets).

llenburg, Harold A. (1974) Geothermal studies in north-central Nevada, (abs.), in; Geol. Soc. Am., Abstracts with programs, v. 6, n. 7, p. 1009.

der, H. S. (1955) Role of water in metamorphism, Geol. Soc. Am., Spec. Paper 62, p. 505-524.